AN INVESTIGATION INTO THE MOSSBAUER EFFECT IN Fe^{57}

by

JANICE EMILY JEAN WOODROW

B. Sc., The University of British Columbia, 1960

A THESIS SUBMITTED IN PARTIAL FULFILMENT OF

THE REQUIREMENTS FOR THE DEGREE OF

MASTER OF SCIENCE

in the Department of

PHYSICS

We accept this thesis as conforming

to the required standard

THE UNIVERSITY OF BRITISH COLUMBIA

April, 1964

In presenting this thesis in partial fulfilment of

the requirements for an advanced degree at the University of

British Columbia, I agree that the Library shall make it freely

available for reference and study. I further agree that per-

mission for extensive copying of this thesis for scholarly

purposes may be granted by the Head of my Department or by

his representatives. It is understood that copying or publi-

cation of this thesis for financial gain shall not be allowed

without my written permission.

Department of _____*Physics*_____

The University of British Columbia,
Vancouver 8, Canada

Date _____*May 5, 1964*_____

ABSTRACT

In this thesis the Mossbauer effect in metallic iron has been studied as a function of the length of time of diffusion of the Co^{57} source into metallic iron, of the source temperature over the range $156^{o}K$ to $478^{o}K$, and of the absorber thickness. In each case, the line shape, width, intensity and shifts were measured.

Measurements showed that the appearance of an appreciable Mossbauer effect, .122, arises within the first ten minutes of diffusion time at $900^{o}C$ in a hydrogen atmosphere and that additional time is required to reduce the line width and to increase the intensity to .145.

The observed temperature shift of the resonantly absorbed 14.4 kev radiation followed that which was predicted by the Josephson effect. However, corrections for an isomer and a hydrostatic compression shift were made to the data before comparing the measured shift with the theoretical shift. The results indicated a Debye temperature of $\Theta_D = (420 \pm 20)^{o}K$ for both the source and absorber used.

The measurements made over the temperature range indicated that the internal magnetic field $\underline{H}$ followed the saturation magnetization curve (the Weiss Law) closely. For small temperature differences between the source and absorber, $\Delta\Theta < 50^{o}K$, measurements were made indicating that the minimum line width occurred at $\Delta\Theta = 24^{o}K$. These results indicated that the internal magnetic field at $\Delta\Theta = 0^{o}K$ for the source was $.01 \times 10^5$oe greater than that of the absorber. For $\Delta\Theta \geq 100^{o}K$, the Mossbauer line displayed a hyperfine structure arising from the temperature dependent difference in the internal magnetic field at the nuclei.

The line profile, width, shift and intensity were measured for four absorber thicknesses - .0002", .00035", .00055", and .001". The detailed comparison of these line characteristics with the theoretical values

required an extension of existing treatments, a discussion of which is given in chapter five. In each case it was observed that the Mossbauer line was accompanied by two small peaks, one on either side of the main line. The position of these peaks indicated that they were associated with a small or zero internal magnetic field at the site of some of the Fe^{57} atoms.

ACKNOWLEDGMENT

TABLE OF CONTENTS

LIST OF ILLUSTRATIONS

INTRODUCTION

This thesis describes experimental and theoretical work carried out by the author on certain aspects of the Mossbauer Effect.[1] The Mossbauer Effect has been extensively studied. Summaries of the literature are found in Hans Frauenfelder's book, "The Mossbauer Effect"[2] in the report of the Second Mossbauer Effect Conference[3] and in "The Mossbauer Effect" by A.J.F. Boyle and H.E. Hall.[4](*) Stated simply, the Mossbauer Effect is another name for nuclear resonance fluorescence, and its occurance is due to the fact that there exists a finite probability f, for nuclei bound in crystal lattices to emit and absorb gamma radiation having an energy almost precisely equal to that of the nuclear transition, E_0. The effect is characterized by the facts that the recoil momentum of the nucleus during emission or absorption, E_γ/c, is taken up by the crystal as a whole so that there is no line shift due to recoil and, that there is negligible thermal Doppler broadening of the gamma ray line. In general, f is very small; however, under special conditions, given in Chapter I, it becomes large enough to be measurable.

Observable energy shifts of the Mossbauer absorption spectrum occur because the width of the absorption line is sufficiently small compared with the interaction between the nucleus and the lattice and, the internal fields. Because of this, the Mossbauer Effect has been useful in determining the magnitude and direction of the fields at the position of the radiating nuclei, in determining nuclear values and static multipole moments, in investigating the chemical bonding of atoms in crystals, and in

(*) References to these books will be given as Frauenfelder, p._, Moss II, p._ and Boyle, P._.

measuring small, relativistic shifts.

Prior to the writing of this thesis, no completely successful attempt had been made to fit theory to experimental measurements of the Mossbauer velocity spectrum . The most rigorous calculation of the line intensity and the line shape, prior to this work, was that of S. Margulies and J.R. Ehrman.[5] In their theoretical study of the Mossbauer spectrum, they did not take into account the fact that in many cases, of which Fe^{57} in natural iron is an outstanding example, the emission and absorption lines are split by the Zeeman effect rather than composed of single lines. The purpose of this thesis therefore, was to make a thorough investigation of the Mossbauer absorption line obtained by the use of Fe^{57} in a natural iron lattice and to determine whether or not certain features of this line could be understood theoretically. The features considered were the line intensity as a function of source diffusion into the source lattice and of absorber thickness, the profile of the line as a function of temperature difference between the source and absorber, the diffusion of the source and of absorber thickness and, line shifts as a function of temperature differences between source and abosrber and the diffusion of the source.

This study of the absorption line width and intensity has a double importance. First, it is possible that the current theory put forth to explain the intensity and width of the Mossbauer spectrum is insufficient to explain all the features of the spectrum adequately. All the features of the line should be predictable by theory so that any new features would be recognizable as such, rather than attributed to experimental errors. Second, the study has a practical importance, that of learning how to achieve narrow lines, i.e., measured line widths equal to those expected on the basis of the half life of the radiating nucleus.

The thesis, in Chapter I deals with the fundamentals of the Mossbauer Effect . Chapter II deals with the theoretical aspects of the Mossbauer velocity spectrum line shape, width, intensity and line shifts for the case of Fe^{57}. Chapter III describes the experimental equipment and techniques used. Chapters IV, V and VI describe the experimental work done - Chapter IV, the annealing of the source; Chapter V, the dependence on the absorber thickness; Chapter VI, the temperature dependence of the line width and shifts. Throughout the thesis the phrase, "Mossbauer velocity spectrum" will be abbreviated to "Mossbauer spectrum" or "Mossbauer line".

Chapter I

GENERAL FEATURES OF THE MOSSBAUER EFFECT
and
ITS USES AS AN EXPERIMENTAL TOOL

1.0 Introduction

Nuclear resonant absorption of gamma rays cannot usually be observed, for two reasons. First, the recoil of the emitting and absorbing nuclei displace the emission line from the absorption line so that little or no overlap of the two occurs and resonant absorption does not take place. Second, the Doppler broadening due to the thermal motions of the nuclei greatly increase the effective width of the emission and absorption lines so that any overlapping is spread out. However, under certain conditions (to be given later in this chapter), there exists a finite probability f, that the emitting (or absorbing) nucleus is so tightly bound to the lattice that the whole lattice rather than the emitting (or absorbing) nucleus recoils. In this case, the recoil energy is characterized by the mass of the whole lattice rather than by the mass of the atom, and the Doppler broadening by the thermal motion of the whole lattice rather than that of the nucleus. Hence, both the recoil energy and the Doppler broadening of such gamma rays is negligible and the gamma rays have the energy and width associated with the nuclear transition.

This chapter has been designed primarily to present a background of the Mossbauer Effect. Since this background theory has been well summarized in Frauenfelder's book, "The Mossbauer Effect"[2] and by A.J. Boyle and H.E. Hall in their article, "The Mossbauer Effect",[4] the theory contained herein will be given in abbreviated form. Theory relating specifically to the experimental work described in this thesis is given in Chapter II

1.1 Recoiless Emission and Absorption

A gamma ray emitted by a free nucleus has an energy spectrum centered at energy

$$E_\gamma = E_o - E_o^2/2mc^2 \qquad\qquad \text{I-1}$$

where E_o is the energy of the nuclear transition, m is the mass of the emitting atom and $E_o^2/2mc^2 \equiv k\theta_R$ is the recoil energy of the emitting atom where θ_R may be called the "recoil temperature". In order to be absorbed by an identical nucleus, this gamma ray must have energy

$$E_\gamma = E_o + E_o^2/2mc^2 \qquad\qquad \text{I-2}$$

since the absorbing nucleus will also recoil. In such a case the resonant absorption would occur only if $E_o^2/2mc^2 < 2\Gamma$ where Γ is the natural line width defined by the nuclear transition. However, for 10 kev $< E_o <$ 100 kev, the energy range in which resonant absorption could be expected (Boyle, p.445), it is found that $E_o^2/mc^2 > \Gamma$ so that very little overlap of the emission and absorption spectra occur. For example, for Fe^{57}, $E_o^2/mc^2 = .004$ ev. and $\Gamma = 4.5 \times 10^{-9}$ev. and hence negligible resonant absorption is expected. In addition, when a gamma ray is emitted from a free nucleus, Doppler broadening of the gamma spectrum is produced by the thermal motions of the emitting atoms. For example, for a gas of atomic mass m = 57, the broadening expected at temperature $\theta = 300^\circ$K is

$$\begin{aligned} \triangle E &= (k\theta/mc^2)^{\frac{1}{2}} E_\gamma \\ &= .01ev \end{aligned} \qquad\qquad \text{I-3}$$

where k is the Boltzmann constant.

In marked contrast to the gamma emitted from a free nucleus, is

the one which is emitted from a nucleus that is tightly bound in the crystal lattice. In this case it is found that subject to the conditions listed in Table I-1, there exists a finite probability f, that the recoil energy given above is replaced by $E_0^2/2Mc^2$ and the Doppler broadening by $(k\theta/Mc^2)^{\frac{1}{2}}E$ where M is the mass of the whole lattice. Since $M \gg m$, the recoil energy loss and the Doppler broadening of such gamma rays would be so small that the emission and absorption spectra would overlap, producing nuclear resonant absorption, i.e., the Mossbauer Effect. Table I-1 lists the conditions under which a measurable Mossbauer Effect may be obtained.

When a gamma ray is emitted without recoil energy loss to the lattice, the state of the lattice is unchanged. In other words, the emission of the gamma ray is not accompanied by the emission of a phonon. If L_i indicates the initial state of the lattice, then the fraction of recoilless gamma rays emitted from the source is given by the expression (Frauenfelder, p.30)

$$f = \left| \langle L_i \left| \exp(i\underline{k} \cdot \underline{X}) \right| L_i \rangle \right|$$
$$= \left| \langle L_i \left| \exp(- X^2/\lambda^2) \right| L_i \rangle \right|$$

where $\underline{X}$ is the distance of the emitting atom from equilibrium position.   I-4

The fraction of gamma rays absorbed without recoil is given by a similar expression. f is called the Debye-Waller factor. In the Debye approximation to the lattice vibration this factor is given by the equation

$$f = \exp(-2W)$$
$$= \exp\left(-3\frac{E_0^2}{mc^2} \frac{1}{k\theta_D} \left[\frac{1}{4} + \left(\frac{\theta}{\theta_D}\right)^2 \int_0^{\theta_D/\theta} \frac{x\,dx}{e^x - 1} \right] \right)$$ I-5

where θ_D is the Debye temperature of the solid. Using $x = \frac{\theta_D}{\theta}$, the function $\phi\ (\theta_D/\theta)$ is plotted in figure I-1. In chapter VI, f has been calculated for Fe^{57} as a function of θ for $\theta_D = 420°K$. At $\theta = 300°K$, $f = .78$ for Fe^{57}. At $\theta = 0$, the Debye approximation for f reduces to

$$f = \exp(-3E_0^2/2mc^2/2k\theta_D)$$ I-6

$$\phi(x) = \frac{1}{x} \frac{ydy}{e^y - 1}$$

$$x = \Theta_b / \theta$$
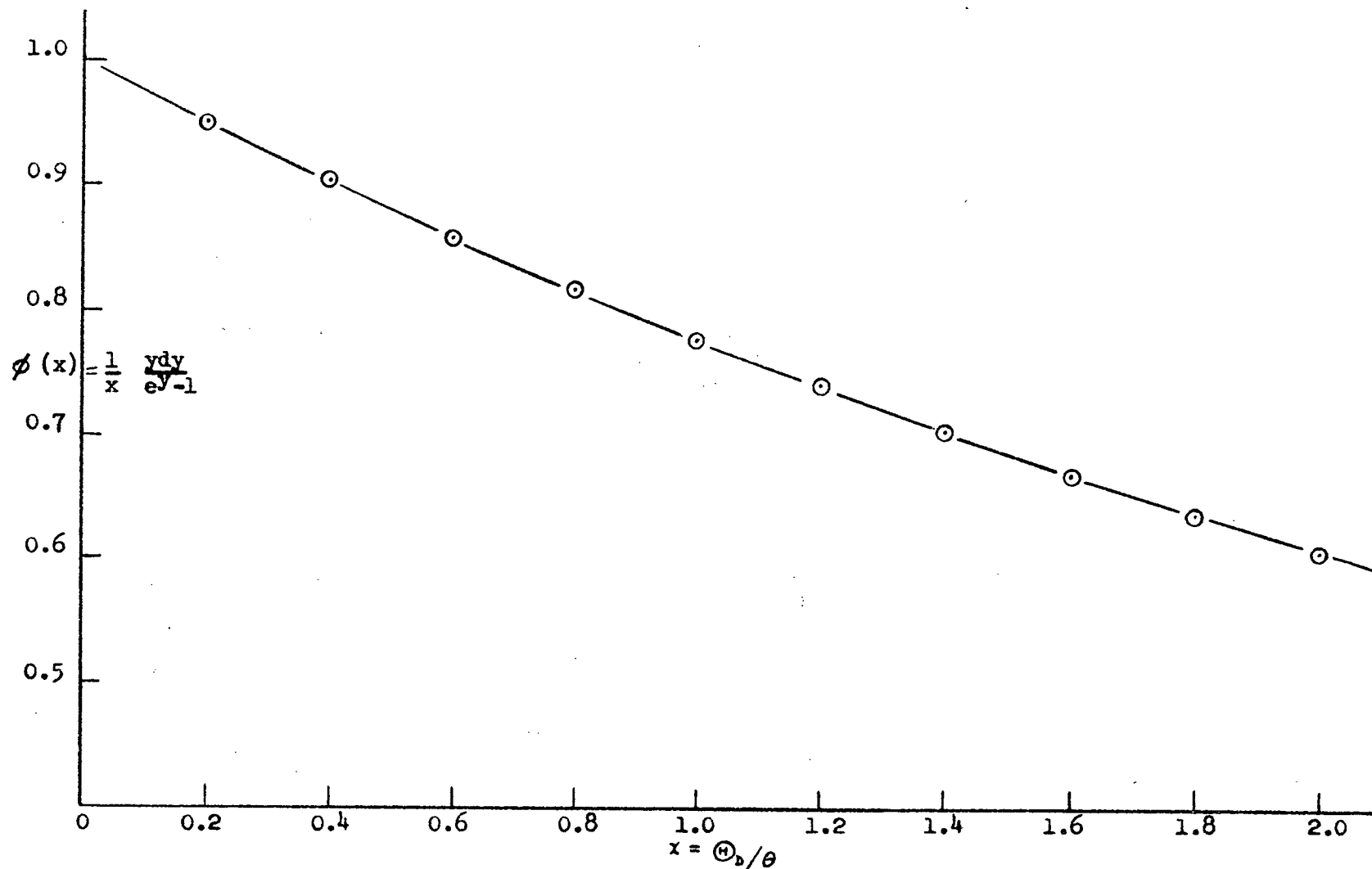
FIGURE I-1   The value of the Debye function,   (x), as a function of the ratio of the Debye temperature, Θ_b, to the ambient temperature, θ.

THE CONDITIONS WHICH MUST BE SATISFIED TO PRODUCE AN OBSERVABLE MOSSBAUER EFFECT

a) The excited state must decay to a ground state in the same nucleus.

b) The ambient temperature must be low compared with both the recoil temperature and the Debye temperature.

c) The cross section, σ_o, of the gamma transition at resonance, must be large.

d) The excited state must have a large probability for gamma decay.

e) The Debye temperature, Θ_D, of the crystal must be of the same magnitude as or larger than the recoil temperature, θ_R.

f) The ground state must be available in sufficient quantity to make an absorber.

g) The excited state must be available in sufficient quantity to make a source.

Table I-1

Transmission through a resonance absorber can be varied by varying the velocity between the source and absorber (see sec. 1.4). The resulting Mossbauer spectrum has a width greater than or equal to twice the width of the nuclear transition. The transmitted line intensities are temperature dependent as a result of the temperature dependence of the Debye-Waller factor, f (in the expression for the line intensities, Eqn. II-18).

1.2 Internal Field Effects

An important feature of the Mossbauer Effect is the fact that the line width of the Mossbauer absorption spectrum is narrow - in many cases, narrower than the Zeeman splitting of the nuclear magnetic substates. For example, for Fe^{57} in Fe, the line width is 9×10^{-9} ev. whereas the Zeeman splitting of the first excited state and the ground state of Fe^{57} are 1.07×10^{-7} ev. and 1.90×10^{-7} ev.[6] Therefore, the Mossbauer Effect has been

used to observe directly the Zeeman splitting of various nuclear states,[7] and also to measure the small shifts due to differences of chemical structures in source and absorber, the isomer shifts, and the electric quadrupole moments. The isomer shift arises from a difference in the s electron density $|\psi(0)|^2$ at the nucleus between the source and absorber. The shift is seen only if the nuclear charge radii of the excited and ground states are different. $|\psi(0)|^2$ is influenced by the electron configuration of the electrons (primarily, the 3d configuration in the case of iron) and, to a limited extent, by the chemical environment. For Fe^{57} in Fe, the only other element present is Co which, like Fe, is a 3d metal, and the isomer shift arises only from the effect of the chemical bond and hence, should be very small.[8]

1.3 Lattice Dynamics

The dynamics of the lattice in which the source or absorber nuclei are imbedded influence the Mossbauer effect in several ways. First, f is primarily determined by the lattice dynamics. Second, differences between the lattice dynamics of source and absorber determine the velocity at which the maxima of the Mossbauer absorption spectrum occur. A difference in Debye temperature , a difference in average mass between the source and absorber and a difference in temperature between the source and absorber (the Josephson Effect) all produce shifts of the Mossbauer spectrum. Third, the fact that the emitting nucleus is essentially an impurity in the lattice affects the lattice vibrations and establishes a localized mode. This localized mode gives rise to both a shift and broadening of the Mossbauer absorption spectrum. Chapter II contains a detailed analysis of these effects .

1.4 Mossbauer Experiments

The equipment necessary to perform a Mossbauer experiment consists of

a) a source of gamma radiation, b) an absorber, the velocity of which, relative to the source, is controllable and c) a detector of gamma radiation. The quantity measured is the transmission of the gamma rays through the absorber as a function of the relative velocity between the source and absorber. In the case in which both the emission and absorption spectra consist of a single line of Lorenzian shape, the transmission displays only one absorption dip as shown in figure I-2a. This transmission spectrum is called the Mossbauer spectrum. Its width is determined primarily by the half life of the nuclear transition, Γ, and, the depth by the Debye-Waller factor, f, and the cross section for gamma absorption. If, as is the case with Fe^{57}, the emission and absorption spectra consist of several Lorenzian lines, the Mossbauer spectrum will then appear as in figure I-2b. Each absorption dip in this Mossbauer spectrum arises from the overlap of at least one of the emission lines with one absorption line. The centre line, called the Mossbauer line in this thesis, arises from the overlap of all the emission lines with the corresponding absorption lines. If the source and absorber are identical, the Mossbauer line should be centered at $v = 0$.
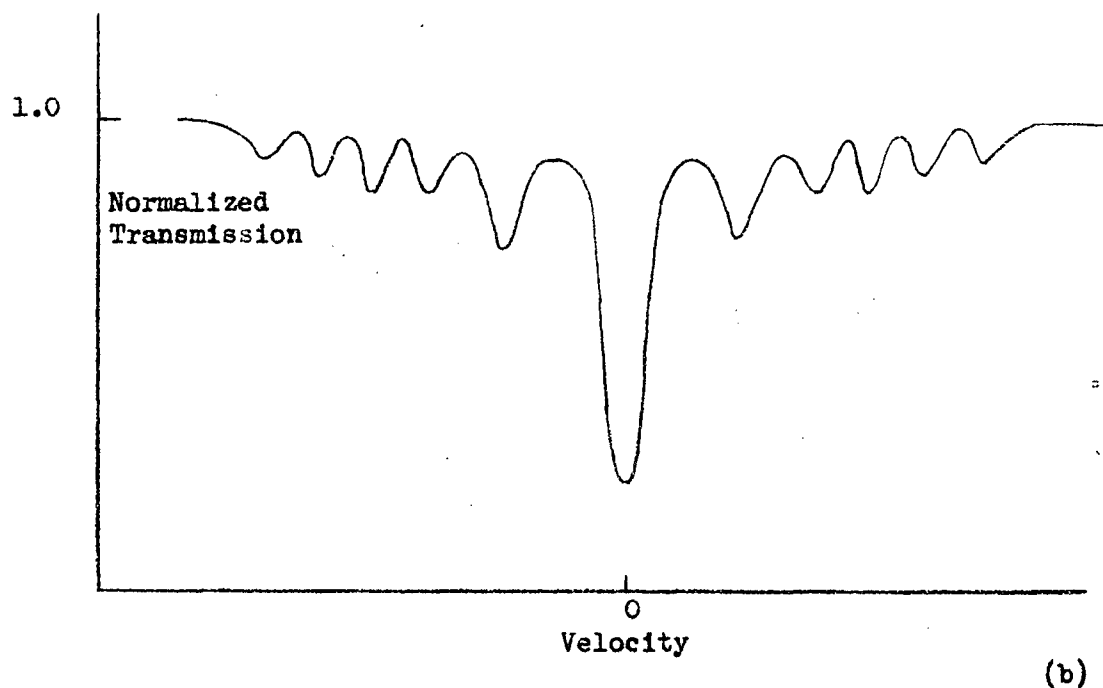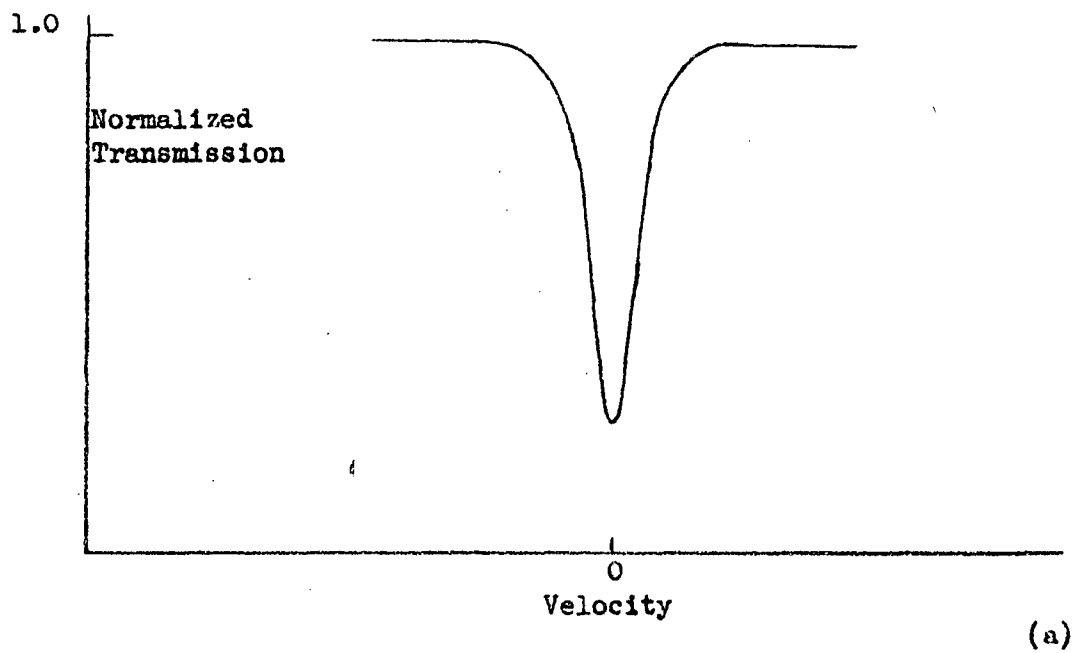
FIGURE I-2 Typical Mossbauer spectra for (a) a single line
emission and absorption spectrum, and (b) a six
line emission and absorption spectrum.

Chapter II

THEORY OF LINE WIDTH, SHIFTS and INTENSITIES

2.0   Introduction

The prime objective of the experimental work described in this thesis was to correlate the line shape, width, shift and intensity of the Mossbauer spectrum obtained with a source of Fe^{57} in iron and an iron absorber, with the relevant theory which will be discussed in this chapter with special attention being given to the Mossbauer spectrum obtained with a source of Fe^{57} embedded in natural iron and a natural iron absorber. This particular case was chosen so that various velocity shifts etcetera, could be discussed with greater ease than would have been possible had a stainless steel lattice or some other alloy lattice been used for the absorber or the source. Effects found could then be attributed to the iron or possibly to the Co^{57} embedded in the natural iron source rather than to an unknown cause. For reference purposes, the properties of Fe^{57} pertinent to the Mossbauer Effect are given in Table II-1, below.

The delay scheme of Fe^{57} is:

$I = +7/2$ K⁻ —— Co^{57}

$I = +5/2$ 0.136 mev.

$I = +3/2$ 0.0144 mev. (10^{-7}sec)

$I = +1/2$ 0.0 (Fe^{57})

    10% 90%

Line width: $\Gamma = 4.5 \times 10^{-9}$ ev.

Cross section of resonance: $\sigma_0 = 1.4 \times 10^{-18}$ cm^2

Internal conversion coefficient: $\alpha = 15$

Debye temperature: $\Theta_D = 420°K$

Mean lattice energy: $\Theta 2/3k = 0.023$ ev.

Free recoil energy: $R = 0.002$ ev.

Abundance of Fe^{57} in natural iron: $a = 2.17\%$

Table II-1

Selected Characteristics of Fe^{57}

The Mossbauer spectrum of the Fe^{57} radiation transmitted through a natural Fe absorber is calculated in the first section of this chapter. The facts that the ground and excited states of the emitting and absorbing nuclei are split into their magnetic substates by the Zeeman effect and that the souce has a finite thickness, are both considered in the calculations. The final equation (Eqn. II-18) was programmed for the I.B.M. 7090 computer and the results of the calculation appear in Chapter V. Also calculated is the ratio of the intensity of radiation from a natural iron source transmitted through a natural iron absorber (where both the emission and absorption spectra are split) to the intensity of radiation from a stainless steel source through a stainless steel absorber (where both emission and absorption are unsplit).

The remainder of the chapter is devoted to the discussion of the various mechanisms by which the Mossbauer spectrum is either shifted from its unperturbed position or increased in width. One such mechanism is the effect of a temperature difference between source and absorber. This effect is composed of two factors, the Josephson effect and the thermal expansion effect, both of which are calculated and plotted herein as a function of temperature. A difference in Debye temperature and of average mass between the source and absorber cause shifts similar to that of the Josephson effect. The possible size of such shifts for the source/absorber combination considered herein, have been calculated.

Another mechanism that causes shifts of Mossbauer spectra is a difference in chemical environment of the Fe^{57} nuclei in the source and in the absorber. This effect, the isomer shift, is discussed and an estimate of the magnitude and sign to be expected with Fe^{57} is given.

Considerable attention is then given to the magnetic field producing the hyperfine splitting of the Fe^{57} radiation. The importance of this magnetic field is twofold. First, the size of the field determines the magnitude of the splitting so that any difference in the magnetic field at the Fe^{57} nuclei in the source and absorber results in an incomplete overlapping of the emission and absorption spectra, thereby giving a broadened Mossbauer spectrum. Second, the magnetic field is temperature dependent so that the width of the transmitted spectrum will also be temperature dependent.

The electric quadrupole moment produces an effect similar to that of the magnetic field. Since Fe is approximately a cubic lattice, this effect is expected to be small but could lead to a broadened transmission spectrum.

The final mechanism considered is that of the localized modes. In the Mossbauer effect, the emitting nucleus is essentially an impurity in the source lattice thereby giving rise to a localized mode which affects the spectrum of normal modes of the source atoms. There are two consequences of the localized modes. First is the existence of a one phonon process peak in the transmitted spectrum at the localized mode frequency and second, the shifting and broadening of the recoilless peak of the transmitted spectrum. The derivation of the theory predicting the second effect concludes this chapter.

2.1 Transmission of the Six line Spectrum of Fe^{57}

The following theory arises from that given by J.G. Dash et al,[6] and S. Margulius and J.R. Ehrman[5]. However, the facts that the source has

a finite thickness and the emission and absorption spectra each consist of six lines, are considered. An exact equation giving the transmission as a function of velocity between the source and absorber is derived.

Since Fe is a ferromagnetic material, the Zeeman effect or, the coupling between the nuclear magnetic moments of each energy level and the internal magnetic field H, acting in each ferromagnetic domain removes the degeneracy of the nuclear magnetic substates producing a set of equally spaced spin sublevels of energies

$$E_{nfs} = mg\mu_n H \qquad -I \le m \le I \qquad \qquad II-1$$

where m is the magnetic quantum number, g is the nuclear gyromagnetic ratio and μ_n is the nuclear magneton. By letting m_j refer to the magnetic quantum number of the 14.4 kev state of Fe^{57} and m_k to the ground state and by employing the selection rule $\Delta m = 0, \pm 1$, (since the 14.4 kev gamma ray of Fe^{57} is known to arise from a dominantly magnetic dipole transition) the transition between the 14.4 kev sublevels to the ground state levels results in a gamma spectrum of six components as shown in figure II-1.
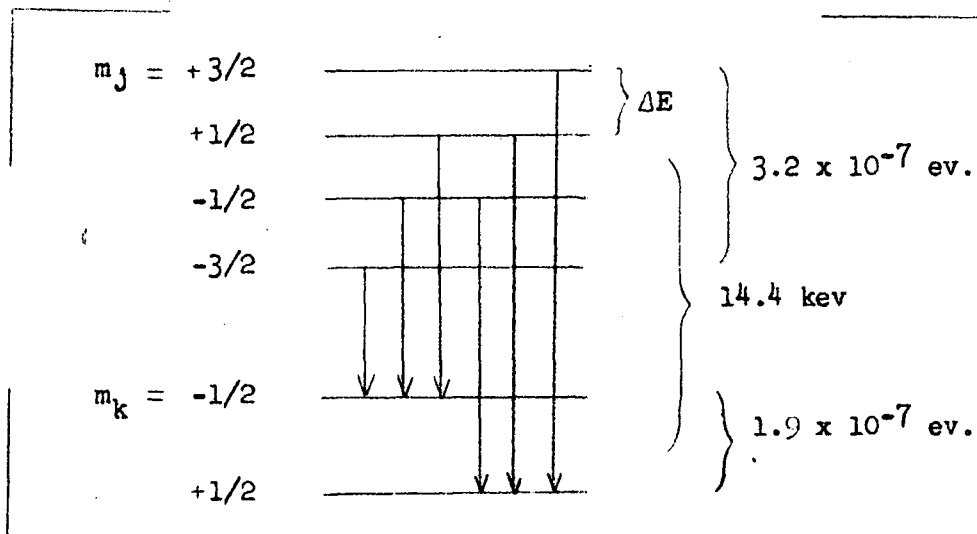
Fig. II-1

The relative intensities of these six gamma rays are given by the rules governing magnetic dipole radiation[9], i.e.,

$$
\begin{aligned}
\text{For } I \to I\text{-}1 \qquad & m_j \to m_j + 1 & I_n &= 1/2C(I\text{-}m)(I\text{-}m\text{-}1) \\
& m_j \to m_j & I_n &= C(I^2\text{-}m^2) \qquad\qquad \text{II-2} \\
& m_j \to m_j \;\text{-}1 & I_n &= 1/2C(I\;m)(I\;m\text{-}1)
\end{aligned}
$$

where I_n is the intensity of the gamma ray and C is a constant. The normalized probability that the transition $j \to k$ will occur is given by the transmission probabilities, W_{jk}. Hence, for the transition given in figure II-1, the relative intensities of the six lines are 3C, 2C, C, C, 2C, 3C for lines one to six and the normalized relative transition probabilities W_{jk} are: 1/4, 1/6, 1/12, 1/12, 1/6 and 1/4. A dilute Fe^{57} absorber (Boyle, p.459) has a similar pattern of absorption line probabilities. For Fe^{57} in a natural iron lattice, the splitting of the 14.4 kev state and the ground state is greater than 4.5×10^{-9} ev., the line width of the 14.4 kev radiation so that the full six line emission and absorption spectra must always be considered.

The Mossbauer velocity spectrum consists, for indentical source and absorber, of a central strong line with a complicated set of satellite lines symetrical in velocity about the central line (See Fig. I-2b). In the following, the phrase "Mossbauer line" will be used to denote the centre line of the Mossbauer velocity spectrum. This line is the easiest to study experimentally and allows the greatest sensitivity in experiments studying line profiles. However, the satellite lines are subject to the same shift and broadening mechanisms as the Mossbauer line. When any distinction is to be made between the source and absorber in the following, primed subscripts will be used to denote the absorber.

The intensity of any component of this spectrum is calculated as follows:

The transition $m_j \rightarrow m_k$ is proportional to:
a) the transition probabilities W_{jk} and
b) the population p_j of the sublevel at which the transition originates.

Above the temperature of liquid nitrogen (88°K) the population of the sublevels can be assumed to be equal and therefore, are not considered in the following. Therefore, the hyperfine resonant absorption cross section is composed of lines of cross section $W_{k'j'} \sigma_{k'j'}$ where:

$$\sigma_{k'j'} = \frac{\sigma_o \Gamma^2/4}{(E - E_{k'j'})^2 + \Gamma^2/4}$$

II-3

and σ_o, the total resonant absorption cross section is

$$2\pi \lambda^2 \frac{2I_1 + 1}{2I_o + 1} \left(\frac{1}{1+\alpha} \right) = 1.48 \times 10^{-18} \text{ cm}^2$$

II-4

and $E_{k'j'}$ is the energy at which the absorption line $k \rightarrow j$, is centered. Then, considering both the resonance emission spectrum and absorption spectrum to be composed of six lines of Lorenzian shape, each line having a width Γ, the intensity transmitted at a relative source/absorber speed v, is for the $j \rightarrow k$ transmission:

$$I_t(j,k) = \frac{I_e}{\pi} W_{jk} \int_o^\infty \frac{\Gamma/2\pi}{(E - E_{jk} + E_{jk}v)^2 + \Gamma^2/4} \exp\left[-naf't\sum_{j'k'} W_{k'j'} \sigma_{k'j'} \delta(k-k', j-j')\right] dE$$

II-5

The summation is: j 1,...6
k 1,...6
where: f' = probability of absorption without recoil.
n = number of atoms/cm^3
a = fractional abundance of Fe^{57}
I_e = total emitted intensity
t = absorption thickness

When $E_{jk}(1-v/c) = E_{k'j'}$, i.e., at the centre of one of the resonant absorption dips,

$$I_t(J,k) = \frac{I_e W_{jk}}{\pi} \int_{-\infty}^{\infty} \frac{dy}{1+y^2} \exp\left[\frac{-W_{k'j'}x}{1 \quad y^2}\right] \qquad \text{II-6}$$

(where $y = 2(E-E_{k'j'})/\Gamma$, $x = n a f' \sigma_0 t'$)

Which has the solution:

$$I_t(J,k) = I_e W_{jk} J_o(iW_{k'j'}\frac{x}{2})\exp(-W_{k'j'} \cdot x/2) \qquad \text{II-7}$$

where $J_o(iW_{k'j'}\frac{x}{2})$ is the Bessel Function and may be found tabulated in conventional form in Tables of Functions, by Eugene Jahnke and Fritz Emele.[10] Hence, if both the absorber and the source have split ground and 14.4 kev levels, the total transmitted intensity (considering resonant absorption only) is:

$$I_t(\text{Total},v) = I_e \sum_{jkk'j'} J_o(iW_{k'j'}\frac{x}{2})\exp(-W_{k'j'}\frac{x}{2})\delta(k-k', J-J') \qquad \text{II-8}$$

In particular, the intensity of the Mossbauer line, henceforth called the Mossbauer intensity ($v = 0$), can be calculated from this equation. However, if the source and absorber have unsplit lines as in the case of nonmagnetic stainless steel source and absorber, the total intensity becomes:

$$I_t(\text{Total},v) = I_e J_o(ix/2) \exp(-x/2) \qquad \text{II-8'}$$

The above expressions for the intensity considered only the resonant part of the gamma ray spectrum. When the electronic absorption is also considered, the transmitted intensity becomes:

$$T(\text{Total},v) = (1-f)I_e \exp(-\mu't') + fI_t(\text{Total},v) \exp(-\mu't') \qquad \text{II-9}$$

where μ' is the electronic absorption coefficient of Fe for 14.4 kev gamma rays. In order to illustrate with a simple example, the results of the calculations, it is useful to determine the relative transmitted intensities for the two cases of a split and an unsplit line, assuming for the moment that a thin source and absorber are used. For this simple example $J_o \to 1$, and $\exp(x) \to 1 + x$, so that equation II-9 becomes:

$$T(\text{Total},v) = (1-f)I_e\,{}^{-\mu't'} + e^{-\mu't'}\,fI_e\sum_{jk,k'j'} W_{jk}(1-W_{k'j'}\frac{x}{2})$$

$$x\ \delta(k-k', j-j') \qquad \text{II-10}$$

for the split line and:

$$T'(\text{Total},v) = (1-f)I_e\,{}^{-\mu't'}\ e^{-\mu't'}\,fI_e(1-\frac{x}{2}) \qquad \text{II-11}$$

for the unsplit line. The Mossbauer intensity as defined above is:

$$\zeta = \frac{T(\text{Total},v=\infty)\ -T(\text{Total},v=0)}{T(\text{Total},v=\infty)} \qquad \text{II-12}$$

This, for the split line case becomes:

$$\zeta = \frac{fx}{2}\sum_{jk,} W_{jk}^2 = \frac{fx}{2}\frac{28}{144} \qquad \text{II-13}$$

whereas for the unsplit line case:

$$\zeta = \frac{fx}{2}\sum_{jk,k'j'} W_{jk}W_{k'j'} = \frac{fx}{2} \qquad \text{II-14}$$

Therefore, the ratio of the central line (v=0) for the split case to the unsplit case in the thin source and absorber approximation for Fe^{57} is 7/36. In practice, this ratio is reduced by a) saturation effects in non-thin sources and absorbers and b) non-resonant backgrounds.

In the discussion above of the transmitted intensities, it was implicitly assumed that the source thickness was negligible whereas in practice, it is not. In fact, the width of the Mossbauer line depends both upon the source and absorber thickness. Assuming that both emission and absorption lines have a Lorenzian shape of width Γ, that a fraction f, of all decays occur without energy loss and that the emission and absorption spectra are split into six lines, equation II-10, representing the transmission through a resonant absorber for the Mossbauer line becomes:

$$T(Total,v) = e^{-\mu' t'}\left[(1-f)\int_0^\infty \rho(x)e^{-\mu x}dx + \sum_{jk} W_{jk} \frac{f\Gamma}{\pi}\int_{-\infty}^\infty dE \exp\left[-\sum_{kj} W'_{kj} \frac{\overline{\tau}\,\Gamma^2/4}{(E-E_0)^2 + \Gamma^2/4}\right]x$$

$$\int_0^\infty \frac{\rho(x)\,dx}{(E-E_0+\xi E_0)^2 + \Gamma^2/4} \exp\left[-\left(\sum_{kj} W_{kj} \frac{\overline{\tau}\,\Gamma^2/4}{(E-E_0+\xi E_0)^2+\Gamma^2/4} + \mu x\right)\right]\right] \quad \text{II-15}$$

where $\tau = fan\sigma_0 t$ and $\rho(x)dx$ is the number of Fe^{57m} atoms lying between x and $x+dx$ from the surface of the source.

A source prepared by electroplating Co^{57} onto Fe and then diffusing the Co^{57} into the lattice, has a Gaussian distribution of radioactive atoms[5] so that:

$$\rho(x) = \frac{2N}{\sqrt{\pi}} \exp(-x^2/t^2) \qquad x \leq 0 \qquad \text{II-16}$$

where t is the rms diffusion depth of the radioactive atoms and Nt represents the total number of radioactive atoms. Substitution of this function into equation II-15 yields:

$$T(Total,v) = e^{-\mu' t'}\left[\left(1-f\right)e^{(\mu t/2)^2}\left[1 - \Phi(\mu t/2)\right] + \sum_{jk} W_{jk} \frac{f\Gamma}{\pi}\int_{-\infty}^\infty \frac{dE}{(E+S)^2 + \Gamma^2/4}\, x\right.$$

$$exp\left(-\sum_{k'j'} W_{k'j'} \frac{\Gamma'\Gamma^2/4}{E^2+\Gamma^2/4}\right) \times \left[1-\Phi\left(\sum_{k'j'} W_{k'j'} \frac{\Gamma\Gamma^2/4}{2(E+S)^2+\Gamma^2/4} + \frac{\mu t}{2}\right)\right] \times$$

$$exp\left[\sum_{k'j'} W_{k'j'} \frac{\Gamma\Gamma^2/4}{2(E+S)^2+\Gamma^2/4} + \frac{\mu t}{2}\right]^2\right] \qquad\qquad\text{II-17}$$

Thus, for a given source and absorber thickness the transmission can be calculated as a function of the relative velocity between the source and the absorber. The ratio:

$$R(v) = \frac{T(\text{Total},v)}{T(\text{Total}, \ )}$$

$$= 1-f + \sum W_{jk}\frac{\Gamma'\Gamma}{\pi} \int_{-\infty}^{\infty} \frac{dE}{(E+S)^2+\Gamma^2/4} \ exp\left(\frac{-W'_{jk}\Gamma'^2/4}{E^2+\Gamma^2/4}\right) \left[1-\Phi\left(\frac{W_{jk}\Gamma\Gamma^2/4}{2(E+S)^2+\Gamma^2/4} + \frac{\mu t}{2}\right)\right]$$

$$\times \ exp\left(\frac{W_{jk}\Gamma\Gamma^2/4}{2(E+S)^2+\Gamma^2/4} + \frac{\mu t}{2}\right)^2 \div exp\left(\frac{\mu t}{2}\right)^2\left[1-\Phi\left(\frac{t}{2}\right)\right] \qquad\text{II-18}$$

is plotted as a function of v to produce the Mossbauer velocity spectrum (see Sec. 3.7). The calculated line widths and Mossbauer intensities for various absorber thicknesses are given in Chapter V.

2.2 The Josephson and Related Effects

When a nucleus emits a gamma ray, it loses mass $\delta m_1 = E_0/c^2$. The energy of the lattice vibrations is thereby affected and so, by the conservation of energy, is the gamma ray energy. This effect was first discussed by Josephson, who assumed that the crystal was a conservative system in which the potential energy of the atoms in the crystal was a function of the position only. It follows therefore, that the Hamiltonian for the system has the form:

$$H = \sum_i P_i^2/2m_i + V(r_1, r_2 \ldots) \qquad\qquad\text{II-19}$$

and that $H = \mathcal{E}$, the total lattice energy. Upon emission of the gamma ray, the change in $\mathcal{E}$ is therefore given by:

$$
\begin{aligned}
\delta\mathcal{E} &= \langle \Delta H \rangle \\
&= \delta m_i / m_i \; \langle P_i^2 / 2m_i \rangle \\
&= E_o / m_i c^2 \langle Y_i \rangle
\end{aligned}
\qquad \text{II-20}
$$

The average kinentic energy of the ith nucleus is $\langle Y_i \rangle$ and it is assumed that the ith nucleus emits the gamma ray. Therefore, since the lattice energy is increased by $\delta\mathcal{E}$ when the gamma ray is emitted, the gamma ray energy must be correspondingly reduced by $\delta\mathcal{E}$ in order to conserve energy. This results in a relative shift for the gamma ray of:

$$
\delta\mathcal{E} / E_o = -\langle Y_i \rangle / m_i c^2 \qquad \text{II-21}
$$

In order to estimate $\langle Y_i \rangle$, Josephson made the following assumptions about the crystal:

a) The atoms all have the same mass and the kinetic energy is equally distributed among them.

b) The kinetic energy is half the total lattice energy (i.e., he assumed that the forces coupling the atoms were harmonic).

These assumptions lead to the conclusion that:

$$
\langle Y_i \rangle / m_i = 1/2U \qquad \text{II-22}
$$

where U is the lattice vibrational energy per unit mass. Hence, the relative shift of the gamma ray energy is:

$$
\delta\mathcal{E} / E_o = -1/2U \; / \; c^2 \qquad \text{II-23}
$$

The Debye temperature of iron is approximately $420^\circ K$ and therefore, at room temperature, (θ), U can be approximated by its classical value $\frac{3k\theta}{m_i}$, giving a relative shift of:

$$\delta\mathcal{E}/E_0 = -3k\theta/2m_i c^2$$
$$= -2.53 \times 10^{-15} \text{ per } {}^\circ K$$
$$= -7.6 \times 10^{-13} \text{ for } 300^\circ K$$

<div align="right">II-24</div>

When the gamma ray is absorbed, it will gain energy, resulting in another relative energy shift of

$$\frac{\delta\mathcal{E}}{E_0} = 1/2 \frac{U'}{c^2}$$

<div align="right">II-23'</div>

From the Debye model of the crystal, the total vibrational energy per unit mass of the lattice is:[12]

$$U = \frac{1}{M}\int_0^{\vartheta_D} \frac{Z(\vartheta)h\vartheta d\vartheta}{\exp\left(\frac{h\vartheta}{k\theta}\right) -1} + 1/2\int_0^{\vartheta_D} Z(\vartheta)h\vartheta d\vartheta$$
$$= \frac{9Nk}{M}\left[\left(\frac{\theta}{\Theta_D}\right)^3 \theta\int_0^{\Theta_D/\theta} \frac{x^3 dx}{\exp(x) -1} + \frac{\Theta_D}{8}\right]$$

<div align="right">II-25</div>

wherein the second term is the zero point energy of the lattice. It can be seen that U and U' are functions of the crystal temperature, the Debye temperature and the mass of the atoms comprising the lattice. The net shift of the gamma ray energy considering both the emission and absorption processes, i.e., the shift of the position of the Mossbauer line, is given by the expression:

$$\Delta(\delta\mathcal{E}/E_0) = \left(\frac{\delta\mathcal{E}}{E_0}\right) + \left(\frac{\delta\mathcal{E}}{E_0}\right)'$$
$$= 1/2 \frac{9Nk}{Mc^2}\left[\left(\frac{\theta}{\Theta_D}\right)^3\theta\int_0^{\Theta_D/\theta}\frac{x^3 dx}{\exp(x)-1} + \frac{\Theta_D}{8}\right] - \frac{9N'k}{2M'c^2}\left[\left(\frac{\theta'}{\Theta'_D}\right)^3 \theta\int_0^{\Theta_D/\theta}\frac{x^3 dx}{\exp(x)-1} + \frac{\Theta'_D}{8}\right]$$

<div align="right">II-26</div>

Thus, a shift can be caused by any or a combination of these three factors:

a) a temperature difference $(\Delta\theta)$ between source and absorber

b) a Debye temperature difference $(\Delta\theta_D)$ between source and absorber

c) a difference in the average mass $(\Delta\frac{M}{N})$ of the source and absorber

By considering $\Delta\theta_D = 0$, but $\Delta\theta \neq 0$, (which are the conditions associated with the Josephson Effect), it seems that:

$$\Delta(\frac{\mathcal{E}}{E_O}) = \frac{1}{2c^2}\Big[\int_0^\theta C_L \, d\theta - \int_0^\theta C_L \, d\theta\Big] \qquad \text{II-27}$$

where

$$\int_0^\theta C_L \, d\theta = \frac{9Nk}{M} \Big(\frac{\theta}{\theta_D}\Big)^3 \theta \int_0^{\theta_D} \frac{x^3 dx}{\exp(x)-1} \qquad \text{II-28}$$

and C_L is the lattice specific heat of the crystal.[12]

Equation II-27 is plotted as a function of the temperature of the source and Debye temperature of the source and absorber, in Fig. II-2. The temperature of the absorber remained constant at $297^\circ K$ and the Debye temperatures used were $355^\circ K$ and $420^\circ K$. Hence, it can be seen that the Josephson shift is not very sensitive to the precise value of θ_D.

In the above calculation of the temperature dependence of the gamma ray energy, it was implicitly assumed that the volume of the crystal remained constant. Empirically however, the thermal expansion of the crystal must be taken into account when examining the temperature dependent line shift. Thus the temperature coefficient of the gamma ray energy at constant pressure has two contributions:[13]

$$\frac{1}{E_O}(\frac{\partial\mathcal{E}}{\partial\theta})_P = \frac{1}{E_O}(\frac{\partial\mathcal{E}}{\partial\theta})_V + \frac{1}{E_O}(\frac{\partial\mathcal{E}}{\partial P})_\theta (\frac{\partial P}{\partial\ln V})_\theta (\frac{\partial\ln V}{\partial\theta})_P \qquad \text{II-29}$$
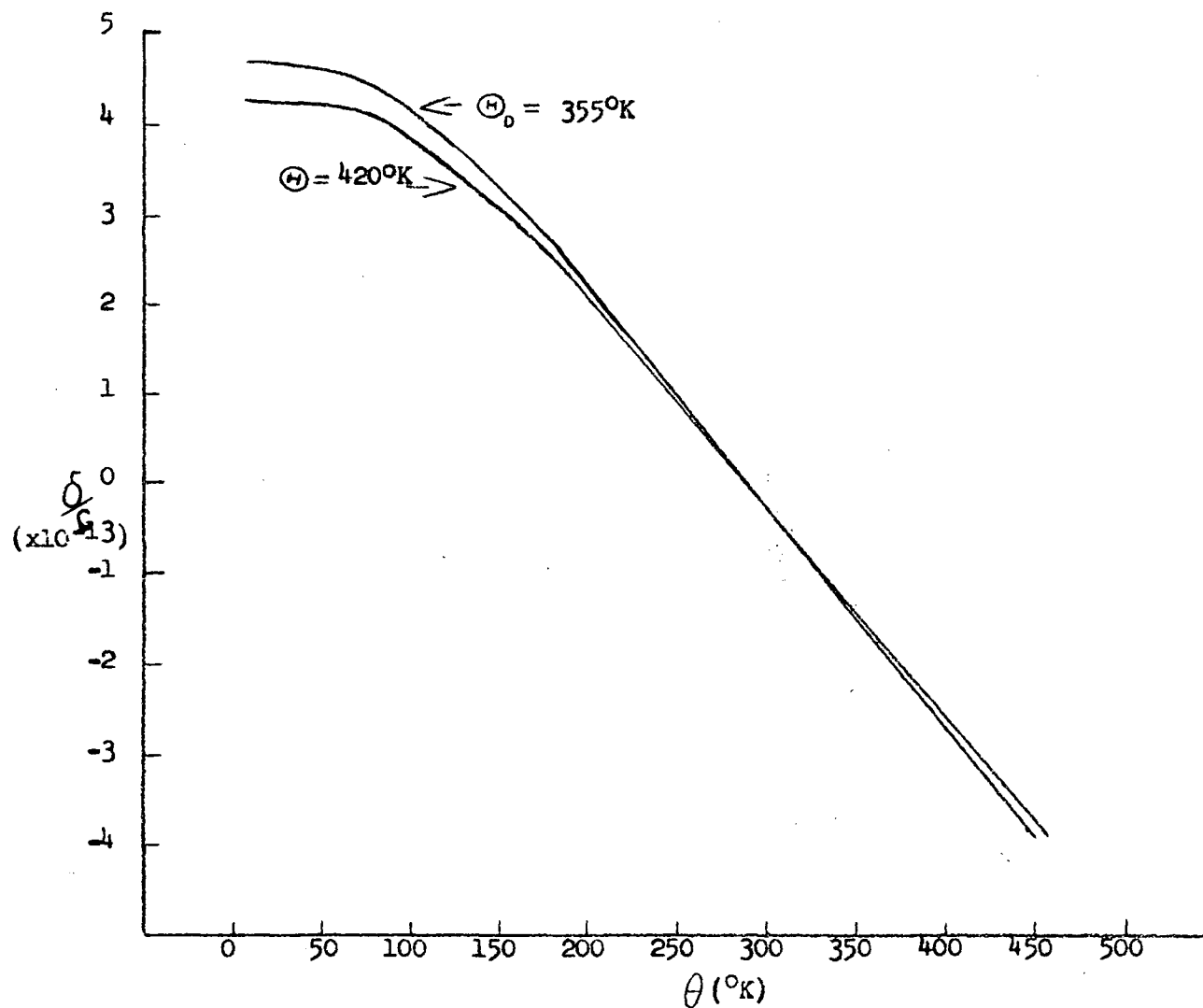
FIGURE II-2   The theoretical Josephson effect as a function of the absolute
temperature of the source. The two curves shown are those ob-
tained for an absorber temperature of 293°K, and Debye temper-
atures of 355°K and 420°K.

where the first term is the Josephson term and the second if the effect of the thermal expansion which, at $295^{\circ}K$, is

$$\frac{1}{E_o} \left(\frac{\partial \xi}{\partial P}\right)_\theta \left(\frac{\partial P}{\partial \ln V}\right)_\theta \left(\frac{\partial \ln V}{\partial \theta}\right)_P = +0.15 \times 10^{-15} \text{ per } {}^{\circ}K \qquad \text{II-30}$$

which is opposite in sign to the Josephson shift and approximately ten times smaller. This term is temperature dependent because of the temperature dependence of the isothermal instantaneous compressibility $K = \frac{-1}{V} \left(\partial V / \partial P\right)_\theta$. The second term is plotted as a function of θ in figure II-3. The total shift caused by a difference in temperatures between source and absorber is therefore the difference between these two temperature dependent terms.

Consider now the more complicated case in which $\Delta \theta = 0$, but in which $\Delta \Theta_D \neq 0$. Under these circumstances, equation II-26 can be written as follows:

$$\Delta\left(\frac{\delta \xi}{E_o}\right) = \frac{9N}{2Mc^2} K\theta^4 \left[\frac{1}{\Theta_D^3} \int_0^{\Theta_D/\theta} \frac{x^3 dx}{e^x - 1} - \frac{1}{(\Theta'_D)^3} \int_0^{\Theta'_D/\theta} \frac{x^3 dx}{e^x - 1}\right] + \frac{9Nk}{16Mc^2} \left[\Theta_D - \Theta'_D\right]$$

$$\text{II-31}$$

which, when $\theta = 0$, reduces to

$$\Delta\left(\frac{\delta \xi}{E_o}\right) = \frac{9Nk}{16Mc^2} \Delta(\Theta_D) \qquad \text{II-32}$$

In order to the estimate the maximum value of such a shift for Fe^{57} in Fe, the assumption is made that the source is essentially a Co^{57} lattice with a Debye temperature of $\Theta_D = 385^{\circ}K$ and that the absorber is an iron lattice with a Debye temperature of $\Theta_D = 420^{\circ}K$. Using these values, equation II-32 gives

$$\Delta\left(\frac{\delta \xi}{E_o}\right) = -3.2 \times 10^{-14} \qquad \text{II-33}$$

$$\frac{1}{\nu}\left(\frac{\partial \nu}{\partial P}\right)_T \left(\frac{\partial P}{\partial \ln V}\right)_T \left(\frac{\partial \ln V}{\partial T}\right)_P$$

$(x10^{-15})$
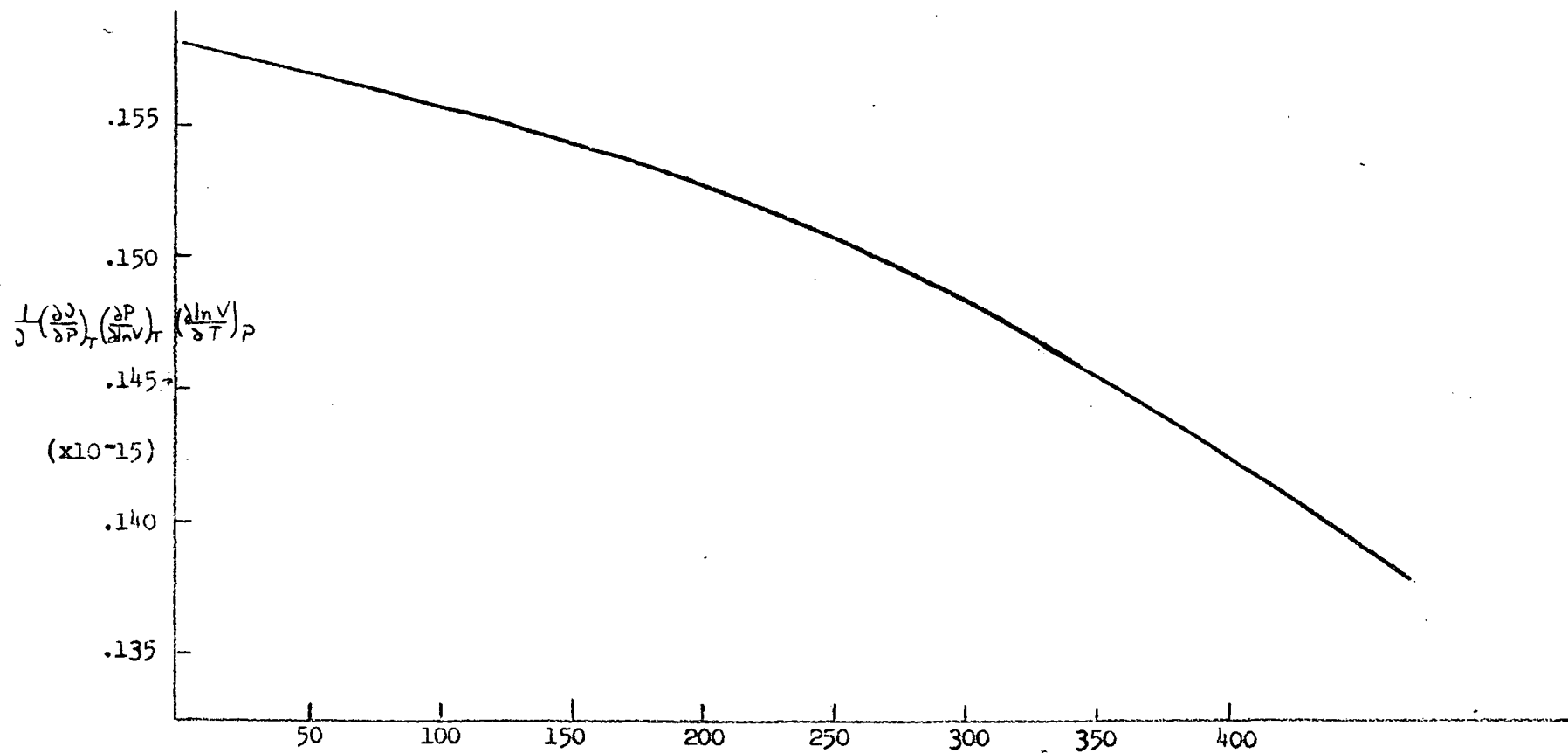
FIGURE II-3 The temperature dependent line shift arising from the thermal expansion of the crystal plotted as a function of the absolute temperature of the crystal.

which corresponds to a relative velocity between source and absorber
of -9.6 x 10^{-4} cm/sec. The negative velocity implies that the distance
between the source and absorber increases. When $\theta \neq 0$, the first term in
equation II-31 must also be considered. Under the same assumptions as
above, this term results in a shift of:

$$\Delta(\frac{\delta E}{E_0}) = 1.9 \times 10^{-14} \qquad\qquad \text{II-34}$$

or a velocity of 5.6 x 10^{-4} cm/sec. Hence, these two effects tend to
annul each other and give a maximum net shift of the Mossbauer line of:

$$\Delta(\frac{\delta E}{E}) = -1.3 \times 10^{-14} \qquad\qquad \text{II-35}$$

However, since the source contains only small amounts of Co^{57}, it is
reasonable to expect that the Debye temperature of the source will not be
as low as $385°K$ but nearer to, if not exactly equal to the Debye temper-
ature of the absorber, such that the actual shift caused by a difference
in Debye temperature of source and absorber will be expected to be much
less than 1.3 x 10^{-14}. In the above discussion, the assumption was that
the Debye temperature of the lattices was independent of the temperature
of the lattice. This assumption is usually valid for crystals above ap-
proximately $60°K^{14}$ (the temperature region will be considered later).

Finally, consider the case in which the average mass of the
atom of the source and absorber crystal differ, but in which the temper-
ature and the Debye temperature of each is the same. Since the source con-
tains Co^{57} atoms, the average mass of the source will be larger than the
average mass of the absorber by an amount:

$$\Delta M = M-M' \qquad\qquad \text{II-36}$$

and hence:

$$\Delta(\frac{\delta\epsilon}{E_0}) = \frac{\Delta M}{2M'c^2} \int_0^\Theta C_L d\theta - \frac{\Delta M}{(M')^2 c^2} \frac{9K\Theta_D}{16} \qquad \text{II-37}$$

Under the assumption that the average mass of the source atoms is 57 and that the average mass of the absorber atoms is 55.85, a shift of:

$$\Delta(\frac{\delta\epsilon}{E_0}) = -1.25 \times 10^{-14} \qquad \text{II-38}$$

would be obtained. However, in the preparation of the source, the ratio of Co^{57} to Fe was kept to less than .01 so that the maximum shift possible through this mechanism is:

$$\Delta(\frac{\delta\epsilon}{E_0}) = -1.25 \times 10^{-16} \qquad \text{II-39}$$

which can be neglected (See also, localized modes due to mass difference between radiating nucleus and host lattice).

2.3 Isomeric Shift

The decay of Fe^{57} from the isomeric state to the ground state is accompanied by an electrostatic interaction between the nuclear charge and the electronic charge within the nuclear volume. The interaction causes a change in the nuclear energy levels (the isomeric shift) but is observed only if a) the nuclear charge radii of the two states are different, b) the electronic wave function overlaps appreciably with the nuclear wave functions and c) these functions are sensitive to external (chemical) changes. In order to see the nuclear isomeric shift, the same nuclear transition in the two atomic systems which have different electronic wave functions at the nucleus, are compared.

Only the difference in the isomer shifts between the two systems will be thus measured.

Using a simple model, Frauenfelder (Frauenfelder, pp.53-57), derived the following expression for the isomeric shift:

$$\delta = \frac{2}{3}\pi Ze^2 \left[\langle R_e \rangle^2 - \langle R_g \rangle^2 \right]\left[|\psi'(0)|^2 - |\psi(0)|^2 \right] \qquad \text{II-40}$$

in which Ze is the nuclear charge, $\langle R \rangle^2$ is the root mean square charge radius and $|\psi(0)|^2$ is the total electron density at the nucleus. It is expected that the major contribution arises from the s electrons as only these have a finite probability density at the nucleus. In deriving this equation, it was assumed that the wave function of the electrons involved in the isomer shift remained constant over the nuclear volume and that:

$$\langle R \rangle^2 = 4\pi \int \rho(r)\, r^2\, dr \qquad \text{II-41}$$

where $\rho(r)$ is the nuclear charge density. Equation II-40 therefore, includes the three requirements listed above. Although the equation is based upon a simple model, it gives the correct magnitude for the isomer shift.

The measured isomeric shift with Fe^{57} therefore, measures the combination of the difference between the charge radii of the excited and ground states and, the difference between the total electron density at the nucleus of the source and absorber nuclei. Measured values[15] indicate that for Fe^{57}, the charge radius of the ground state is larger than that of the chemical environment of the atoms and therefore, depends upon the lattice in which the embedding and absorbing nuclei are located. The presence of an isomer shift in the source/absorber combination considered in this work would imply a difference between the chemical structures of

the source and absorber. The Fe^{57} atoms in the source do not lose electrons as a result of the recoil due to the preceding 121 kev transition as happens in the case of ionic compounds, so that such a shift, if observed, is probably due to the presence of the Co^{57} in the source lattice. Measurements made by L. R. Walker et al[15] indicate that $|\Psi(0)|^2$ for Co is greater than that for Fe. Hence, knowing that $\langle Re \rangle^2 - \langle Rg \rangle^2$ is negative, any expected isomer shift should have positive sign and magnitude less than .003 cm/sec, according to the results of L. R. Walker et al.[15]

In the absence of phase changes, $|\Psi(0)|^2$ should not change appreciably with temperature, and hence, it can be assumed that the isomeric shift is not temperature dependent. The above analysis assumes that the isomeric shift in the given source/absorber combination is uniform for all emission and absorption events. If this assumption is invalid and instead, the isomeric shift is not uniform, a broadening of the Mossbauer line would result rather than a line shift. Such a line broadening should also be temperature independent.

2.4 Hyperfine Splitting

The effect of the internal magnetic field on the energy levels of the Fe^{57} nucleus was mentioned briefly at the beginning of this chapter. At this point, it is appropriate to begin a detailed discussion of this magnetic field and its effects.

The internal or hyperfine magnetic field of a system of atoms is intimately related to the electronic structure of the magnetic material. Since the actual contributions of the electrons to this field is not well known, the field at the Fe nucleus cannot be accurately predicted. It is

expected however, that the field will depend upon the following quantities as well as the local magnetic field at the nucleus:

a) the field arising from the polarization of the core s electrons (-300kg)

b) the field from the 4s conduction electrons which are polarized by the 3d electrons in the same way as the core is polarized (80kg to 100kg)

c) the field from the 4s conduction electrons which are admixed into the overlapping 3d band (90kg)

d) the orbital contribution from any unquenched angular momentum of the 3d electrons (50kg)

The values given for each cause is that estimated for Fe (MossII, p. 120). The measured internal magnetic field at $\theta = 300^{\circ}K$ for Fe is -333koe[7] which indicates that a fifth mechanism (in addition to those listed above) must contribute a negative field to the net magnetic field. A reasonable hypothesis (Moss II, p.122) for this mechanism states that in addition to the positive contribution which comes from a mixing of the 4s and 3d bands there is a negative term which comes from a covalent mixing of the d-wave functions on one atom with s-like conduction band wave functions from another atom. The negative hyperfine field so produced would cancel the field produced by quantity (c) above. The total hyperfine field therefore is the sum of several quantities. It must be kept in mind however, that each quantity itself is a sum of the magnetic fields of the electrons of one atom, although each electron separately contributes a magnetic field many orders of magnitude larger than the observed field but with the sign depending upon the electron spin. Hence, each quantity contributing to the magnetic field is the sum of large contributions of opposite signs yielding a small result..

A ferromagnetic subject such as Fe, of macroscopic dimensions, contains a number of domains which are spontaneously magnetized. The net magnetization of the sample is the vector sum of the magnetic moments of these domains. In the presence of a small external field such as that of the earth, the atomic dipole moments of the Fe atoms in the domain are essentially aligned to produce saturation of the spontaneous magnetization in that region so that in each domain the effective magnetic field acting upon the nucleus has a single direction in space. Thus, the effective internal field at the nucleus can be represented by:

$$\underset{\sim}{H}_{eff} = H_{no}\underset{\sim}{M} + \underset{\sim}{H}_{ext} \qquad\qquad \text{II-42}$$

in which $\underset{\sim}{M}$ is a unit vector along the direction of the magnetization in the ferromagnetic domain and H_{no} is the magnitude of the effective field in the absence of the external field, $\underset{\sim}{H}_{ext}$. The latter quantity includes the demagnetization field which is negligible for the sample used. Since Fe has $\underset{\sim}{H}_{ext}/\underset{\sim}{H}_{eff} << 1$, it is assumed that $\underset{\sim}{H}_{eff}$ is not appreciably influenced by $\underset{\sim}{H}_{ext}$. The internal magnetic field at the nucleus however, is strongly correlated with the spontaneous magnetization of the domain. In fact, it has been found that the two follow essentially the same temperature dependence as that predicted by the Weiss law. This temperature dependence is shown in Figure II-4.

The effect of the internal field was seen to remove the degeneracy of the nuclear spin orientation to produce a set of equally spaced spin sub-levels of energies $\Delta E = mg\mu_n H$. Therefore, the transition energy of the transition $-3/2 \to -1/2$ denoted by L_1 will be:

$$L_1 = E_0 + (m_e g_e - m_g g_g)\mu_n H$$
$$= 14.4 \text{ kev} + (.2433)\mu_n H \qquad\qquad \text{II-43}$$
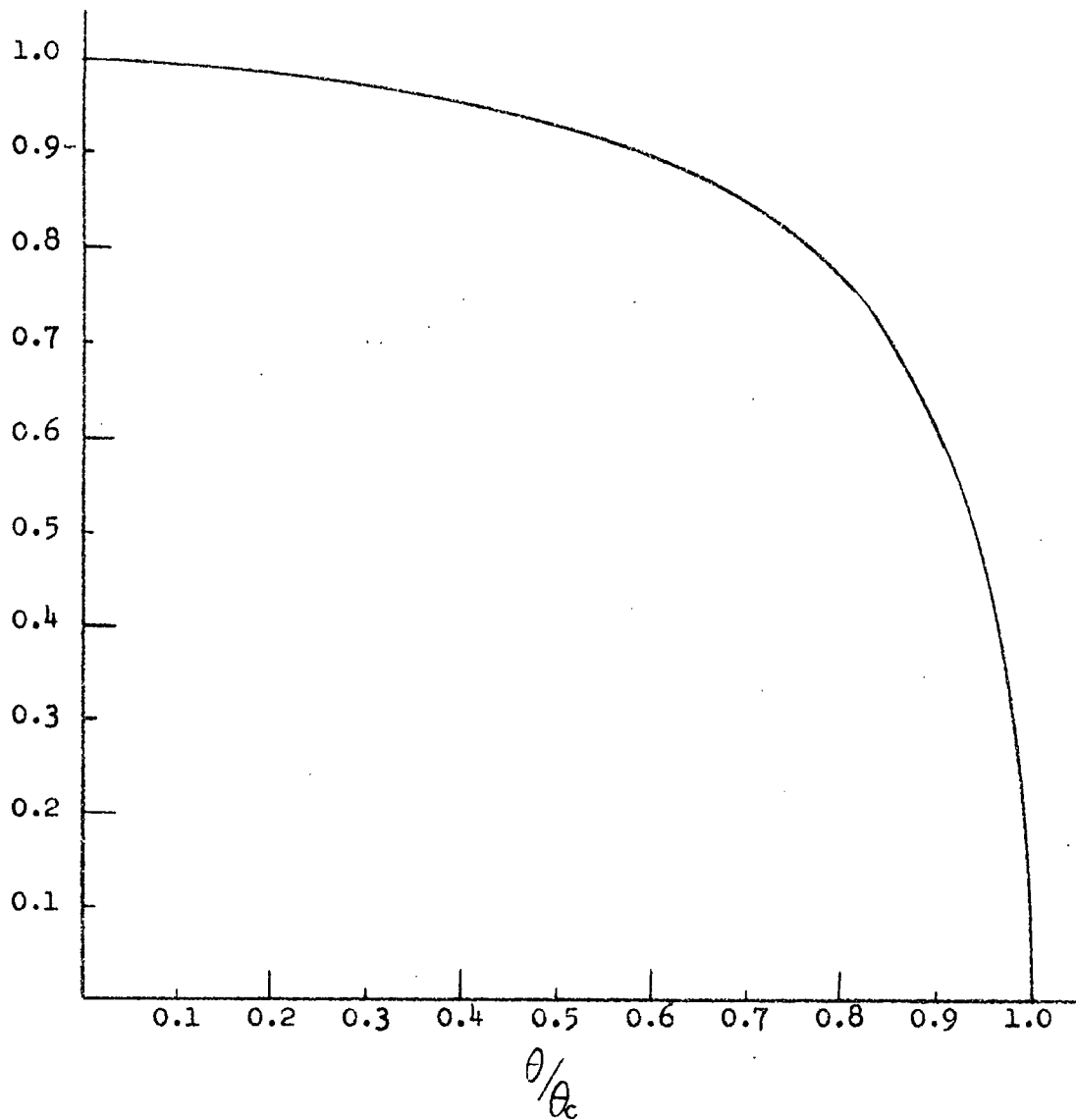
FIGURE II-4 The temperature dependence of the internal magnetic
field of a ferromagnetic material as given by the
Weiss law.

where the subscripts refer to the excited and ground states of the nucleus. The energies for the six transitions are given in Table II-2, below. From this table it is evident that the energy or position of the emission or absorption lines depends upon the internal magnetic field at the nucleus.

	m_j	m_k	Transition Energy
L_1	$-\frac{3}{2} \longrightarrow$	$-\frac{1}{2}$	$E_o + .2433\mu_n H$
L_2	$-\frac{1}{2} \longrightarrow$	$-\frac{1}{2}$	$E_o + .1413\mu_n H$
L_3	$\frac{1}{2} \longrightarrow$	$-\frac{1}{2}$	$E_o + .0393\mu_n H$
L_4	$-\frac{1}{2} \longrightarrow$	$\frac{1}{2}$	$E_o - .0393\mu_n H$
L_5	$\frac{1}{2} \longrightarrow$	$\frac{1}{2}$	$E_o - .1413\mu_n H$
L_6	$\frac{3}{2} \longrightarrow$	$\frac{1}{2}$	$E_o - .2433\mu_n H$

Table II - 2

The transition energies of the six spectral lines of Fe^{57} in terms of the internal magnetic field at the nucleus.

However, since the positions of the lines are symmetric with respect to E_o, The position of the Mossbauer line is independent of the internal field although the remaining lines of the Mossbauer spectrum do depend upon this field. But should the internal fields at the nuclei in the source and absorber differ, then the width of the Mossbauer line would be observed to be wider than the lifetime of the state predicts. To completely appreciate this statement, one must remember that the Mossbauer line arises from the overlap of all six emission lines with the same six absorption lines. An exact overlapping indicates that the internal fields in the source and absorber are identical. If the fields are different, the splitting of the hyperfine structure of the source will differ from that of the absorber

so that the emission spectrum must be Doppler shifted in order to achieve resonance. However, the magnitude of the shift depends upon which emission line is considered so that the size of the necessary Doppler shift depends upon the emission line. The Mossbauer line is produced by the overlapping of all six components of the emission and absorption spectra so that if the shift of the emission lines is small, these six lines will be unresolved, thereby producing a broad Mossbauer line.

Since the internal field at the nucleus is temperature dependent, the difference between the internal fields at the nuclei in the source and absorber depends upon the temperature difference between the source and absorber thereby producing (by the above-mentioned mechanism) a temperature dependent line width for the Mossbauer line. Using the transition energies given in Table II-2, the broadening of the Mossbauer line caused by this mechanism is calculated as a function of the temperature difference between the source and absorber. If $\Delta H = H-H'$, then the difference in transition energy for the L_1 line is:

$$\Delta E_{\frac{3}{2} \ -\frac{1}{2}} = .2433\mu_n\Delta H \qquad \qquad \text{II-44}$$

The broadening of the line is the sum $\sum_{j=1}^{6}|\Delta E_{jk}|W_{jk}$. The result of this calculation is given in Table II-3.

$\theta°K$	$\theta'°K$	$\Delta\theta°K$	$Hx10^5 oe$	$H'x10^5 oe$	$\Delta Hx10^5 oe$	Increase in Line Width
148	293	-145	3.39	3.33	-.06	.0178 cm/sec
179	295	-116	3.38	3.33	-.05	.0115 cm/sec
253	296	- 63	3.35	3.33	-.02	.0046 cm/sec
293	293	0	3.33	3.33	0	0 cm/sec
352	294	58	3.31	3.33	.02	.0046 cm/sec
405	295	110	3.27	3.33	.06	.0138 cm/sec
458	294	164	3.21	3.33	.12	.0276 cm/sec

Table II - 3

The increase in line width as a function of temperature difference between source and absorber. The value of 3.42×10^5 oe was used for the internal field at the Fe nucleus at θ $0°K$

2.5 Electric Quadrupole Splitting

In a manner similar to that by which the nuclear magnetic moment of Fe^{57} interacts with the effective internal field at the nucleus to split the $I = 3/2$ spin state into four sub-states, the electric quadrupole moment of this state interacts with the effective internal electric field gradient to produce, in the absence of the magnetic hyperfine splitting, two sub-states. For a pure quadrupole interaction in the case of axially symetric electric field gradients, the two sub-states are shifted by an energy:

$$E = \frac{e^2qQ}{4I(2I-1)} \left[3m^2 - I(I+1) \right] \left[1 - \gamma \right] \qquad \text{II-45}$$

where $q = (1/e)(\partial^2 V/\partial z^2)$, the maximum principal field gradient, I is the spin of the state ($3/2$ for the excited state of Fe^{57}), Q is the electric quadrupole moment, m is the magnetic quantum number of the magnetic sub-state and γ is the anti-shielding factor. In the presence of non-symetric field gradients, the above expression must be increased by a factor $(1 + 1/3\eta^2)^{\frac{1}{2}}$, where

$$\eta = (\frac{\partial^2 V}{\partial x^2} - \frac{\partial^2 V}{\partial y^2})/\partial^2 V/\partial z^2 \qquad \text{II-46}$$

the asymmetry parameter (Moss II,p.169). When the quadrupole interaction is combined with the Zeeman splitting of the sublevels of the $I = 3/2$ state, the precise energy shifts for the individual m states due to the quadrupole interaction, depend upon the orientation of the magnetic axis relative to the axis of symmetry for the electric field gradient and, in general, are not the same for all m states. The energy shift then becomes

$$\xi = \frac{e^2qQ}{8} (3\cos^2 \phi - 1) \qquad \text{II-47}$$

where $\emptyset$ is the angle between the magnetic field and the crystal axis. The angle depends upon the temperature of the crystal so that the magnitude of the electric quadrupole interaction is temperature dependent (Moss II, p.160).

For a crystal structure having cubical symmetry, the electric field gradient is zero and hence, the electric quadrupole interaction is also zero. Since natural Fe is a good approximation of a cubically symmetrical lattice, it is expected that no electric quadrupole interaction would be present in the absorber. It is possible however, that the presence of Co^{57} in the iron lattice of the source could destroy the cubical symmetry of this lattice so that a net electric field gradient could exist at the Fe^{57} nuclei. In this case therefore, the presence of the quadrupole interaction in the source would shift the energies of the lines in the emission spectrum so that the Mossbauer line would split. If, on the other hand, the shifts were small, the line splitting would be unresolved so that the observed effect would be a broadened Mossbauer line rather than a split line. Since the electric quadrupole interaction is temperature dependent, the line broadening would also be temperature dependent. In the special case in which the source or absorber consisted of a single line, the presence of an electric quadrupole interaction would shift the positions of the resonant absorption lines. Such a shift would be temperature dependent due to the temperature dependence of the quadrupole interaction.

2.6 Localized Modes

In the source being discussed in this thesis, the emitting nucleus (Fe^{57}) is an impurity in the host source lattice and as an impurity, it has a mass m_0 which is different from the mass m of the lattice atoms. Further, the coupling constant k_0 of the impurity atoms is different from the coupling

constant k of the lattice atoms. The impurity atom therefore has a frequency of:

$$w_o \doteq \sqrt{k_o/m_o} \qquad\qquad \text{II-48}$$

which differs from that of the lattice atoms, w_E. Moreover, in the Debye approximation, the impurity causes a shift in the phonon frequencies of the lattice atoms by an amount which is of the order $1/N$ of that expected from the Einstein model, where N is the total number of atoms in the lattice. If the mass difference $\Delta m = m_o - m$ is positive, the the phonon frequencies are shifted to lower frequencies and a quasi-localized mode of frequency w_o is established within the normal phonon spectrum of frequencies (i.e., $w \propto w_D$, where w_D is the maximum frequency of the Debye continuum). The difference between w_o and w_D depends upon Δm and increases as Δm increases. The number of atoms involved in the localized mode is very small, consisting primarily of the closest neighbours of the impurity atom.

As seen in Table II-1, the establishment of the 14.4 kev state of Fe^{57} is preceeded by the emission of a 121 kev γ ray. The recoil energy of the 121 kev γ ray is:

$$E_r = E_\gamma^2/2m_o c^2 \qquad\qquad \text{II-49}$$
$$= 7.9 \text{ ev.}$$

which is much larger than that of the mean lattice energy of .023 ev. The localized mode therefore, may be highly excited by the emission of the 121 kev γ ray. Since $w_o < w_D$, the localized mode can decay easily by exchanging a phonon with the Debye continuum of normal phonon frequencies. The lifetime of a localized mode is[18]

$$\tau_o = \frac{6\Delta m h}{\pi m \, w_D} \qquad\qquad \text{II-50}$$

Equation II-52 assumes that $w_0 \ll w_D$ and $\Delta m/m \gg 1$. If these conditions are not valid (as is the case of Fe^{57} in Armco iron) then the actual lifetime is much less than this equation gives.

Using a one dimensional model of a lattice, it has been shown that the Debye-Waller factor increases if the impurity mass is greater than the host mass. In this case the Debye-Waller factor is given by the expression (Moss II, p.81):

$$f = e^{-2W} \quad \text{where} \quad W \propto \frac{1}{m(m + \Delta m)} \qquad \text{II-51}$$

In order that the increase in f be appreciable, it is necessary that the mass of the impurity be appreciably less than that of the host lattice. Since this is not the so in the case of Fe^{57} in a natural iron lattice, the Debye-Waller factor in this case is that of the natural iron lattice.

For comparison purposes the case in which $\Delta m < 0$ will also be considered. In this case all frequencies of the lattice phonons are shifted but this time, to higher frequencies by an amount of the order $1/N$, except the highest frequency which separates from the Debye continuum to form a localized frequency mode of frequency w_0 with amplitude localized in the vicinity of the impurity. This localized mode when excited, can decay by exchanging two or more phonons with the Debye continuum.[17] This interchange of energy between the normal phonon frequencies and the localized mode arises from the anharmonic forces coupling the impurity and the lattice atoms. At absolute zero the lifetime of the mode is given by[17]

$$\frac{1}{\tau_0} = w_0 \, 8 \gamma^2 \, I(\frac{w_0}{w_D}) \frac{\hbar w_0}{m_0 v^2} \, (\frac{k'D}{k'})^3 \, (\frac{w_0}{w_D})^2 \qquad \text{II-52}$$

where v is the velocity of sound, γ is the Gruneisen constant, m_o is the atomic mass, k' and k'_D are attenuation lengths and $I(x) =$ $\int_o^{'} y^3(1-y^{\frac{1}{2}})dy$. At higher temperatures the anharmonic interaction is increased. For this case, it has been shown that the Debye-Waller factor is reduced by the presence of the impurity (Moss II, p.29).

In both of the cases of localized modes considered, the Mossbauer effect can be used to detect the mode. The presence of the mode is indicated by a peak centered at w_o, superimposed upon the broad single or multiple phonon - γray emission and absorption processes. Since the lifetime of the mode is short in either case, the peak will be broad enough so that slow high resolution scanning of the Mossbauer spectrum should not be necessary.

The localized mode can also exert some effect upon the zero phonon spectrum (i.e., upon the recoilless γray spectrum). To establish qualitatively this effect, the Einstein model of a lattice is used. This model may be used as a good approximation in this case of a localized mode since the extent of the interaction between this mode and the rest of the lattice is limited to the first few neighbours. Based on this model, the impurity is oscillating in a potential well and has ground state energy of $\frac{1}{2}\hbar w_o$. For small mass diferences Δm, w_o is approximately equal to w_D and the probability of the occupation of the localized state is small. Hence, as a result of the emission of the 121 kev γray, the energy of the localized mode will be approximately

$$E_1 = (n+\tfrac{1}{2})\hbar w_o$$
$$= \frac{E'_{\gamma}}{2m_oc^2}$$

II-53

$E'_\gamma = 121$ kev, which is the recoil energy of the 121 kev γ ray. If m'_0 represents the mass of the radiating nucleus in its excited state (i.e., Fe^{57m}), then

$$m'_0 = m_0 + \frac{E_\gamma}{c^2} \qquad (E_\gamma = 14.4 \text{ kev})$$
$$= m_0 + \delta m_0 \qquad\qquad\qquad\qquad\qquad\qquad \text{II-54}$$

Hence the frequency before the emission of the γ ray is given by:

$$w'_0 = (k'_0/m_0 + \delta m_0)^{\frac{1}{2}} \qquad\qquad\qquad \text{II-55}$$
$$= w_0(1 - \tfrac{1}{2}\delta m_0/m_0)$$

Assuming that the γ emission preceeds the phonon emission from the localized mode, the energy of the excited state of the nucleus is

$$E^m_1 = \langle (n + \tfrac{1}{2}) \rangle \hbar w'_0 \qquad\qquad\qquad \text{II-53'}$$

where $\langle n + \tfrac{1}{2} \rangle$ is the expectation value of $n + \tfrac{1}{2}$, and the energy of the ground state is given by equation II-53. Hence the change in lattice energy caused by the emission of the γ ray is:

$$\Delta E_1 = \langle n + \tfrac{1}{2} \rangle \hbar (w'_0 - w_0)$$
$$= -\langle n + \tfrac{1}{2} \rangle \tfrac{1}{2}\hbar w_0 \delta m_0/m_0 \qquad\qquad \text{II-56}$$
$$= -\tfrac{1}{2}E'_\gamma /m_0 c^2 \langle n + \tfrac{1}{2} \rangle \hbar w_0$$

Since $w_0 \approx w_D$, n will be small (of the order of 10) hence, large dispersions of n are possible. As a consequence of the fluctuations in n, a broadening of the zero phonon spectrum of the order

$$\Delta = \tfrac{1}{2}E'_\gamma/m_0 c^2 \ (\langle n^2 \rangle - \langle n \rangle^2)^{\frac{1}{2}} (\hbar w_0) \qquad\qquad \text{II-57}$$

is expected. Furthermore, the absorbing nucleus, also an impurity in the

lattice, should be in the ground state since it is not subjected to a recoil from a preceding decay as is the case of the source atom. Hence, the change in the lattice energy of the absorber when a ray is absorbed is

$$E_1' = (\tfrac{1}{2}E_\gamma'/m_0 c^2)(\tfrac{1}{2}\hbar w_0) \qquad \text{II-58}$$

Hence, there will be a shift in the zero phonon peak of the order

$$\delta(\Delta E_1) = \tfrac{1}{2}E_\gamma'/m_0 c^2 <n> \hbar w_0 \qquad \text{II-59}$$

For both cases considered earlier, the magnitude of these two effects depend upon the ratio of the lifetime of the source to the life-time of the localized mode which, in turn, depends upon $|\Delta m|$. For the same $|\Delta m|$, the lifetime for $\Delta m < 0$ is somewhat greater than that for $\Delta m > 0$. For the example of Fe^{57} in Armco iron source and an Armco iron absorber, it is seen that $m_0 = 57$, $m = 56$ and $\Delta m = 1$. Since Δm is small compared with m, the effect of the localized mode on the position and width of the Mossbauer line is expected to be very small. Further, the effect should decrease as temperature increases since the lifetime decreases as the temperature increases.

In the discussion of the localized modes, it is to be remembered that the introduction of the impurity may result in a change of the chemical bond strength, thus giving rise to the isomer shift discussed earlier.

Chapter III

EXPERIMENTAL APPARATUS and METHOD

3.0 Introduction

The source, absorber and gamma ray spectrometer used in the gathering of the experimental data for this thesis are described in this chapter. The method by which the source was electroplated is given but the subsequent thermal treatment of this source to produce the Mossbauer effect, is covered in Chapter IV. The absorber was mounted on a lathe carriage so that its velocity relative to the source could be controlled. Arrangements were made so that the temperature of the source could be varried and the temperature of both the source and absorber could be monitored. A proportional counter was constructed to detect the gamma radiation. The details of this construction as well as the characteristics of the counter are summarized in this chapter.

The second part of this chapter describes the method by which the transmission of the gamma rays through the absorber as a function of velocity was determined. Corrections to the measured transmission were necessitated by the presence of the background radiation, the counter drift and the experimental geometry. Further, an analysis was made to determine the thickness of absorber which would give the most significant results.

3.1 Detectors
a) NaI Crystal

The experimental data contained in this thesis was obtained with

the use of two types of detectors. For the preliminary investigations an
NaI crystal gamma ray spectrometer was used; for the final measurements
an Ar-CH$_4$ (methane) proportional counter was used.

The NaI crystal used was $1\frac{1}{2}$" in diameter and 1/8" thick, covered
with a .010" Be window to allow the highest transmission possible for low
energy gamma rays (those less than 16 kev) emitted by the source. The
crystal was mounted on an R. C. A. 6342 photomultiplier tube #12-4-444 by
means of Dow Corning 200 fluid (silicon grease with viscosity 1,100,000 cs)
and the assembly was wrapped with black electricians tape to prevent light
from entering the photomultiplier tube. The tube was operated at an EHT
of 1300 volts. Pulses from the photomultiplier were fed through the ap-
paratus shown in Fig. III-11 with the photomultiplier replacing the proportion-
al counter. Fig. III-1 illustrates typical spectra of Fe^{57} radiation obtained
with this crystal. Calibration pulses from the pulse generator are in-
cluded in this figure. These peaks were obtained with one volt across
the helipot and helipot settings of 2.50 to 7.00 in steps of .50. The set-
tings on the other electrical apparatus were a) for the amplifier, dif-
ferentiation time constant of .8 μsec; integration time constant of .16
μsec; attenuation, coarse, 0, fine, 12 dbs., b) of the nuclear data kick-
sorter, live time 10, window 9.74, gain f 8.00, c 16, and c) for the
scaler, discriminator bias 60, dead time 5 μsec.

The spectra shown in Fig. III-1 are those obtained using a .001"
stainless steel absorber, a .001" shim steel absorber, and no absorber.
Each spectrum in this figure was obtained in the same counting time, T,
and with the same electronic settings. The use of the stainless steel
absorber considerably increases the separation of the 6.9 kev and 14.4 kev
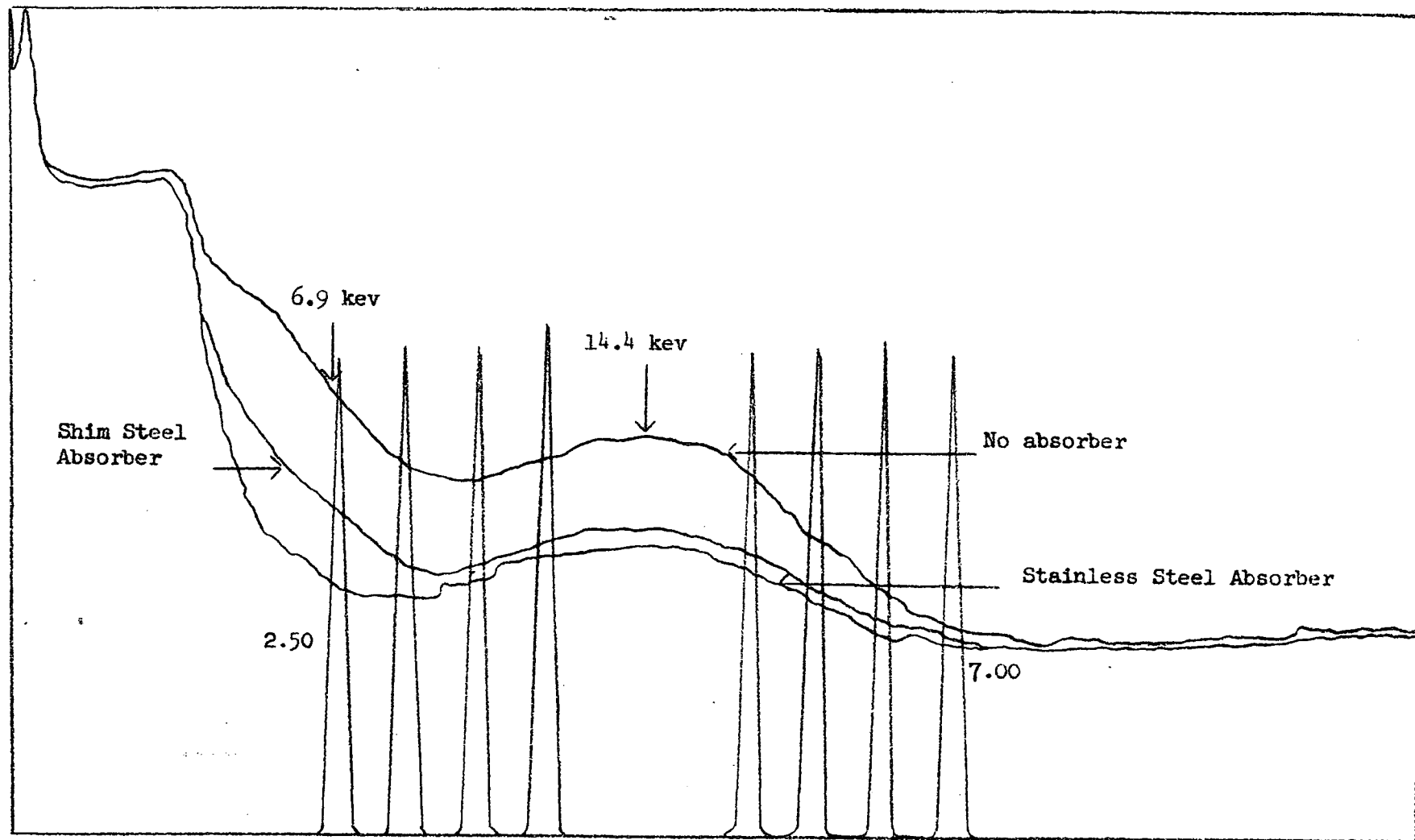
FIGURE III-1 Typical Fe^{57} spectra obtained by the use of a NaI crystal with (a) No absorber, (b) .001" shim steel absorber, and (c) .001" stainless steel absorber. Calibration pulses are also shown.

gamma ray peaks and increases the absorption of the 6.9 kev gamma ray. The component of the stainless steel responsible for this selective absorption is the element chromium (type 30321 stainless steel used is 17-19% Cr) which has a linear absorption coefficient of 792cm^{-1} for the 6.9 kev gamma ray and 396cm^{-1} for the 14.4 kev gamma ray. A second substance found to absorb the 6.9 kev gamma ray more strongly than the 14.4 kev gamma ray was the silicon grease mentioned above. Both of these substances, however, absorb the 14.4 kev gamma ray as well as the 6.9 kev gamma ray and therefore, were not used for the detailed investigations.

b) Ar-CH$_4$ Proportional Counter

i) Sensitivity

The poor resolution of the NaI crystal for the 14.4 kev gamma ray in the absence of either Cr or the silicon grease and consequently its insensitivity to small energy shifts prompted the construction of the Ar-CH$_4$ proportional counter used to compile the experimental results given in this thesis. The best resolution that can be expected with the use of a proportional counter at 14.4 kev is 5.5% whereas with an NaI crystal the best resolution at 14.4 kev is 33.6% (Moss II, p.70). Experimentally, with proportional counters, resolutions of 10-20% have been obtained - a factor of at least two greater than the best expected with the crystal. Another advantage of the proportional counter is the fact that they can be made very large and hence their efficiencies at low energies can be made higher than those of NaI crystals. Moreover, the proportional counter can be made insensitive to high energies. This latter fact is particularly important when the counter is to be used

with an Fe^{57} source in which there exists a high counting rate compared with that of the transmitted 14.4 kev counting rate, arising from the 120 kev gamma ray of the preceding transition. Pound found that the use of an Ar-CH_4 proportional counter produced a ratio of the counting rate of the 14.4 kev gamma ray to the total rate of 1:1.5, i.e., there were only 50% more counts above the 14.4 kev line than in the line (Moss II,pp.70-71).

Ideally, for 14.4 kev gamma rays, a krypton filled proportional counter should be used (the linear absorption coefficient of Kr at 1 atmosphere pressure, at 14.4 kev is $4.35 \times 10cm^{-1}$) but the expense of the krypton and the satisfactory results obtained with the Ar-CH_4 mixture precluded its use. The use of the Ar-CH_4 mixture, on the other hand, required a very large counter (8" diameter) to get a useful stopping power as the linear coefficient of absorption of Ar at 14.4 kev is $4.27 \times 10^{-2}cm^{-1}$. Assuming the gas to be entirely Ar (a good approximation since the gas used was 90% Ar), the stopping power of the counter for the 14.4 kev x-rays was calculated to be 57% and for the 6.9 kev x-rays essentially 100%. To avoid gas contamination the counter was designed to run with a continuous gas flow. No attempt was made to recover the gas since one cylinder (1600 lbs.) lasted approximately five months.

ii) Construction of the Counter

The body of the counter (see Fig. III-2) was constructed from a 23" length of aluminium pipe, 1/8" thick and 8" inner diameter. In order to make the window of the counter, an area six inches square was cut from the centre of the pipe. This area was covered with a piece of mylar .001" thick. The inside of the counter was ground with a drum sander to remove the dirt, but no attempt was made to remove the remaining small
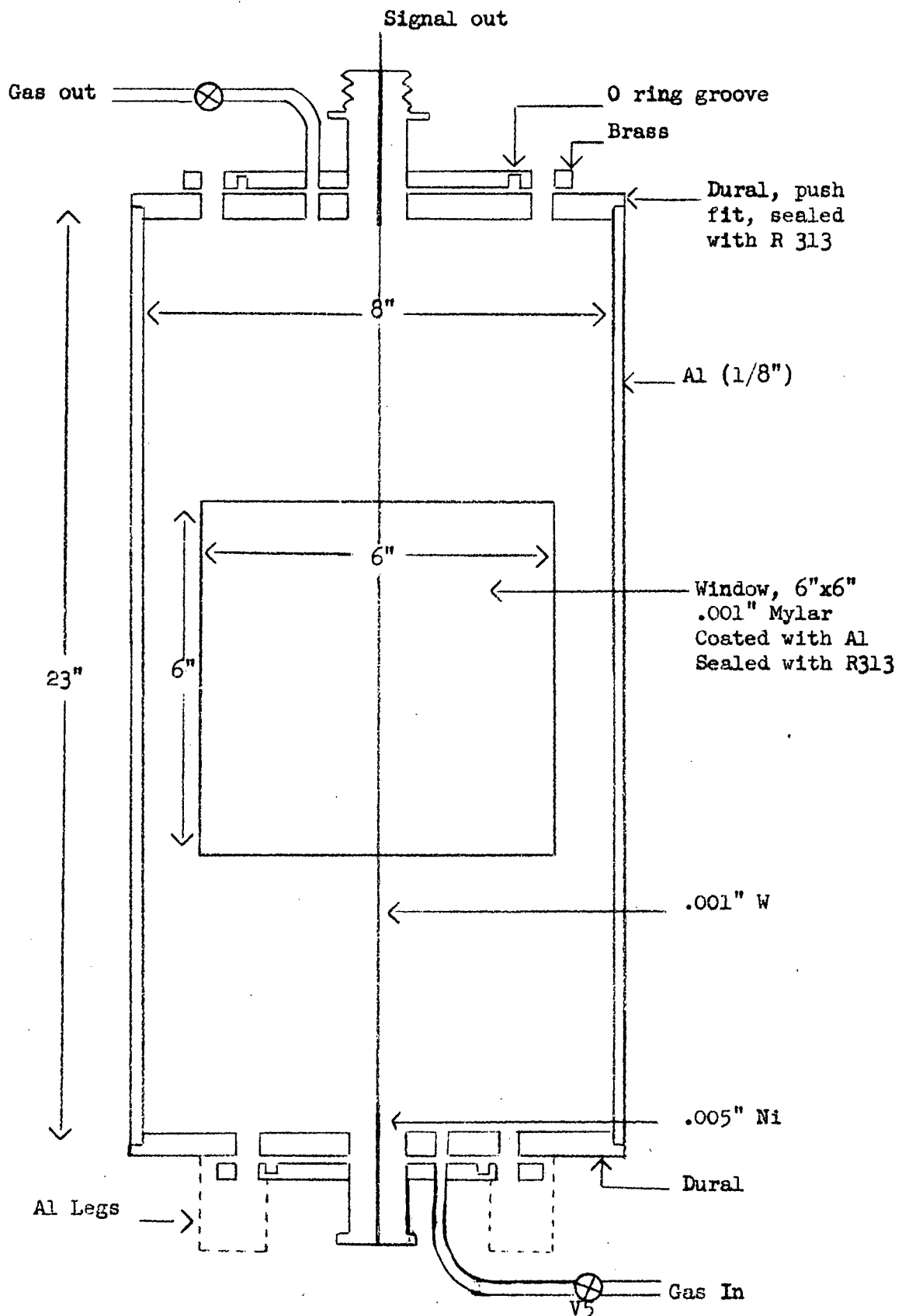
FIGURE III-2 A cross-sectional diagram of the body of the
Ar-CH₄ continuous flow proportional counter.

surface irregularities. The interior was further cleaned with acetone, then alcohol and dried with an infra-red lamp. To provide a conducting surface for the window, aluminium was deposited upon the inner side of the mylar. The mylar was secured to the aluminium with R313.

Both ends were fitted with a gas flow tube and a terminal for the centre wire. Fig.III-3 shows the details of the top terminal. These two terminals were identical except for the fact that the top one was fitted with an R. G. 560/U plug providing the means for connecting the counter to the pre-amplifier. The centre wire was .001" tungsten wire, spot welded to each end of which there was a short piece of nickel wire (.005"). The tungsten wire was positioned in the counter by threading it through the two covar seals and soldering its two nickel ends to these seals. The two removeable plates were fashioned to make this operation possible. Great care was taken to insure that no kinks remained in the tungsten wire in this installation process.

iii) Filling the Counter

The counter was designed to operate at atmospheric pressure so that it was possible to have a very large, thin window. Hence, it was not feasible to merely evacuate the counter and refill with the gas mixture. Instead the counter had to be placed within a slightly larger cylinder of iron and both were evacuated at the same time. Both cylinders were then filled with the gas mixture, the counter gas intake was closed and the counter was removed, essentially ready for operation. Since residual amounts of air still remained in the counter, good resolution was not attained immediately. However, after eight hours with a gas flow of
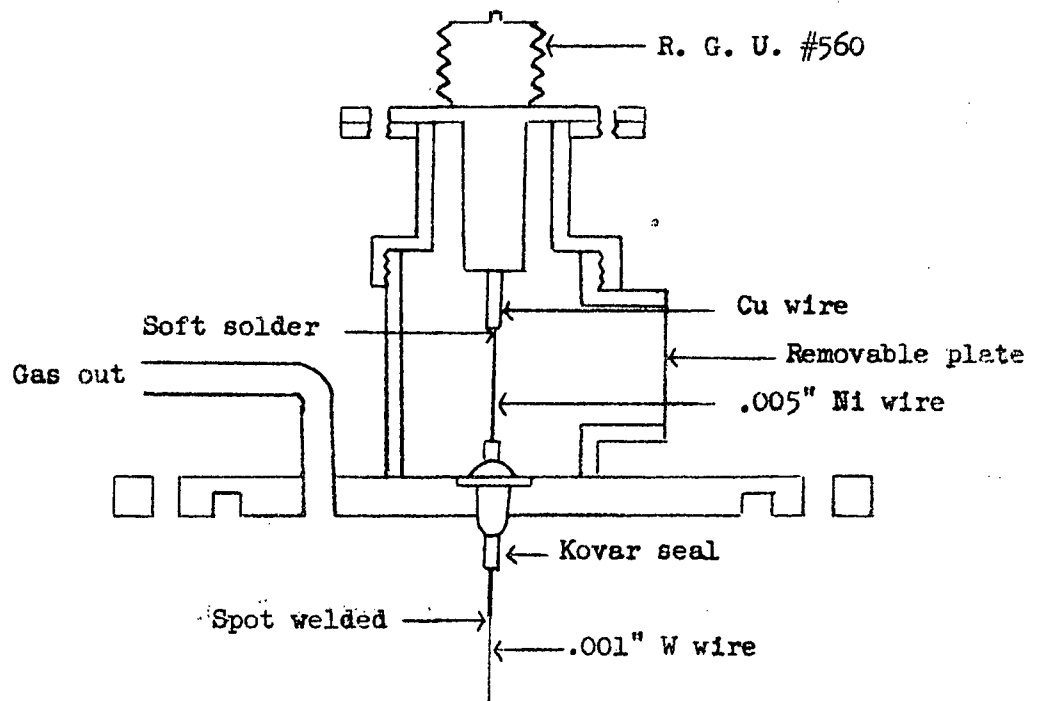
FIGURE III-3 A detailed diagram of the top terminal of the
Ar-CH₄ proportional counter.

.05 cu.ft./hr., a resolution of approximately 20% at 14.4 kev was attained.

iv) Gas Flow System

The system providing the counter with a continuous stream of gas is shown schematically in Fig. III-4. With reference to this diagram, the parts used in this system are given below.

PARTS	DESCRIPTION	MFG
Counter gas	90% Ar; 10% CH_4	Matheson Co. Ltd.
V_2 and V_3	Single stage regulator #1	"
V_4 and V_5	Low pressure "Pancake" Regulator #70-A-B	"
V_6	Needle valve	Rollason
V_7 and V_8	Imperial diamond valves 693-C	Imperial Brass
Flowmeter	#201 Flowmeter	Matheson Co. Ltd.
V_9	Rubber hose clamp	Cenco

Table III-1

The flowmeter was placed in the system so that a) the actual flowrate of the gas could be measured and kept the same when the gas bottles were changed and b) so that fluctuations or instabilities in the gas flow could be detected. The meter was constructed from a block of lucite. The gas flowed through a narrow tube so that the flow rate was indicated by a small metal sphere supported in this tube by a flow of gas. The meter was calibrated from .01 to .08 cu.ft./hr for dry air. The correction curve for other gases is shown in Fig. III-5. The flow
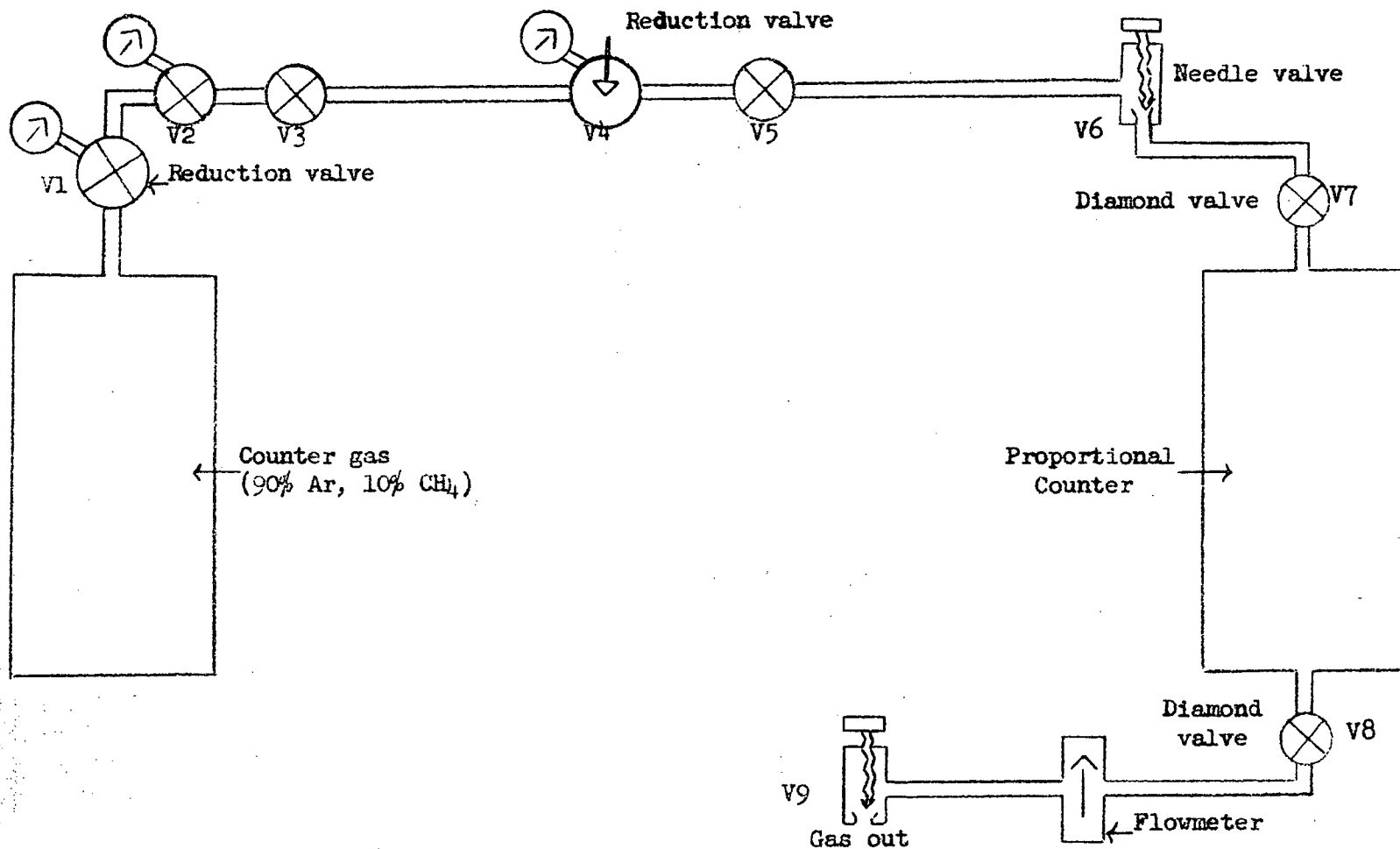
FIGURE III-4   A block diagram showing the gas flow system of the Ar-CH₄ proportional counter.
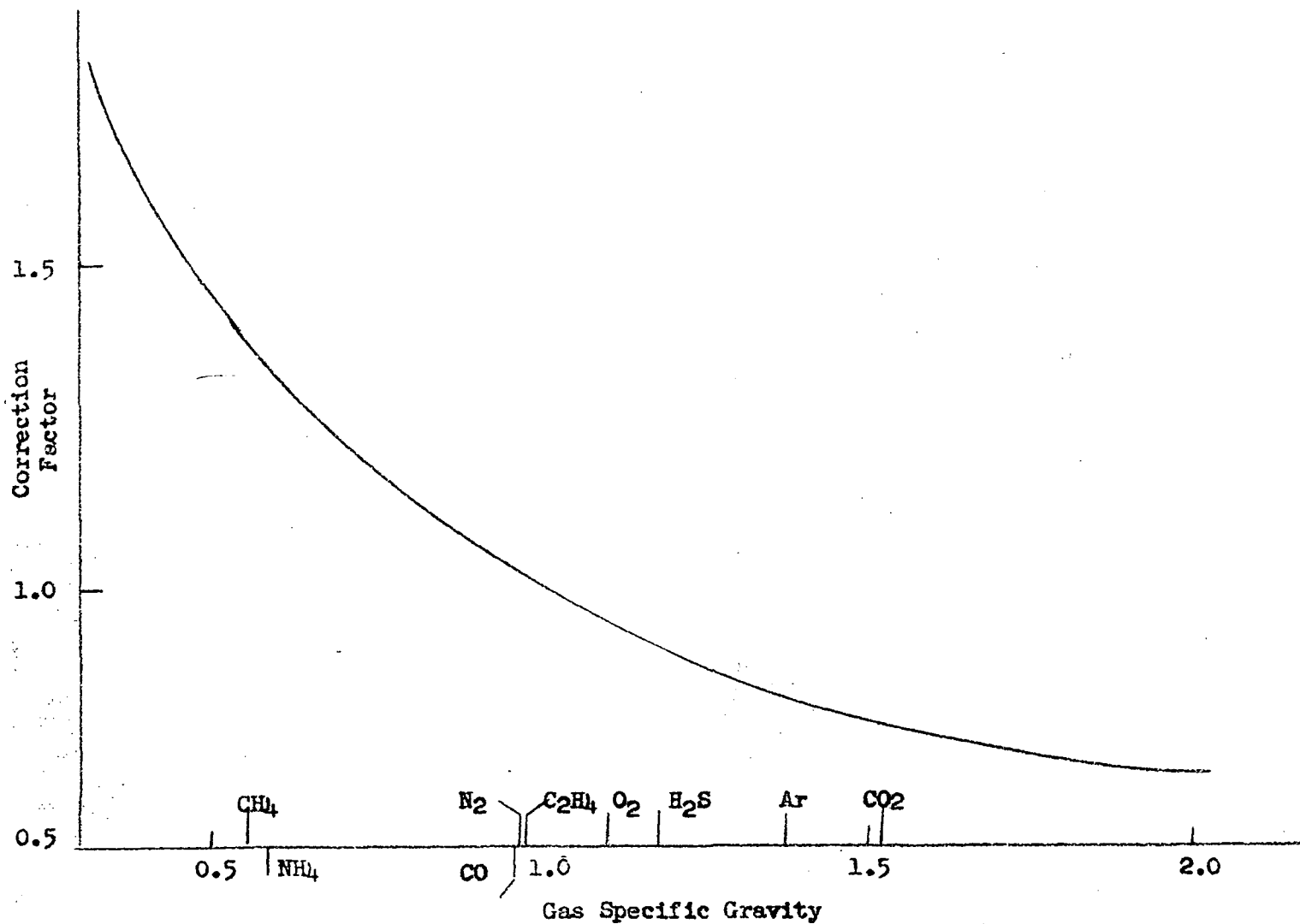
FIGURE III-5   The specific gravity correction curve for the flowmeter. The correction
is made by multiplying the indicated flow by the correction factor.

rate used in the experiments was .05 cu.ft./hr for the Ar-CH$_4$ mixture.

v) Difficulties

Since both the resolution (as noted in the filling procedure) and the gas gain of the proportional counter depends upon the gas purity, it was vital that the gas flow rate be kept constant. The required constant flow rate was obtained by including the needle valve V$_9$ in the flow system because without it the gas flow was essentially determined by P_c-P_a/I_f where P_c and P_a refer to the counter and atmospheric pressures respectively and I_f to the impedance in the gas flow of the flowmeter (I_f appeared to be a function of the flow rate through the meter). These conditions were sufficient to produce positive feedback and fluctuations in the pressure in the counter. V$_9$ acts as a high fixed impedance to the gas flow so that the flow is determined by P_c-P_a/I_{V_9}, which is much smaller than P_c-P_a/I_f so that the flow is dominated by the fixed impedance and the fluctuations are smaller. In fact under these conditions, no fluctuations could be detected by the flowmeter.

The gain of the counter was found to be (as expected) strongly dependent upon the pressure in the counter and hence this pressure had to be kept constant during the operation of the counter. Since it operates at atmospheric pressure, any fluctuations in the room pressure affected the gain of the counter. Small fluctuations due to the ventilating fan in the room were minimized by leaving the door of the room open during the course of the measurements as well as letting the fan run at at a constant speed. However, a strong correlation was found between the value of the atmospheric pressure and the count rate in the 14.4 kev channel. Therefore, changes in atmospheric pressure were monitered and the
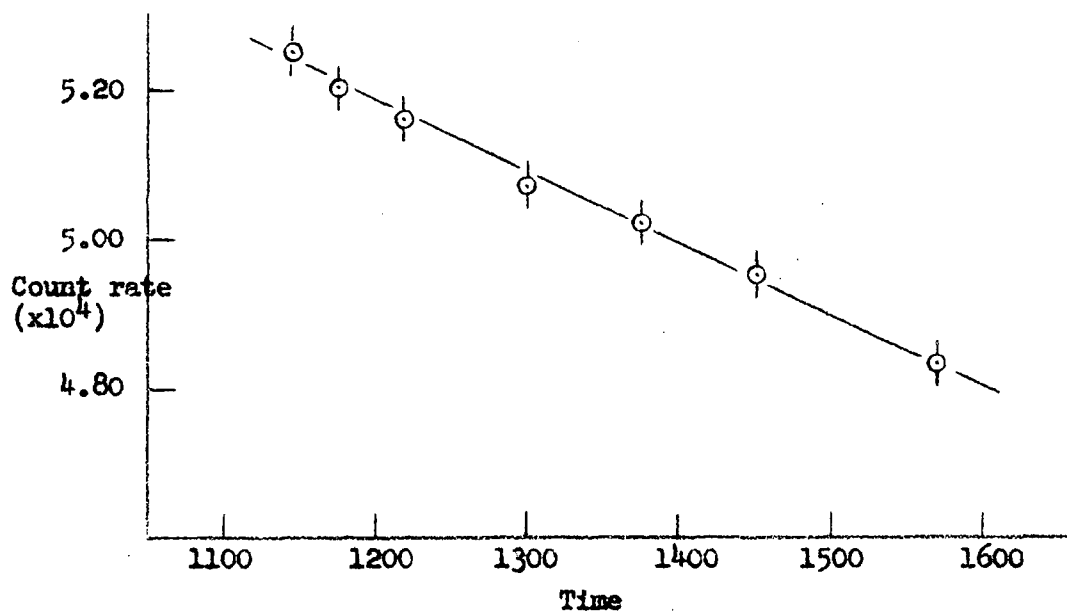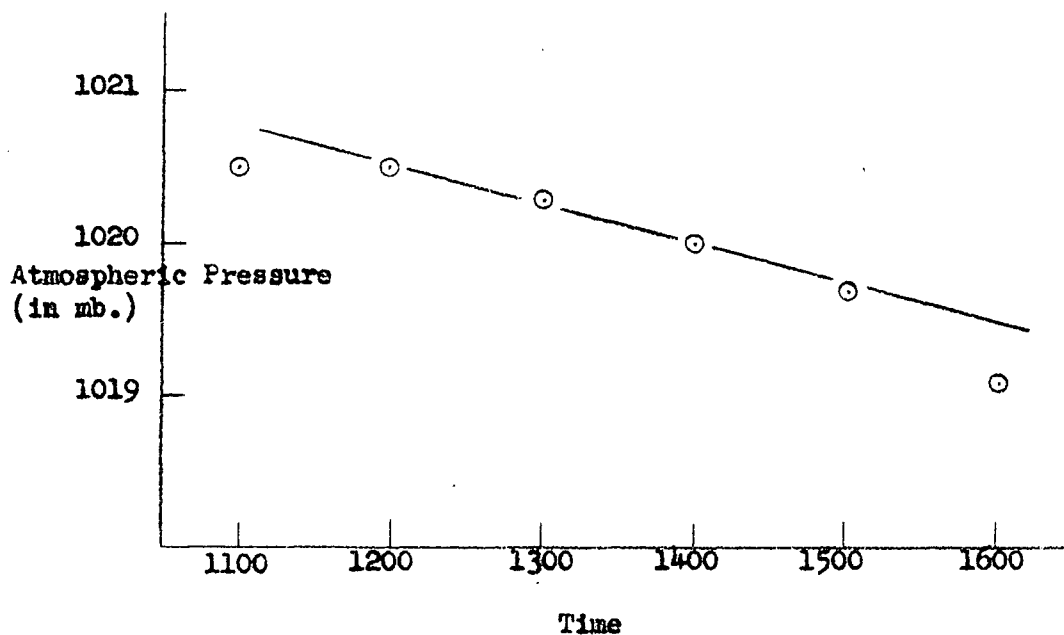
FIGURE III-6 An illustration of the relationship between the atmospheric pressure and the count rate in the 14.4 kev channel. The gamma rays were detected by means of the proportional counter.

results were corrected for this count rate drift.

Another source of difficulty with the counter was the fact that very large pulses of unknown origin occasionally came through the counter, effectively turning it off for periods of approximately 10 milliseconds. The frequency of these break down pulses was found to increase as the E.H.T. of the counter increased. These pulses were random and it was found, as shown in Fig. III-7, that when they occured sufficiently often, they distorted the distribution of count rates about the mean count rate away from the statistically expected distribution to such an extent that the highest E.H.T. at which it was possible to operate the counter was 1800 volts.

In addition to being a function of the gas flow rate and the counter pressure, it was found that the gain of the counter depended upon the total count rate of the source. However, the change in the count rate for the experiment (approximately 17%) was small enough so that the resulting gain shift was negligible.

vi) Characteristics of the Counter

Using the same equipment as used in the experiment and the NSEC #2 source, the characteristics of the proportional counter as shown in Table III-2 were found. In order to determine the gas gain in the counter, the gain of the amplifier and the preamplifier system was measured. The equipment was arranged as shown in Fig.III-8a for this measurement. The gain was determined for six values of V_{in} and averaged. With reference to the figure, the gain of the amplifier is given by:
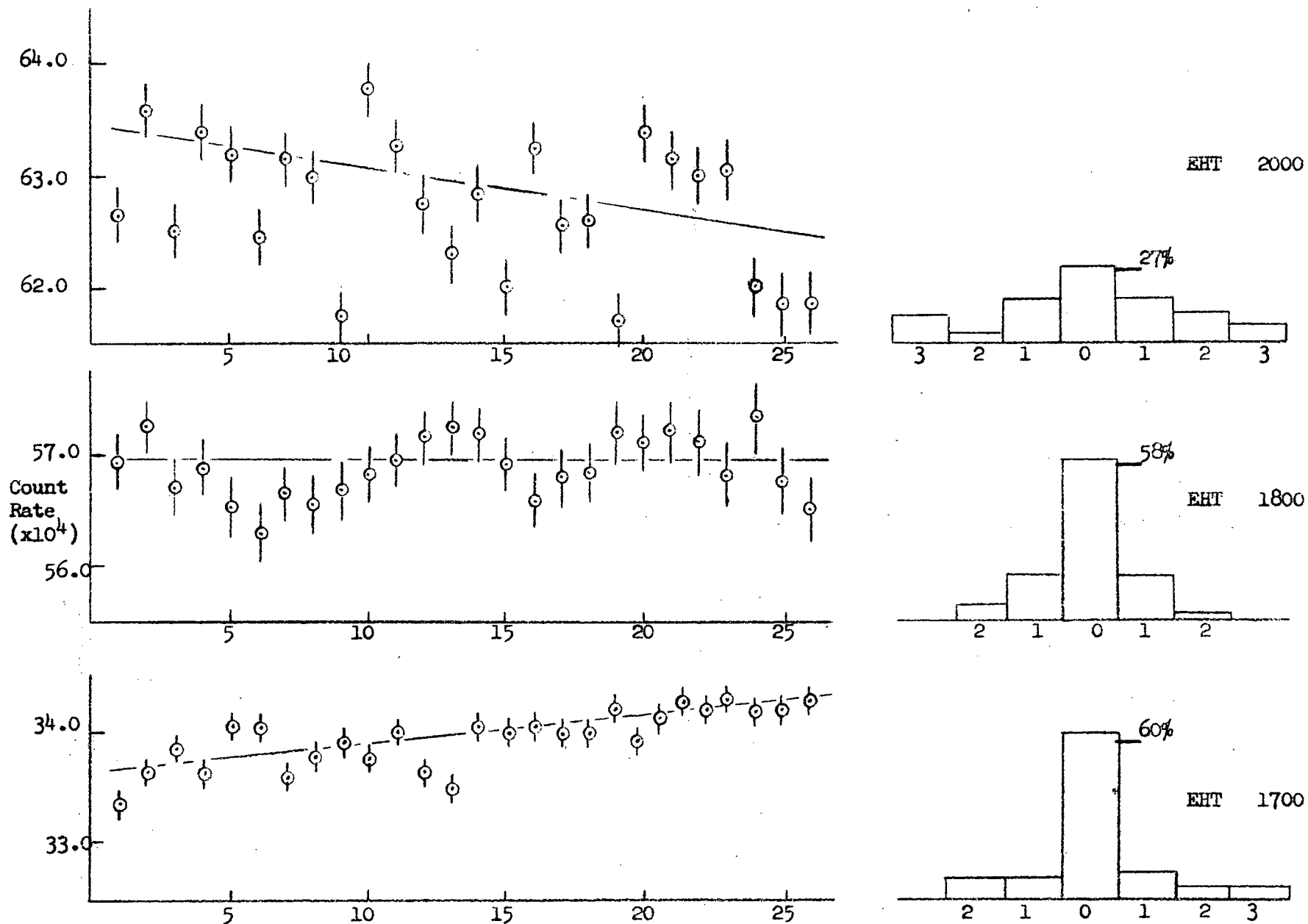
FIGURE III-7 The effect of the random break down pulses in the proportional counter on the statistical distribution of the count rate for various E H Ts.

$$G_a = V_{max}/V_{in}$$
$$= V_{max}/ V(c_1/c_1 + c_2)$$

III-1

The average gain of the preamplifier-amplifier was 2×10^6. The equipment was then arranged as in Fig.III-8b to determine the gas gain of the proportional counter as a function of the E.H.T. In this case

$$V'_{in} = \frac{V'_{max}}{G_a}$$
$$= q/C$$

III-2

where q is the charge collected by the proportional counter. The charge q', produced in the counter when the gamma ray of energy E_γ is absorbed is:

$$q' = E_\gamma/\epsilon$$

III-3

where ϵ is the stopping power of the gas mixture. The value of ϵ for Ar is 26.4 ev/ion pr.[19] The gas gain therefore, is given by:

$$G_g = q/q'$$

III-4

In the calculation of G_g, it was assumed that the effect of CH_4 with $\epsilon = 29.4$ ev/ion pr.[20] on G_g would be within the experimental error and hence was not included in the calculations. The gas gain is plotted as a function of the E.H.T. in Fig.III-9.

In order to determine the resolution of the counter, the spectrum transmitted through the absorber was analyzed by means of the C.D.C. 100 channel kicksorter. The spectrum was plotted by an X-Y recorder and the background correction made. The resolution as taken from this spectrum

Cathode Ray
Oscillascope

Pulse
Generator

V

C_1 2pf

C_2 65pf V_{in}

V_{out}

Proportional
Counter

Pre-amplifier

Amplifier

(a)

V_{in} V_{out}

C
65pf

Proportional
Counter

Pre-amplifier

Amplifier

Cathode Ray
Oscillascope
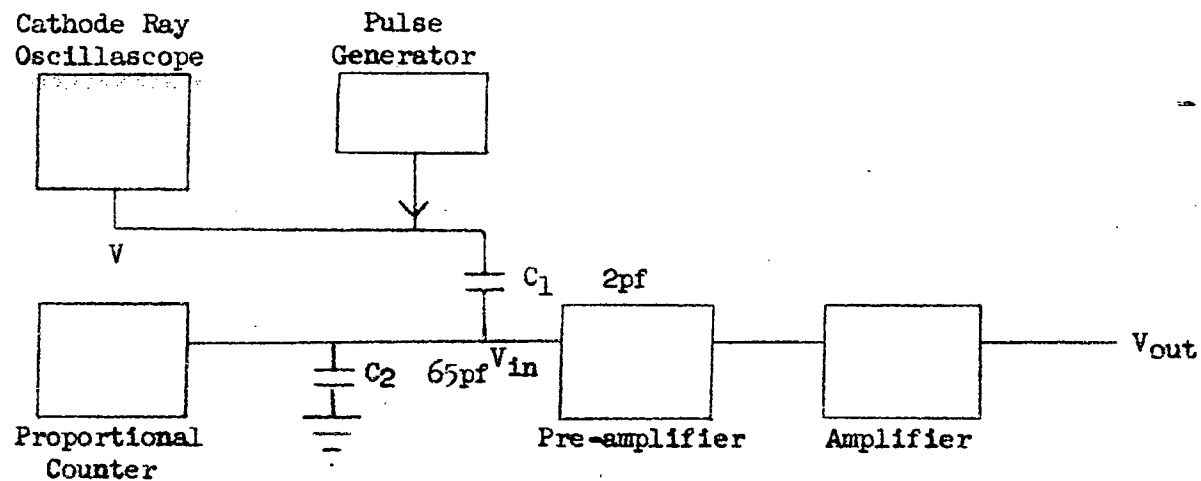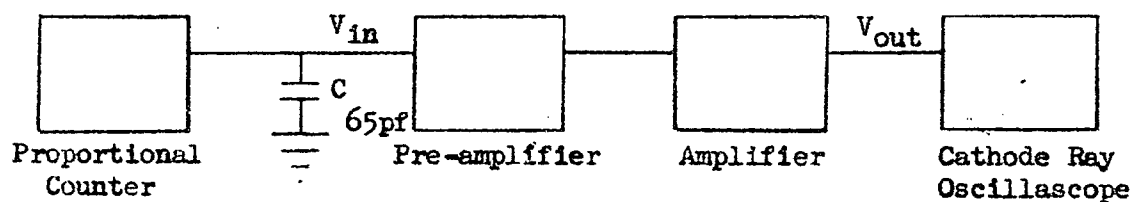
(b)

FIGURE III-8   A block diagram showing the arrangement of the apparatus to
determine (a) the gain of the pre-amplifier and amplifier,
and (b) the gas gain of the proportional counter as a function
of the EHT.

was:

$$R_{es} = W_{\frac{1}{2}}/L \qquad\qquad III-5$$

where $W_{\frac{1}{2}}$ is the width of the 14.4 kev peak at $\frac{1}{2}$ height and L is the distance from the low energy limit to the 14.4 kev peak. The noise, the signal to noise ratio and the rise time of the pulses were all determined by displaying the pulses from the counter and amplifying system into a calibrated oscilloscope.

E.H.T.	Gas Gain	Resolution	Noise	Signal/Noise	Rise Time (20-80%)
1650 volts	28 ± 3	18.9%	2.88 kev	5.00	3.0 μsec
1700 "	34 ± 3	16.0%	2.47 kev	5.83	3.0 "
1750 "	45 ± 3	17.0%	1.80 kev	8.00	3.0 "
1800 "	58 ± 3	16.5%	1.44 kev	10.00	3.0 "
1850 "	74 ± 6	16.7%	1.08 kev	13.30	2.5 "
1900 "	100 ± 6	17.7%	.85 kev	17.00	2.5 "
1950 "	142 ± 9	18.3%	.60 kev	24.00	2.5 "
2000 "	164 ± 9	19.9%	.50 kev	28.80	2.5 "

Table III-2

The Characteristics of the Proportional Counter as a Function of E.H.T.

The solid angle into which the detected x-rays were emitted was determined by the size of the counter window (36 square inches) and the distance of the source from the counter (27"). This solid angle was calculated to be .0495 steradians. The spectrum obtainable with the proportional counter is shown in Fig.III-10.. Again, the calibration pulses from the pulse generator have been included. The settings used for this spectrum were: a) amplifier differentiation: .8 sec; integration time constant: 3.2 sec; attenuation c 0, 20db b) Multichannel (C.D.C.) P.H.A. .3 volts/channel, bias 5 and c) E.H.T. 1850 volts.
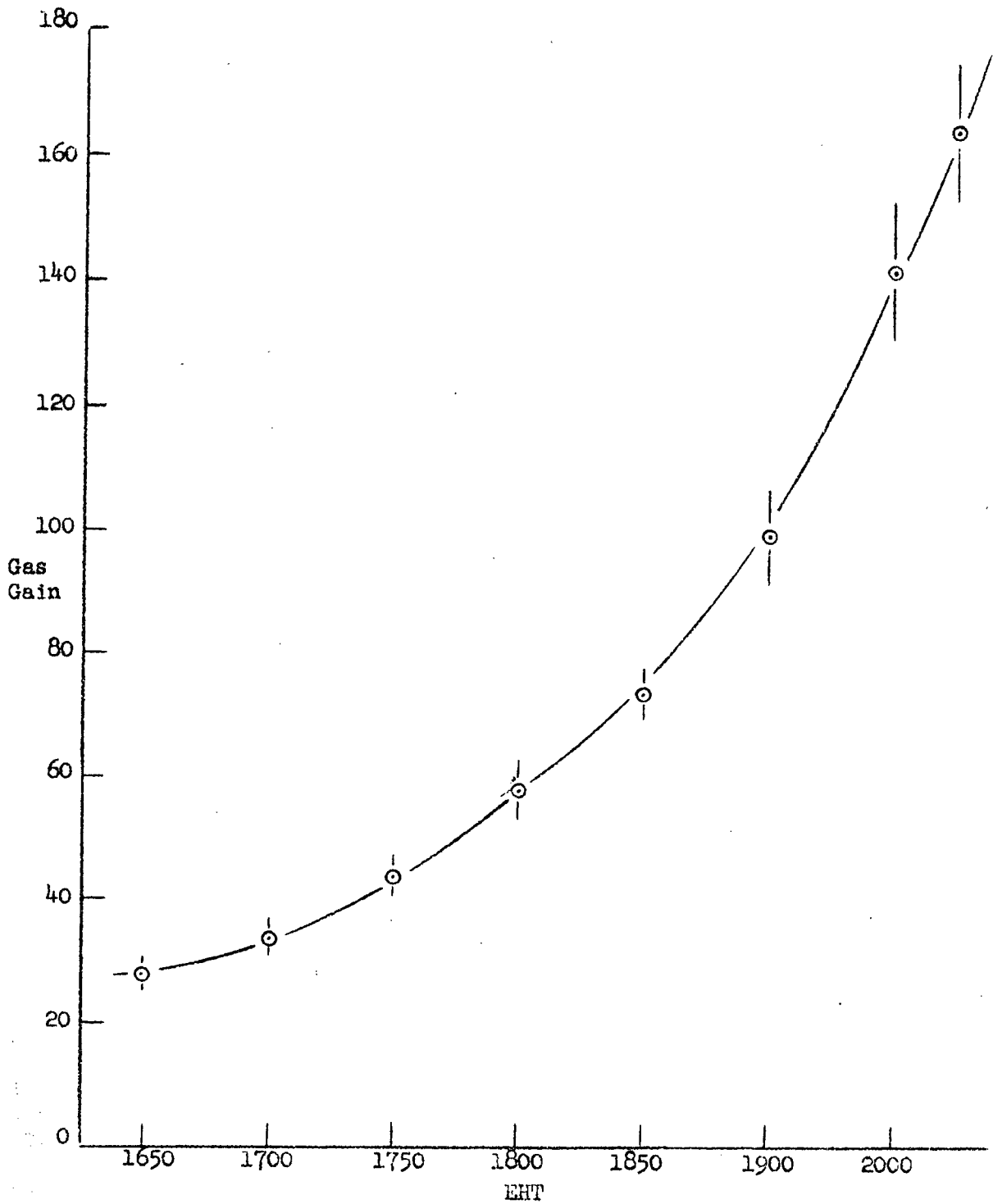
FIGURE III-9 The gas gain of the proportional counter as a function of the EHT on the centre wire.
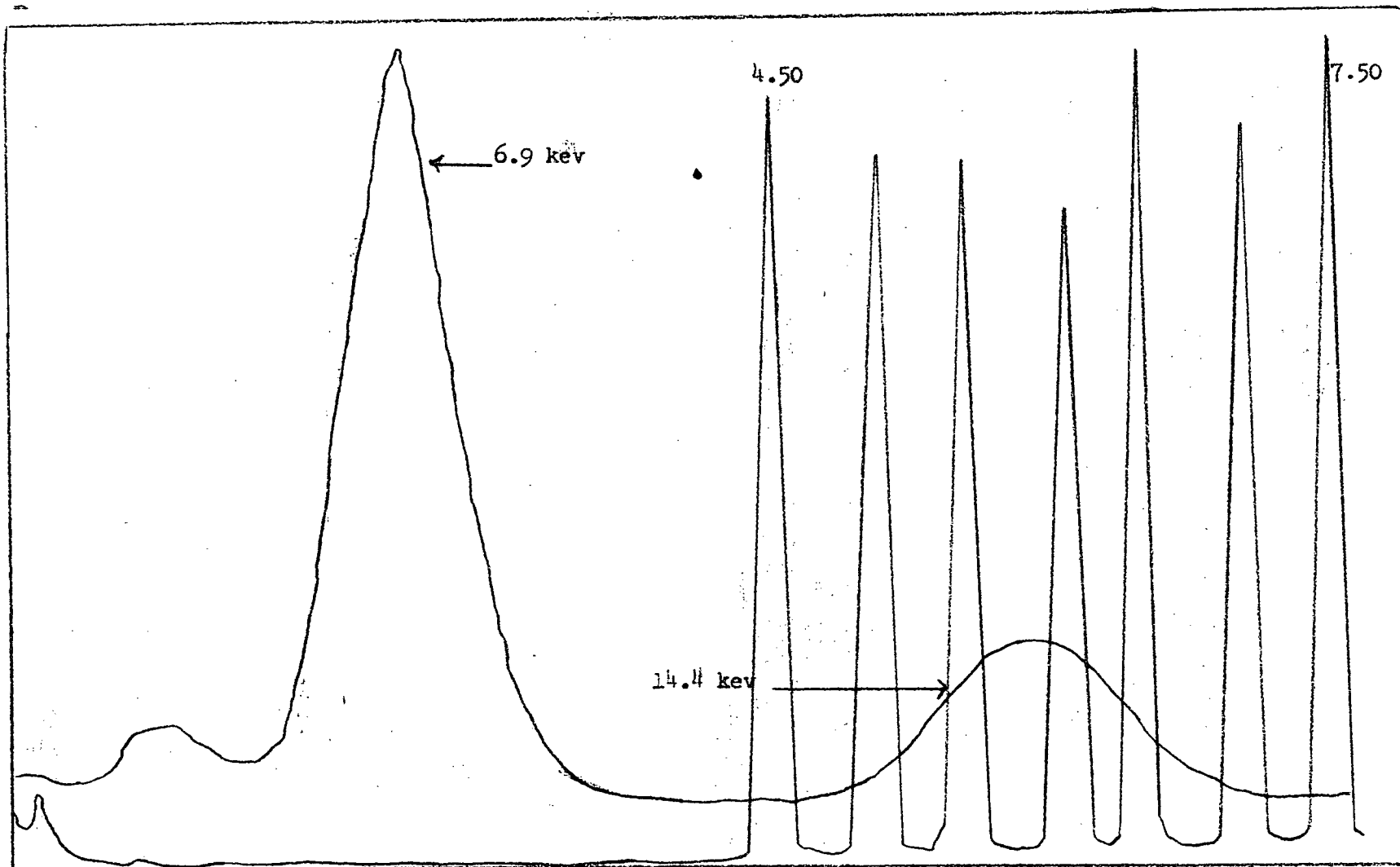
FIGURE III-10   A typical Fe^{57} spectrum obtained with the proportional counter. Calibration pulses are included.

3.2 The Electrical Apparatus

The electrical apparatus used in the experimental work is shown schematically in Fig. III-11. A list of the equipment is given in Table III-3.

Name of Apparatus	Description
Regulated high voltage supply	Model RE-5001AWL, Serial #218 Northeast Scientific Corporation
Pre-amplifier and amplifier	Amplifier unit type 1430A.Serial #1367. Dynatron Radio Ltd.
Single channel kicksorter	Pulse height analyzer, single channel Model 510.Serial #2633
Standard pulse generator	U.B.C. NP Scaler, Serial #7
Lathe drive motor	1/3 HP General Electric Motor
Switch	UND Laboratories Inc. #2HBW1
Scalers	Berkeley type, Made at U.B.C.
Multi-channel pulse height analyzer.	100 channel kicksorter. Computing Devices of Canada Ltd.

Table III-3

A circuit diagram of the pulse generator used for calibration purposes is given in Fig.III-12. Also included in this figure are the AC and DC supply circuits. The helipot used in the DC supply was made by Helipot Corporation.

The U.B.C. NP scaler was modified so that it produced an output signal sufficient to drive the Berkeley scalers. In addition, provision for a dead time of 15 microseconds was made in this scaler for it was found that with the dead times built into the scaler (i.e., .8,.2,5 and 50 microseconds), it was impossible to set the Berkeley so that they would
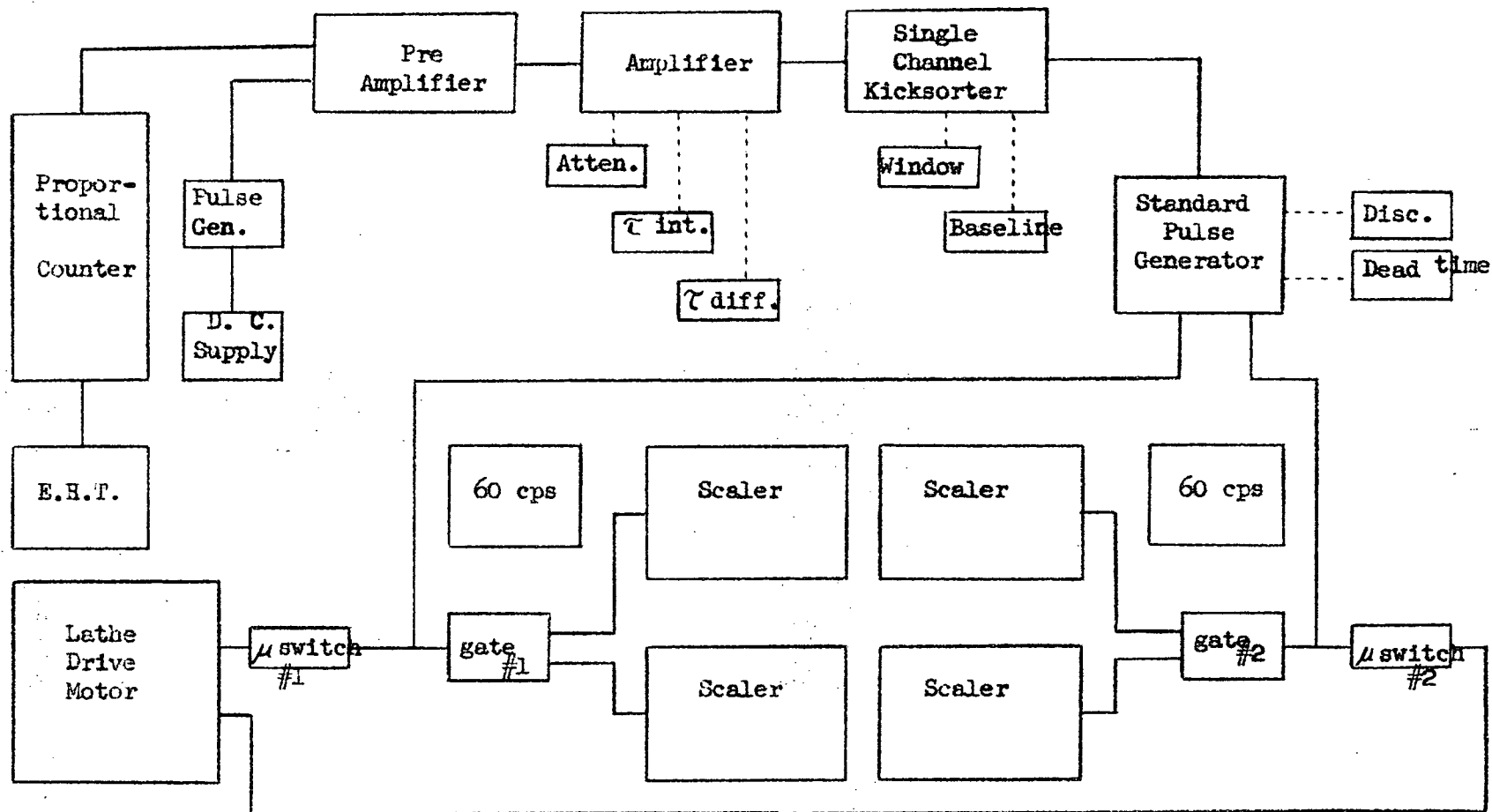
FIGURE III-11 A block diagram of the electrical apparatus.
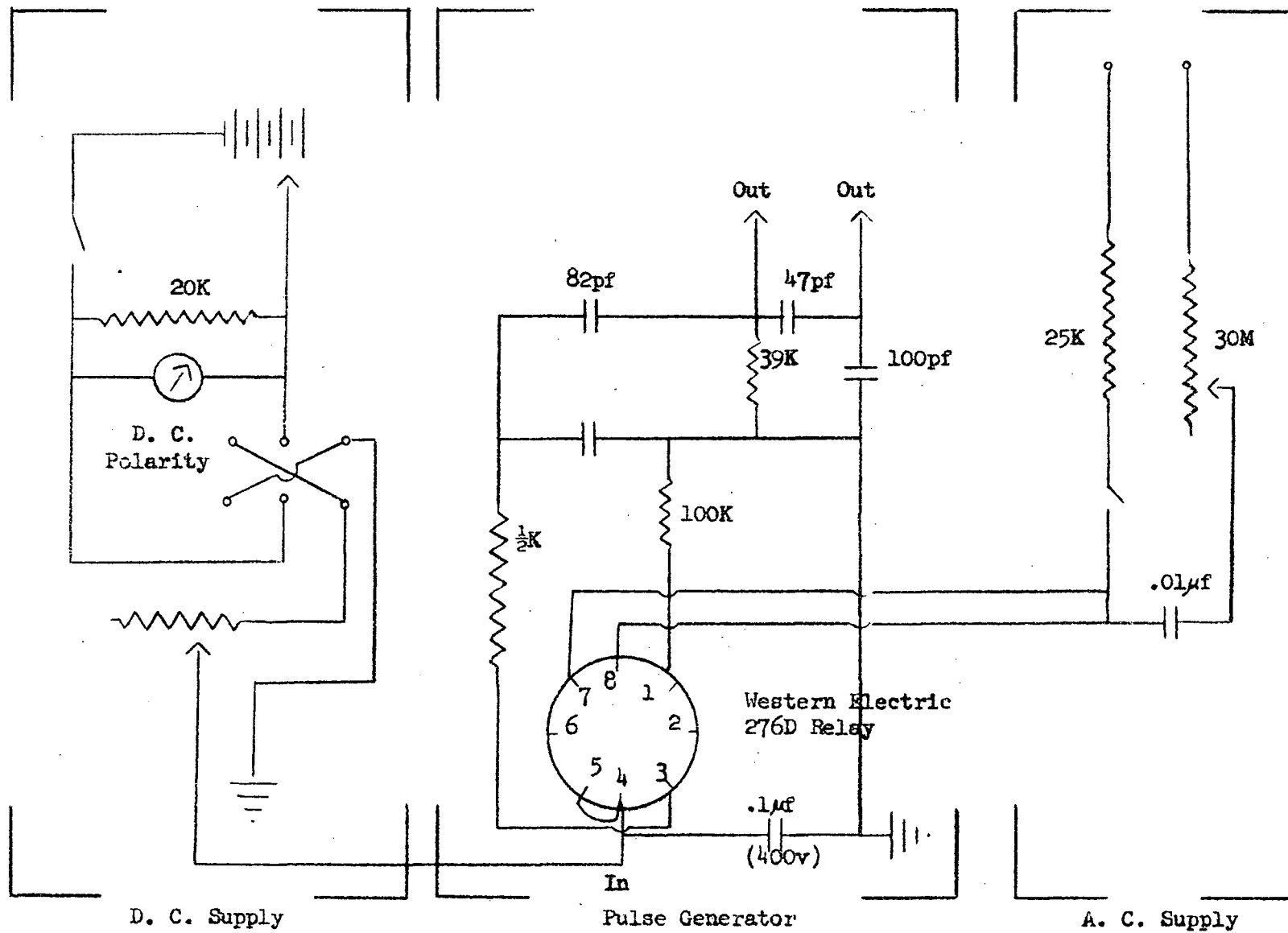
FIGURE III-12 A circuit diagram of the standard pulse generator used to produce the calibration
pulses.

all count in unison.

3.3 The Control System

A South Bend Precision Lathe (Model A, catalogue #Cl 644Z)
with a bed length $3\frac{1}{2}'$ was used to move the absorber relative to the source
at small constant velocity. To prevent vibrations present in the building
from reaching the source or absorber, the lathe was mounted upon a $\frac{1}{8}"$
piece of lead which in turn was mounted upon a 4' stand of cement blocks.
The lathe was accurately leveled and kept well oiled at all times to in-
sure that the motion of the lathe carriage was constant and reproduceable
and free of further vibration. An additional precaution against the ef-
fects of room vibrations was to enclose the lathe and detector in a sound
proof box. This box also tended to reduce temperature fluctuations of the
equipment within the box during the course of the experiments.

The gears of the lathe provided a range of 80 possible speeds,
40 each on direct and clutch drive. A 1/3 hp General Electric motor was
used to drive the lathe. Using a ratio of motor pulley to lathe pulley of
1/5, the range of speeds obtainable was .2cm/sec to .0025cm/sec. An
O-ring #1820-72 was used instead of a pulley belt to reduce vibrations
from the lathe drive. The limits and direction of motion of the lathe
carriage was controlled by means of two microswitches attached to the
lathe bed. These microswitches were arranged so that the lathe carriage
travelled 2.3cm. The microswitches also controlled the operation of the
Berkeley scalers so that they counted only when the lathe carriage was
moving in the correct direction and at the correct speed. One of each
pair of scalers recorded the number of transmitted gamma rays, the other
the 60 cps mains frequency. The switching circuit is shown in Fig.III-13.

Line 115v, AC

V8 V7

Hammond 167D60

6.3v, 2amp, AC

GE Motor Starting Switch CR1061

III Power Relay

B2
B1 B5
B3 B6
B2
B2

See Mossbauer Lab. Book #II, BLW, p5

Drive Motor Reversing Switch B numbers refer to motor terminal labels

KRP11A

X
2
7
4 1
3
5 8
6 IV

Lathe dir. control relay

Lathe travel limit and reversing switches

switch

Black NC
Red
White
Brown

X   X'

guardian switch

Blue NC
Green

Dynatron #2   1 3   Red

Berkeley #2   1 3   Blue

Dynatron #4   1 3   Green

Black

NP-11

White

2 31 46 5

1 3
1 4
8 6

X
2
7

1 3
4

8 6
5

X
2
7

Alternate Sym.   II   KRP11A   KRP11A

FIGURE III-13 A schematic diagram showing the switching circuit used to control the direction of the lathe travel and the operation of the scalers.

The temperature of the source and absorber were monitored at all times by means of a copper-constantan thermocouple attached to them. A Hewlett-Packard DC voltmeter was used to measure the thermocouple voltage.

3.4 The Absorber

a) The Absorber Mount

The absorber was fixed to the lathe carriage by means of a mount consisting of two squares of $\frac{1}{4}$" aluminium, each of which had a 2" diameter circle cut from its centre. The thin absorber was placed between two $\frac{1}{4}$" pieces of styrofoam and then clamped beteen the two pieces of aluminium. The styrofoam acted both as a support for the foil by damping out induced vibration and as a temperature shield tending to keep the absorber at a constant and uniform temperature regardless of the source temperature. The absorber mount was screwed to a 1" diameter brass cylinder which in turn was tightly fixed to the lathe carriage.

b) Armco Iron Absorbers

In the course of the preliminary work on the Mossbauer effect several types of materials were used as absorbers. However, it was decided that since small shifts were to be investigated, that pure Armco iron would be the most satisfactory. The two foils of Armco iron which were used were obtained from the Hamilton Watch Co. These foils were rolled to .0002" and .00035" thicknesses. Also used for certain measurements was a .001" shim steel foil. The Armco iron foils were annealed in an Ar atmosphere for a period of one hour at 950°C before being used. The .001" shim steel foil was likewise annealed but in an H_2 atmosphere. Since the Armco foils were difficult to obtain and were fragile, they were sprayed

with Acrylic plastic to give them added strength and protect them from corrosion. Unless otherwise stated, all absorption curves included in this thesis were obtained using the two Armco iron foils mounted together to give an effective thickness of .00055". The reason for this choice of thickness is given in section 3.9. Appendix B outlines the method that could be used in the preparation of an enriched Fe^{57} absorber.

3.5 The Source

a) The Mount

The source mount had to serve two purposes; to rigidly clamp the source to the lathe bed and to enable the temperature of the source to be varied from $100^{\circ}K$ to $500^{\circ}K$. The mount shown in Fig.III-14 was used for temperatures of $300^{\circ}K$ and higher. The pressure within the pot was reduced to 15 microns when the temperature was increased to prevent the Fe source from oxidizing and to provide sufficient temperature insulation so that a constant source temperature could be maintained. In order to maintain the reduced pressure without pumping, it was necessary to replace the .001" mylar window originally used with the .005" mylar window shown in Fig. III-14 and the covar seals had to be coated with R313. The source was heated with the heating unit from a soldering iron, placed in the inner pot.

Preliminary investigations proved that the use of the above pot filled with liquid nitrogen to obtain the temperatures in the region of $100^{\circ}K$ was not an acceptable method of lowering the temperature of the source. The vibrations from the boiling nitrogen (and other low temperature mixtures) in the pot were transmitted to the source and hence, broad-
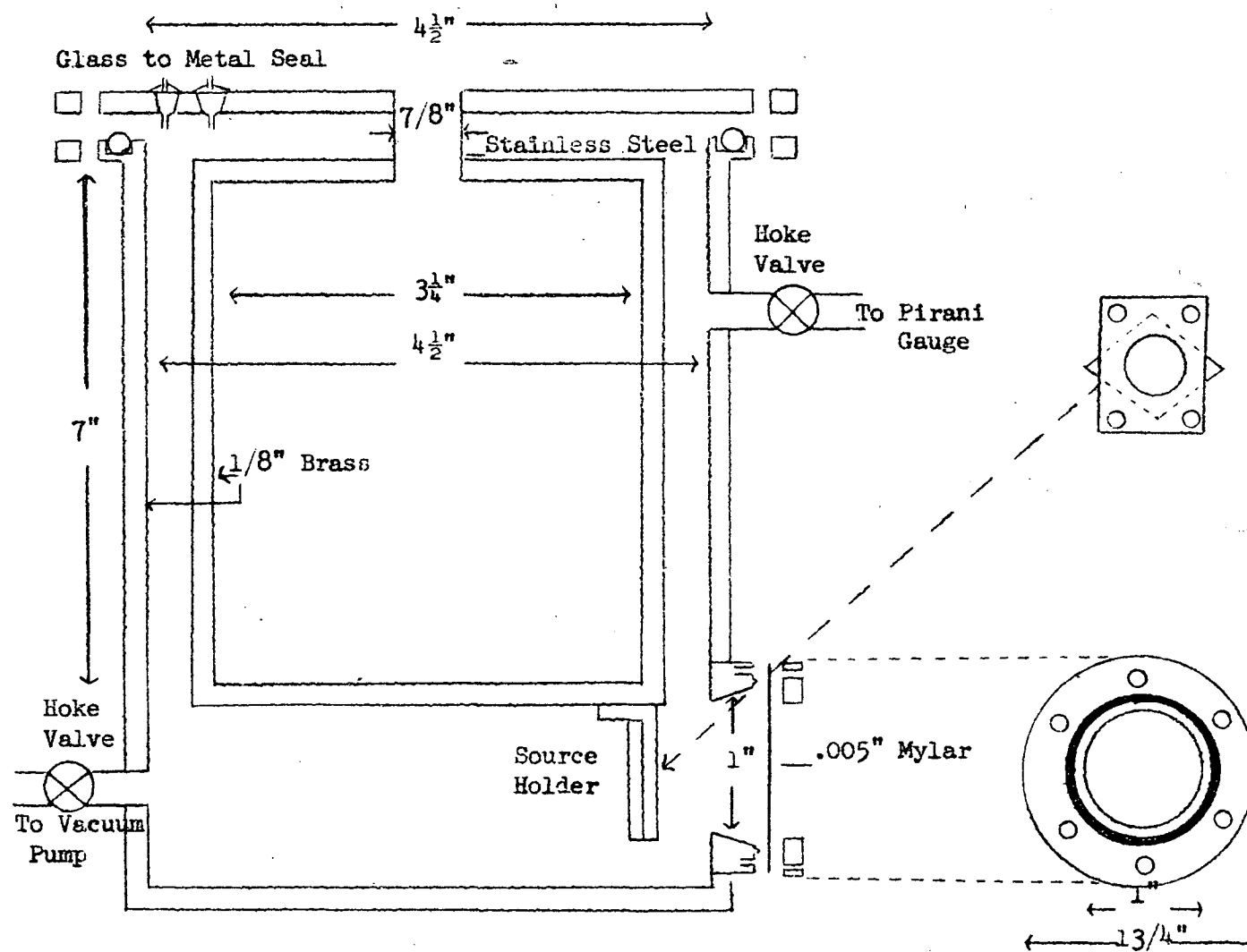
FIGURE III-14   The source mount used for source temperatures at or above room temperature.

ened Mossbauer line to an observable but incalculable extent. To over-
come this difficulty the inner pot shown in Fig.III-14 was replaced with
that shown in Fig. III-15, for all source temperatures below $300^\circ K$. The
low temperatures were obtained by forcing the liquid nitrogen vapour
through the stainless steel tubes. The liquid nitrogen reservoir used was
7" in diameter, 1' deep and surrounded by a layer of 2" styrofoam. The rate
of flow of the vapour and hence, the temperature of the source was controlled
by means of a 600 watt heating unit placed in the liquid nitrogen reservoir
and a variac to which the heating unit was attached. As the level of the
liquid nitrogen decreased, it was found that the voltage of the heater
had to be increased slightly to keep the source temperature constant. To
improve the heat insulation, the pressure of the pot was reduced to 15
microns and an aluminium radiation shield was erected around three quarters
of the inner surface of the outer pot. In order to prevent the vibration
of the liquid nitrogen from reaching the source, polyethylene tubing
was used to connect the nitrogen reservoir and the source mount. It was
found necessary to surround the tubing with 2" of styrofoam in order to
reach temperatures below $200^\circ K$. A piece of rubber tubing was connected
to the output stainless steel tube of the source holder to remove the
cold nitrogen gas from the equipment box and thereby insured that the
absorber temperature remained steady at room temperature.

b) Sources

The source used for the preliminary investigations was prepared
by Dr. J. B. Warren. This, and all other sources, was Co^{57}. 1 mc of
Co^{57} was co-plated with Fe^{56} in the ratio of 1:500 onto a one-quarter inch
square copper bar. The plating solution, $FeSO_4$, was absorbed in a piece
of absorbent cotton wrapped about the platinum anode. The Co^{57}/Fe mixture
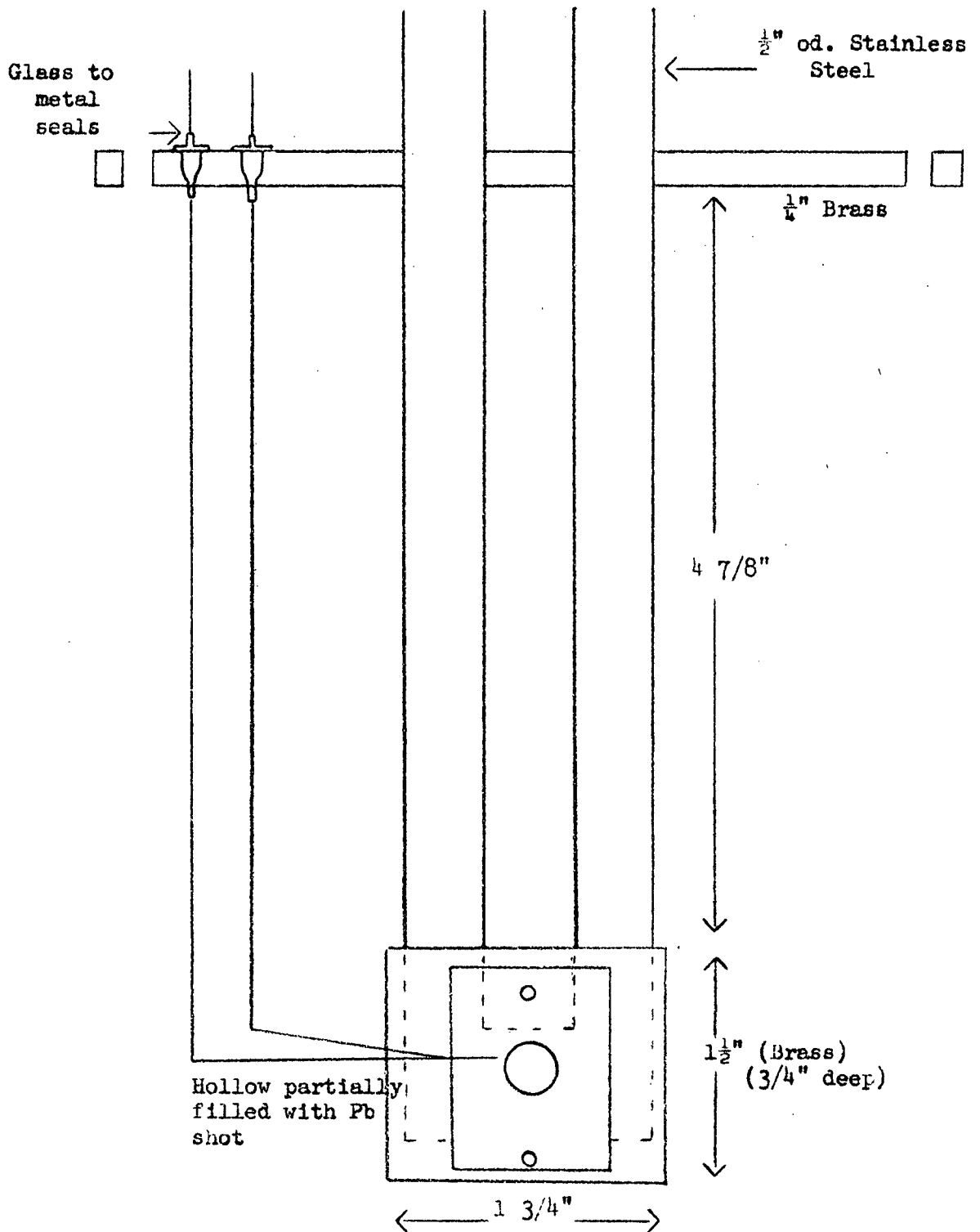
FIGURE III-15 The source mount used for source temperatures below
room temperature.

was deposited by rubbing the copper rod with this anode arrangement. The current density used was 50 ma/cm^2.

The two sources of Co^{57} were obtained from the Nuclear Science and Engineering Corporation. The first of these, NSEC #1, was 1 mc and the second, NSEC #2, was 4 mc. The Co^{57} was 99.9% pure and electroplated upon .005" Armco iron. The cost of the Co^{57} was $75.00 per mc and a charge of $75.00 was made for the electroplating. The active material was confined to an area of .5 square centimetres. The Co^{57} of NSEC #1 was diffused onto the iron (Armco) backing in an argon atmosphere at 900°C for one hour. The annealing of NSEC #2 is described in detail in Chapter IV. Briefly, this treatment consisted of five steps of ten minutes each, during which the source was heated to 900°C in an Ar atmosphere. NSEC #2 was used for the experimental results included in this thesis.

3.6 The Measured Quantity

The quantity measured was the transmission of the 14.4 kev gamma ray of Fe^{57} through an Fe absorber as a function of the velocity of the absorber relative to the source under various experimental conditions. With infinite velocity between source and absorber, electronic absorption occurs only whereas at very small relative velocities, both electronic and Mossbauer (recoilless) absorption occur. This change in transmission with relative velocities produces the Mossbauer velocity spectrum. The measured transmission is normalized by forming the ratio:

$$R_m(v) = \frac{T(v)}{T(v = .14)}$$

where velocity $v = .14$cm/sec (rather than v) was used for experimental con-

venience. The measured line intensity therefore is $h = 1-R_m(v = 0)$ and will differ from the calculated line intensity (Equation II-11). This definition of h also means that the measured Mossbauer line width $\triangle$ (i.e., the width at h/2) will differ from the calculated width, d. In the following, the quantities h and $\triangle$ will be considered except when a comparison between theory and experiment is to be made at which time h and $\triangle$ will be adjusted to fit data for $v = \infty$ rather than $v = .14$cm/sec.

3.7 Geometric Effects on R(v)

In Chapter II the function R(v) was defined as T(total,v) which by the substitution of Eqn.II-17 becomes:

$$R(v) = 1 + f + \sum_{j=1}^{3} W_{jk} \frac{f\Gamma}{\pi} \int_{-\infty}^{\infty} \frac{dE \exp\left[\frac{-W_{jk}\tau\Gamma^2/4}{E^2 + \Gamma^2/4}\right]}{(E+S)^2 + \Gamma^2/4} \left[1 - \Phi\left(\frac{W_{jk}\tau\Gamma^2/4}{2[(E+S)^2+\Gamma^2/4]} + \frac{\mu t}{2}\right)\right] \times$$

$$\exp\left[\frac{W_{jk}\tau\Gamma^2/4}{2[(E+S)^2+\Gamma^2/4]} + \frac{\mu t}{2}\right]^2 \div \exp\left(\frac{\mu t}{2}\right)^2 \left[1 - \Phi\left(\frac{\mu t}{2}\right)\right]$$

<div align="right">III-6</div>

for a six line emission and absorption spectra. This equation is complete in that it accounts for the source thickness and the hyperfine splitting of the 14.4 kev transition of Fe^{57} but the influence of the small but finite solid angle into which the gamma rays can radiate and still be detected by the gamma ray spectrometer, is ignored. This solid angle produces a finite width to the first order Doppler shift obtained with a given velocity and also increases the effective thickness of the absorber and proportional counter and hence, must be taken into account when interpreting the experimental measurements (see Fig. III-16). The parameter which determines the magnitude of the effects is $\emptyset$, the angle between the
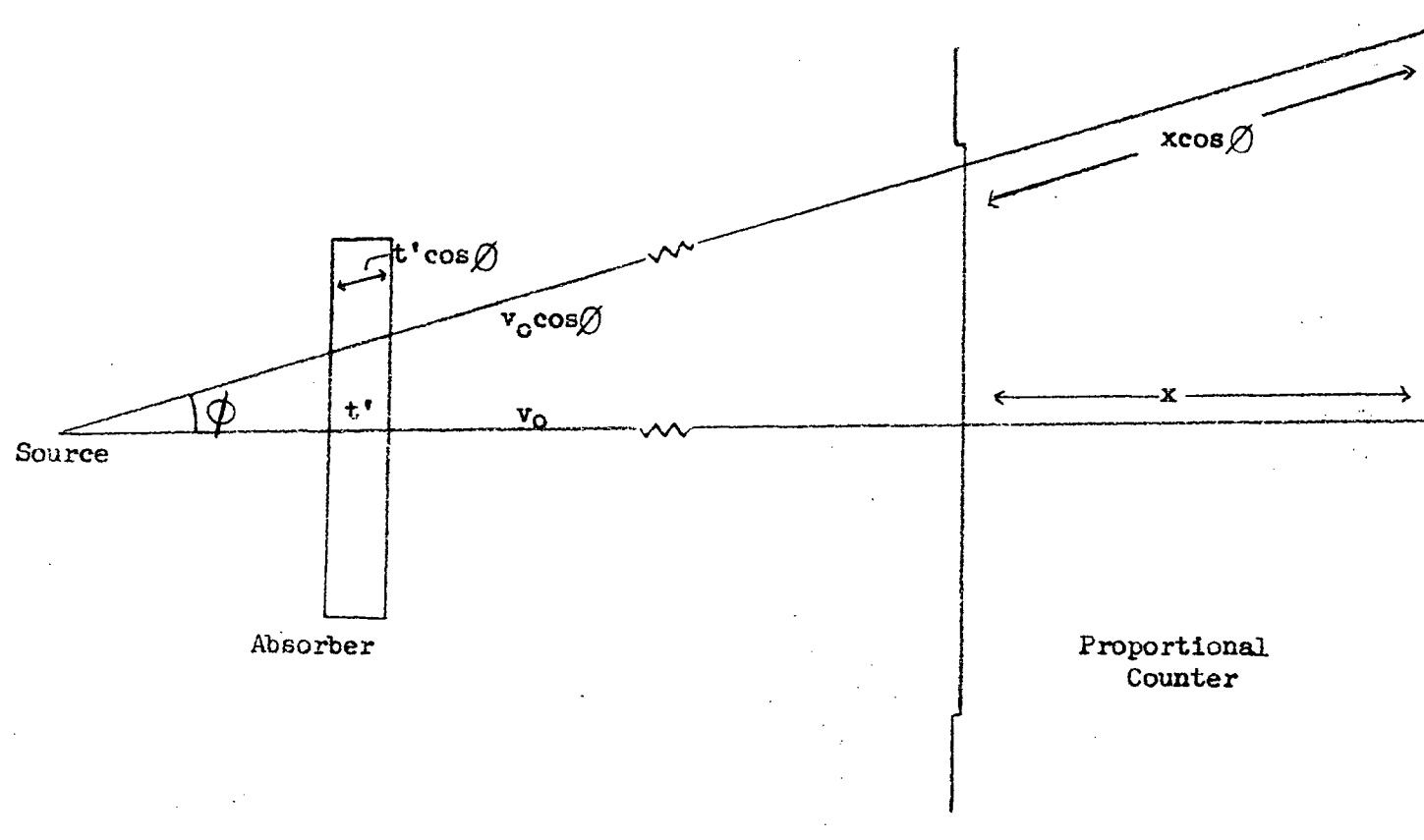
FIGURE III-16   A schematic representation of the arrangement of the source, absorber, and Proportional counter. The scale has been adjusted to emphasize the effect on the velocity, v_0, the absorber thickness, t', and the proportional counter thickness, x, of the geometry.

line joining the source and detector and the vector at relative velocity.

The effect of the experimental geometry on R(v) has been calculated in Appendix C. The result of this consideration is that Eqn.III-6 must be replaced by:

$$R(v,\phi) = 1-f\left[1-.97\sum_{j=1}^{3}\frac{W_{jk}}{\pi}\int_{-\infty}^{\infty}\frac{dE\exp(-W_{jk}\tau\Gamma^2/4)}{(E+S)^2+\Gamma^2/4}\left[1-\overline{\phi}\left(\frac{W_{jk}\tau\Gamma^2/4}{2[(E+S)^2+\Gamma^2/4]}+\frac{\mu t}{2}\right)\right]\right.$$

$$x \quad \exp\left(\frac{W_{jk}\tau\Gamma^2/4}{2[(E+S)^2+\Gamma^2/4]}+\frac{\mu t}{2}\right)\div\exp\left(\frac{\mu t}{2}\right)^2\left[1-\overline{\phi}\left(\frac{\mu t}{2}\right)\right] \qquad \text{III-7}$$

in which the factor .97 corrects the originally calculated $R(v,\phi=0)$ to the experimental conditions under which $R_m(v,\phi)$ is measured. The correction factor .97 is that required for a .001" absorber. Those factors necessary for other absorber thicknesses are given in Appendix C.

3.8 Background Correction

Inspection of the spectrum of Fe^{57} (see for example, Fig.III-10) shows that the 14.4 kev peak is superimposed upon a continuum of background radiation. In the calculation of $R_m(v)$, this background count rate must be subtracted so that only the count rate of the 14.4 kev transition is considered in the results. Therefore $R_m(v)$ is calculated as:

$$R_m(v) = \frac{N(v) - N_b}{N(v=.14) - N_b} \qquad \text{III-8}$$

where N is the total count rate at v and N_b is the background count rate.

For zero relative velocity between the source and absorber, and for equal (dead time corrected) counting times, the Fe^{57} spectra transmitted through the Fe absorber and through a 1/16" aluminium absorber
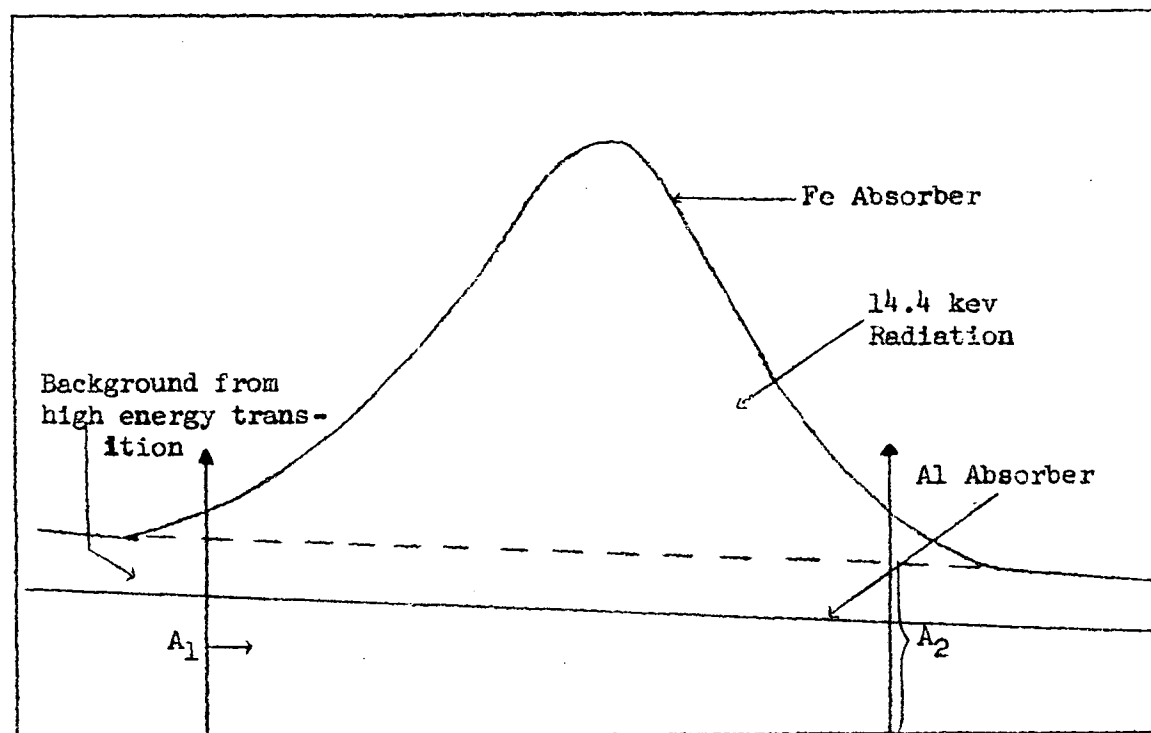
FIGURE III-17   The transmission of 14.4 kev radiation through a .00055"
Armco iron and a 1/16" Al absorber. From such a spectrum
the background correction was made.

were measured thus determining the background rate N_b. Calculations showed that the aluminium absorber would absorb all of the 14.4 kev radiation incident upon it so that only background radiation of reduced intensity would be measured when this absorber was used. The area of the background radiation within the window settings of the single channel kicksorter was measured for both spectra (see diagram, Fig.III-17). The count rate of the background radiation transmitted through the aluminium absorber was measured. Hence, N_b is

$$N_b = \frac{A_{Fe}(N_{Al})}{A_{Al}}$$

where N_{Al} is the count rate of the transmitted through the aluminium absorber.

III-9

and therefore

$$R_m(v) = \frac{N(v) - \frac{A_{Fe}(N_{Al})}{A_{Al}}}{N(v = .14) - \frac{A_{Fe}(N_{Al})}{A_{Al}}}$$

III-10

All experimental measurements involving $R_m(v)$ used in the determination of results given in this thesis are corrected in this manner for the background unless otherwise noted.

The accuracy of the above correction is dependent upon the accuracy with which the dead time was measured. In the experimental work the dead time was $(8 \pm 1)\%$ so that the error in the determination of N_b was approximately 1%. Moreover, since N_b is almost 1/3 $N(v)$, the total error in the determination of the background correction $R_m(v)$ was approximately .3%.

3.9 Selection of the Absorber

As mentioned in section 3.3, a number of absorbers of various thicknesses were available for the experimental investigations. It was necessary therefore, to determine which of these absorbers would give the most significant results in a given time T, that is, maximize the expression X/e, where X is the difference in the count rate transmission at $v = 0$ and $v = .14$ cm/sec and e is the statistical error for the measured count rates. In Appendix D it is shown that

$$X/e = f(N_s)^{\frac{1}{2}} e^{-\mu e^x/2} (1-e^{-\mu_m x/2} I_0(\frac{\mu_m x}{2})$$ III-11

where N_s is the source strength . For Fe^{57}, the absorber thickness x at which X/e is a maximum, depends upon the value of the Debye-Waller factor f and upon the fraction of absorber atoms which are Fe^{57}.

The value of X/e was measured for various absorber thicknesses for both NSEC #1 and #2. Moreover, for the same absorber thicknesses, X/e was calculated using Eqn. III-11 for $f = .4$, .6 and .7.

Absorber Thickness	NSEC #1	NSEC #2	f = .4	f = .6	f = .7
.0002"	25.78	25.78	25.78	25.78	25.78
.00035"	45.70	39.00	35.60	33.63	34.02
.00055"	57.30	54.83	41.41	35.80	37.60
.001"	57.77	55.98	41.70	31.96	34.46
.00155"	49.44	--	39.15	23.81	26.21

Table III-4

The values of X/e for various absorber thicknesses as measured for NSEC #1&2 and calculated for f .4, .6 and .7.

Since the reason for this procedure was to determine the optimum thickness of the absorber, the values found in the above table have been nor-

malized so that X/e for $x = .0002"$ is the same for all calculations. Hence, the trend of X/e for all cases can be compared. The count rates used for the NSEC #1 data required four minutes to accumulate whereas those for NSEC #2 required one minute. Corrections were made for the dead time of the apparatus in each case but correction for background radiation was not made, since only relative values of X/e were required.

The data in Table III-4 is given in graphical form in Fig.III-1B. The dependence of X/e on absorber thickness for NSEC #2 is seen from this figure to be the same, within experimental error. X/e attains a maximum value at $x = 5.7 \times 10^{-4}$ inches for $f = .7$ and at $x = (8.0 \pm .5) \times 10^{-4}$ inches for the NSEC #2. The experimental results show that there is a negligible difference in the significance attained with absorber thicknesses of 5.5×10^{-4} inches and 1.0×10^{-3} inches. The choice of absorber thickness of 5.5×10^{-4} inches was therefore based upon the fact that the accumulation of results was faster with the thinner absorber and its closeness to the theoretically determined optimum thickness (assuming $f = .7$ for Fe^{57}) of 5.7×10^{-4} inches.
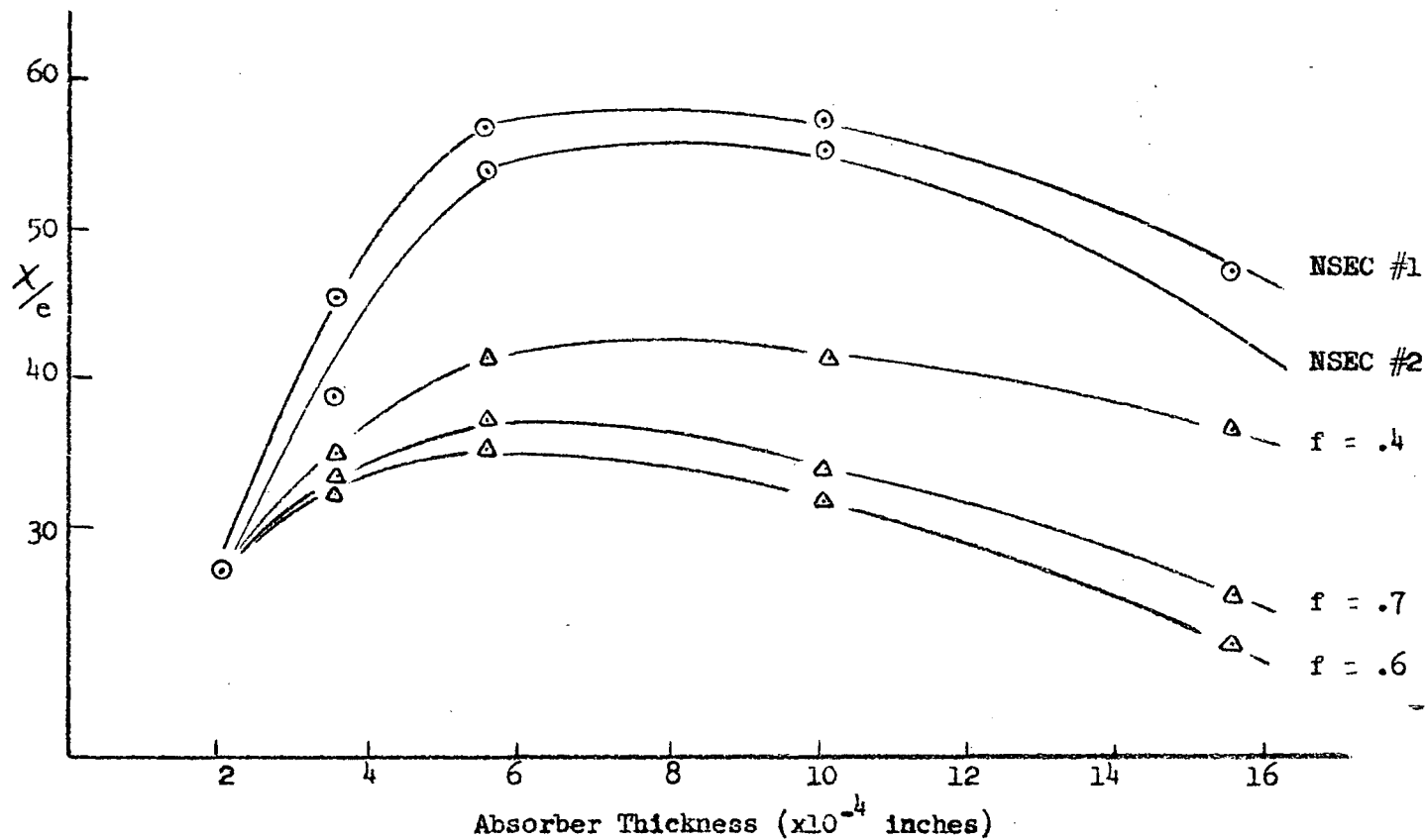
FIGURE III-18 The ratio of the difference of the count rate of the 14.4 kev rays, χ, to the statistical error in the count rate, e, as a function of the absorber thickness.

Chapter IV

DIFFUSION OF Co^{57} INTO NATURAL IRON

4.0 Introduction

The usual method of preparing a radioactive source for a Mössbauer experiment is to electroplate or evaporate the radioactive material onto a non-radioactive metallic lattice and to diffuse the radioactive material into the lattice. Pound and Rebka[20] were the first to notice that the diffusion procedure remarkably improved the magnitude of the Mössbauer effect obtainable. The source used in this experiment was made in a similar manner but the diffusion procedure was done in a series of five short steps rather than in one or two so that the Co^{57} could be diffused in a controlled and continuously monitored fashion to the minimum depth at which the measured Mössbauer effect was equal to the calculated effect (17.9% for a natural iron absorber of thickness .00055"). Such a controlled diffusion results in a source with optimum properties. In addition, this procedure made it possible to measure the Mössbauer line parameters (height h, width Δ, and shift ℓ) as a function of the depth to which the radioactive atoms had diffused.

The dependence of these parameters on diffusion depth is due to the fact that as the Co^{57} diffuses into the natural iron, the lattice surrounding the radiating Fe^{57} nucleus changes from the non-uniform Co^{57} lattice resulting from the initial deposition process to a uniform lattice of a weak solution of Co in Fe. Since accurate measurements of small line shifts and variations in line widths were to be measured with this source,

the diffusion process was continued until a narrow line and a large Mössbauer intensity were produced.

The velocity spectrum showed the presence of two small auxiliary peaks on either side of the main line. These peaks appear to be associated with a zero or small internal magnetic field at the sites of some of the Fe^{57} atoms.

Before the apparatus and method used in the diffusion procedure are discussed, a brief summary of the theory (both general and particular to this thesis) of diffusion is given. The remainder of the chapter contains the experimental results and a discussion thereof.

4.1 Theory of Diffusion

a) General Diffusion Theory

Diffusion of one solid into another is governed by Flick's Law[21]

$$dm = DA \frac{d\ c(x)\ dt}{dx} \qquad\qquad IV-1$$

where dm is the mass diffusing across area A, $c(x)$ is the concentration of diffusing atoms at depth x, and D is the diffusion coefficient. This coefficient (D) gives the rate at which diffusion takes place. It depends strongly upon temperature according to the equation[21]

$$D = D_o \exp(-Q'/\mathcal{R}\theta) \qquad\qquad IV-2$$

where D_o is a constant, $\mathcal{R}$ is the gas constant, θ is the absolute temperature, and Q' is the approximate binding energy of the crystal.

In order to calculate the rms diffusion depth, it is necessary to know the coefficient D. This coefficient can be calculated by measuring the activity of a radioactive solute before and after its diffusion and then substituting these quantities into the equation,[22]

$$r = e^z(1 - \oint \sqrt{z})$$
IV-3

where r is the ratio of counting rates, z is $\mu^2 Dt$ and μ is the linear coefficient of the detected radiation. $\oint$ is $\frac{2}{\sqrt{\pi}} \int_0^y e^{-x^2} dx$. The above equation is subjected to the two assumptions:

a) The radioactive deposit before diffusion is infinitely thin.

b) The radioactive material diffuses into a semi-infinite cylinder along the direction of the cylinder's axis.

The value of D obtained by Carter and Richardson in this was for Co diffusing into Fe compounds at T 850°C, agrees well with that calculated by them by a more accurate method.

Under the same assumptions as above, the concentration of diffused atoms at depth x is given by

$$c(x) = \frac{Q}{\sqrt{\pi Dt}} \exp(-x^2/4Dt)$$
IV-4

from which (see Appendix E) the equation

$$(\overline{x^2})^{\frac{1}{2}} = \sqrt{2Dt}$$
IV-5

giving the rms penetration, is derived.

b) Theory of the Diffusion of Co^{57} into Fe

When a Mossbauer source is prepared by the electrodeposition of Co^{57} onto an Fe lattice, the Fe^{57m} nucleus, when it emits the 14.4 kev

ray, is located in a Co lattice rather than an Fe lattice like the absorbing Fe^{57} nucleus. As the Co^{57} is diffused into the Fe lattice the concentration of Co^{57} diminishes so that the Fe^{57} nuclei become part of an Fe lattice rather than a Co lattice and are subject to essentially the same bonds as are the Fe nuclei. The diffusion treatment therefore, reduces the difference in Debye temperatures and chemical bond effects between the source and absorber lattices which in turn, reduces or eliminates the line shift of the Mossbauer spectrum. The fact that the diffusion treatment increases the observed Mossbauer intensity implies that the bonds on the Co^{57} atoms in the electroplated or evaporated deposit are weak or inhomogeneous. The diffusion process also varies the apparent width of the Mossbauer line.

In section 2.4 it was noted that any difference in the fields at the nuclei of the source and absorber would produce a broadened line. At $300^{\circ}K$, the internal field at an Fe^{57} nucleus embedded in an Fe lattice is 3.33×10^5oe., whereas that in a Co lattice is 3.045×10^5oe. (a difference in internal fields of $.295 \times 10^5$oe.). Using equation II-44, the increase in line width produced by this difference in internal magnetic fields is calculated to be 3.27×10^{-8} ev.(compare with the expected width for this source and absorber of 9.0×10^{-9}ev). As the Co^{57} is diffused into the Fe lattice, the difference in the internal fields decreases, thereby decreasing the line width.

A summary of the conditions described by other authors under which sources for the Mossbauer experiments have been diffused, is given in Table IV-1.

Source Preparation	Source	Lattice Material	Diffusion Temperature	Diffusion Time	Atmosphere	Ref.
Electro.	Ga^{67}	ZnO	1000°C	60 min.	air	22
Electro.	Co^{57}	S.S.	900°C	60 min.	hydrogen	23
Electro.	Co^{57}	Armco Iron	900-1000°C	60 min.	hydrogen	24
Evap.	Co^{57}	S.S.	950°C	-	vacuum	16
Electro.	Co^{57}	CoPd	1000°C	120 min.	vacuum	25

Table IV-1

4.2 Apparatus

The apparatus used in the diffusion of the Co^{57} source into a .005" Armco iron lattice is shown in Figs. IV-1 and IV-2. The apparatus to hold the source in the quartz tube had to be designed in a manner such that its heat capacity was small, thus requiring a very short time to change from room temperature to the temperature used for the diffusion and its heat conductance was low so that little heat was lost down the supporting tube. Also, its strength was sufficient so that the source could be moved in and out of the furnace without the risk of dropping it in the quartz tube. A combination of an iron (.010") boat and thin walled stainless steel tubing met these specifications. The iron boat was spot welded to the steel tubing. The ceramic two-hole tube within the steel tubing ensured that the thermocouple wires did not short either to each other or to the stainless steel tube and in addition, increased the strength of the boat handle. The hot junction of the chromel-alumel thermocouple was attached to the iron boat by laying a piece of .001" shim steel over the junction and spot welding this overlay to the 'boat'.

In order to have a continous record of the temperature during the diffusion, the thermocouple voltage was recorded on a Brown recorder.
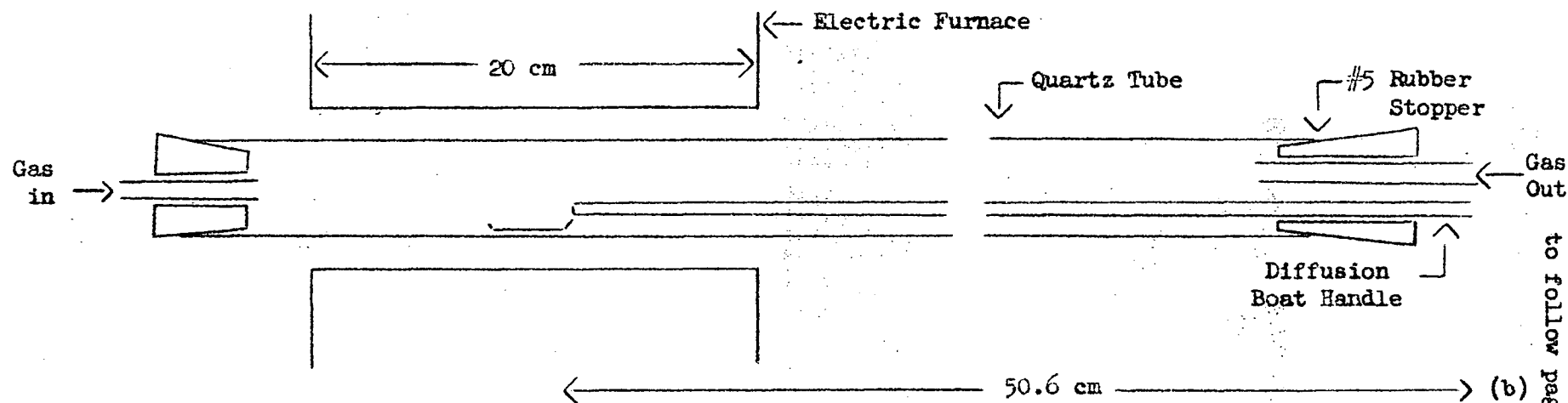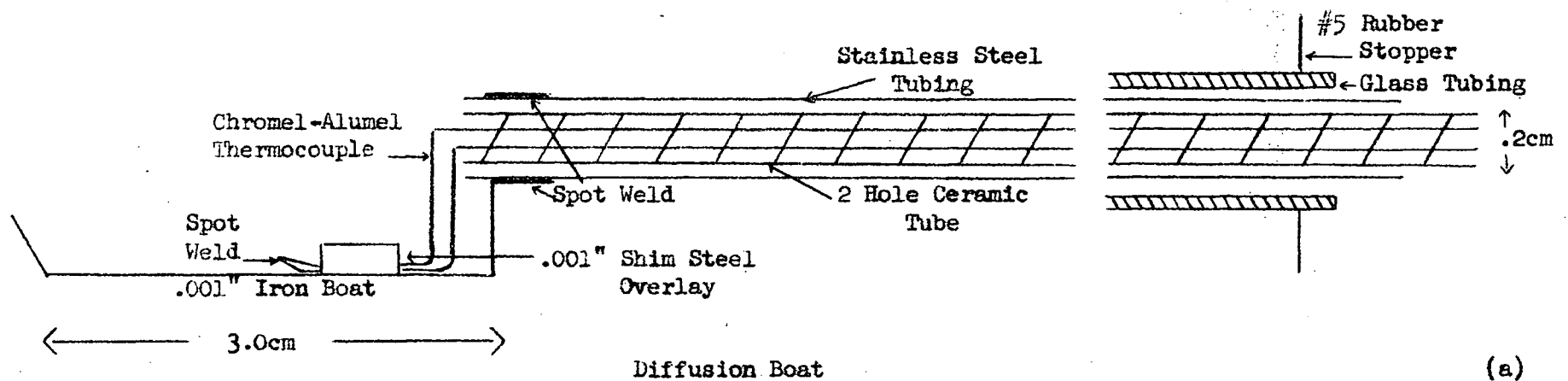
FIGURE IV-1 (a) The boat in which the Co^{57} source was diffused into an Fe lattice. (b) The arrangement of the diffusion apparatus.

The 1K Spectrol helipot (#495086) was used to reduce the thermocouple voltage (at $900^{\circ}C$, $V = 90mv$) to a value that could be fed into the Brown recorder (Model 153X12V-X-30A1, Serial #6471253) which has a full scale deflection of 10mv. The potentiometer was set such that the boiling water-ice temperature difference corresponded to 1mv on the Brown recorder.

The arrangement of the apparatus is shown schematically in Fig. IV-1b. The flow of gas was indicated by a water bubbler. Factors determining the use of argon were a) it is safer to use (particularly at high temperatures) than hydrogen, b) the apparatus needed for an argon atmosphere is much simpler than that required for a vacuum or hydrogen and c) it provides the necessary inert atmosphere. The argon used was 99.9975% Ar, .0008% O_2, .0013% N_2 and .0004% H_2. The oven heater arrangement is shown in Fig. IV-2b where the oven used was a Hoskins Electric Furnace (FD 303A, serial #33553, 110V, 5A). To obtain $900^{\circ}C$ inside the furnace, the variac setting had to be 82.8V. A fan was arranged to blow on the exterior of the quartz tube at the gas exit end to increase the rate at which the diffusion boat and source returned to room temperature at the end of each run.

4.3 Procedure

a) The central section of the quartz tube was heated to a predetermined temperature. This took about thirty minutes.

b) The source was placed in the boat at the gas exit end of the quartz tube. The flow of argon was increased to a flow producing 240 bubbles per minute when the gas tubing was inserted $\frac{1}{4}$" into the water. The flow was maintained at this rate for at least five minutes before a heating cycle commenced to remove any air from the tube.

To Brown Recorder

Spot Welded
Oven Junction

Chromel-Alumel
Thermocouple

1K 3 turn Spectrol

Spot Welded
Ice Junction

Thermocouple Arrangement   (a)

| Mains | | Solar | | Variac | | Furnace |

Set at 82.8v

Ammeter

Oven Heater Arrangement   (b)
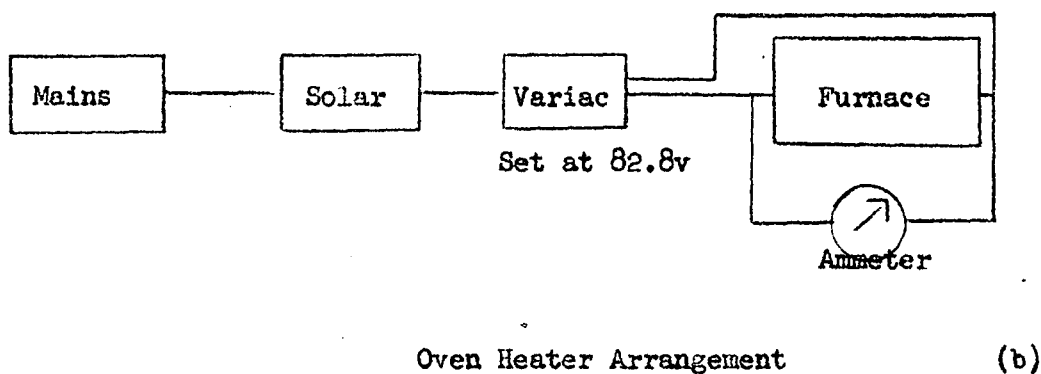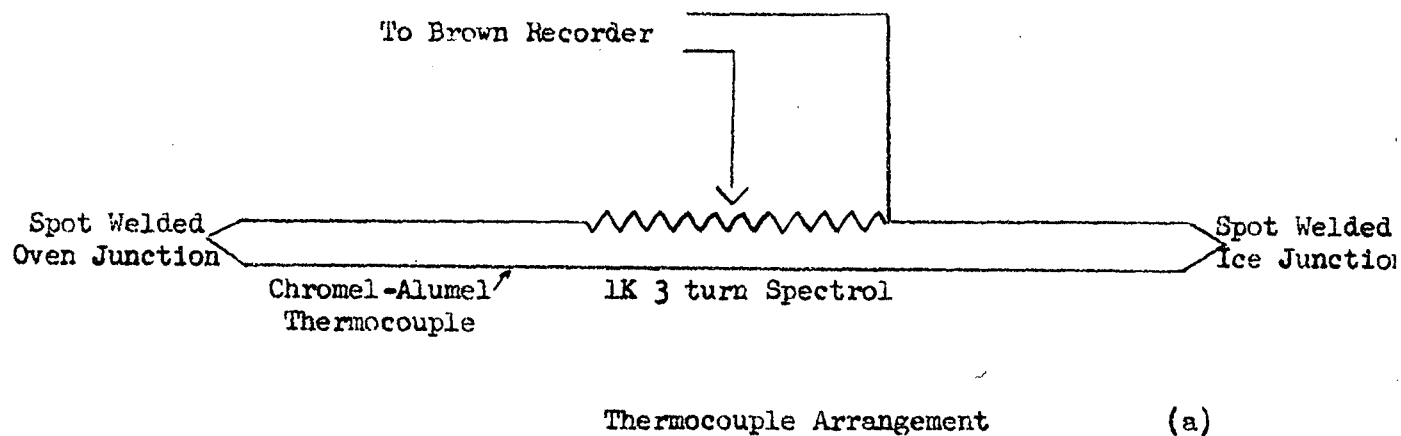
FIGURE IV-2   Schematic diagram showing (a) the thermocouple
               arrangement and (b) the oven heater arrangement
               used in the diffusing of Co^{57} into a Fe lattice.

c) The flow rate was decreased to 85 bubbles per minute and the system was allowed five minutes to reach thermal equilibrium.

d) The source and assembly were quickly inserted into the furnace to the position indicated in Fig. IV-1b, to raise the temperature of the source to 900°C. The temperature of the source was recorded as a function of time.

e) The source and assembly were then quickly withdrawn from the furnace to the cool end of the quartz tube and held there in the Ar atmosphere until the source returned to room temperature.

f) The source was removed and mounted in the Mossbauer apparatus. The count rate of both the 6.9 kev and 14.4 kev gamma rays were measured by putting the spectrum into the C.D.C. kicksorter. The dead time losses were taken into account in determining the count rates. Two source to counter distances were used for this measurement on each cycle - 153.3 cm and 69.2 cm.

g) The Mossbauer intensity and the shape of the resonant absorption spectrum was measured using the 0.00055" Armco iron absorber.

h) The procedure was repeated from step b.

Since the count rate due to the 4 mc source was high enough to cause coding troubles in the kicksorter, only every tenth pulse was put into the kicksorter. In order to do this, the output of the amplifier was fed into the UBC NP scaler and the input to the second unit of the scaler triggered the kicksorter (coincidence mode used). Fig. IV-3 is a reproduction of a typical temperature versus time trace made on the Brown recorder.

$n = 2$

Time (in Minutes)
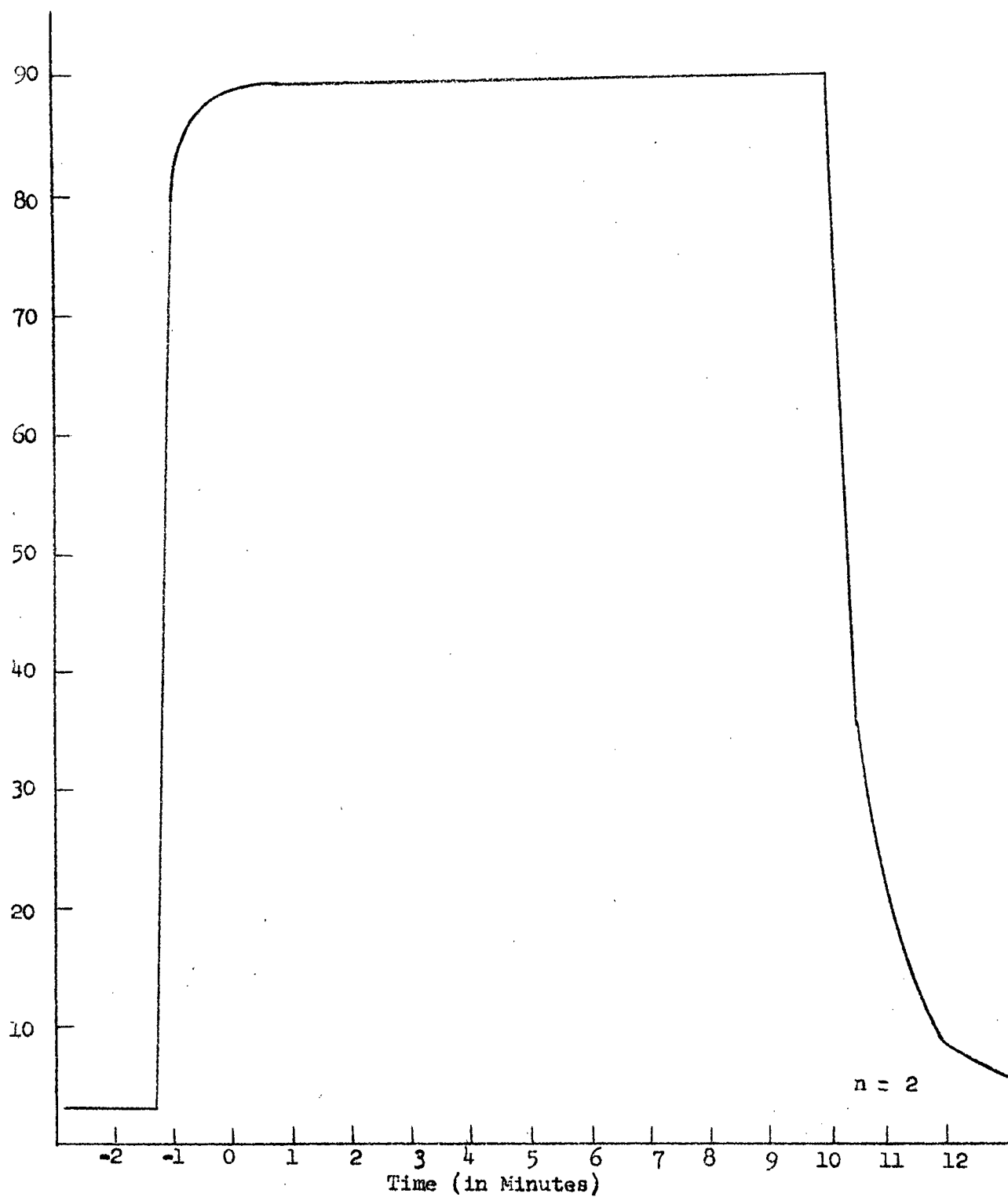
FIGURE IV-3 A reproduction of the temperature versus time record used
for the second diffusion run.

In the measurement of the Mossbauer intensity and the resonant absorption spectrum, correction was made for the non±14.4 kev background count rate within the single channel pulse height analyzer settings. This correction was explained in Chapter III. Diffusion runs 1, 2, and 3 were done as a group, each run lasting approximately $1\frac{1}{2}$ hours. However, at the end of run 3, trouble with the electronics delayed the diffusion runs 4 and 5 until two days later.

4.4 Experimental Results

The resonant absorption line shape after each diffusion run is shown in Fig.IV-4. Also shown in this figure is the line shape obtained from the electroplated source before the source was annealed. From these curves the following quantities were determined: the fractional resonant absorption h, the total line width at one half maximum height $\triangle$, and the size and direction of the line shift ℓ.These three quantities are summarized in Table IV-2. Also, these quantities are plotted as a function of the diffusion time in figure IV-5 and the rms depth of the active layer in figure IV-6. The line shift was calculated by means of the equation:

$$\delta = (\tfrac{1}{2})^v \; \frac{(A+B) - (C+D)}{(A+C) - (B+D)} \qquad\qquad \text{IV-6}$$

where: A is the fractional resonant absorption at $-v_1$

B "   "   "   "   "   " $-v_2$

C "   "   "   "   "   " v_1

D "   "   "   "   "   " v_2

v $= \; |v_2-v_1|$
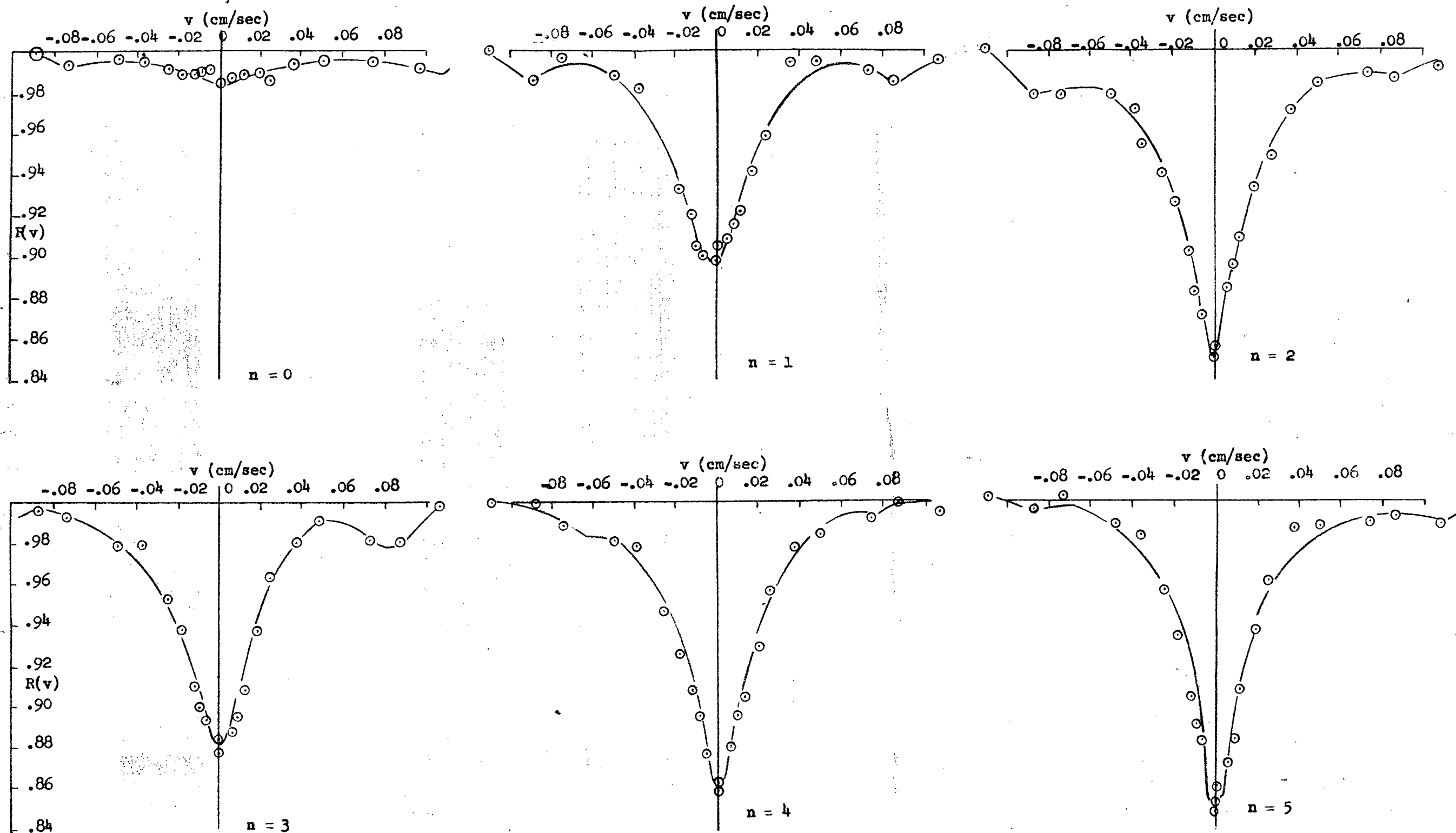
FIGURE IV-4 The resonant absorption line shape after diffusion run.
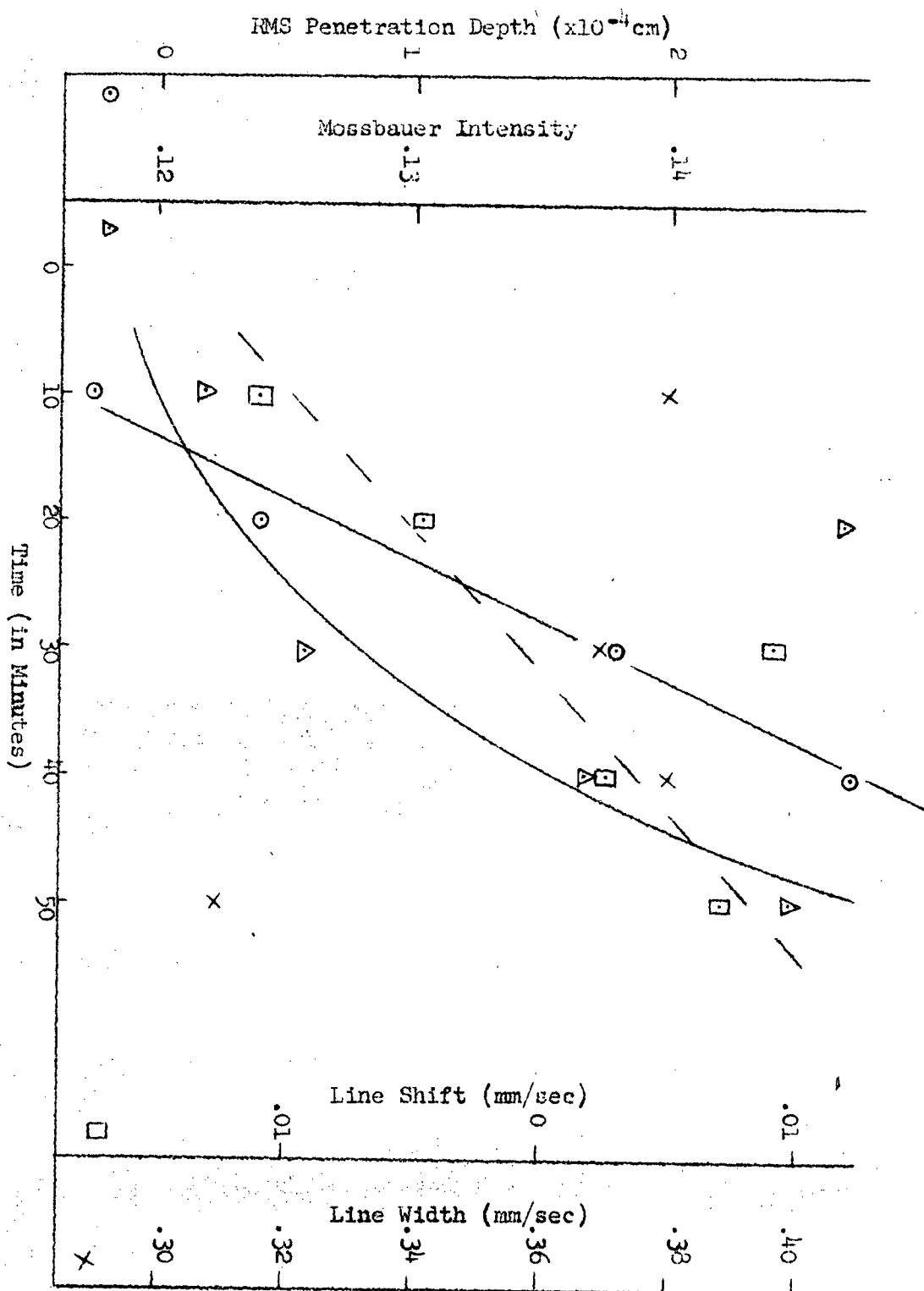
FIGURE IV-5. The variation of h, Δ, δ, and the rms penetration of the Co^{57} with the diffusion time.
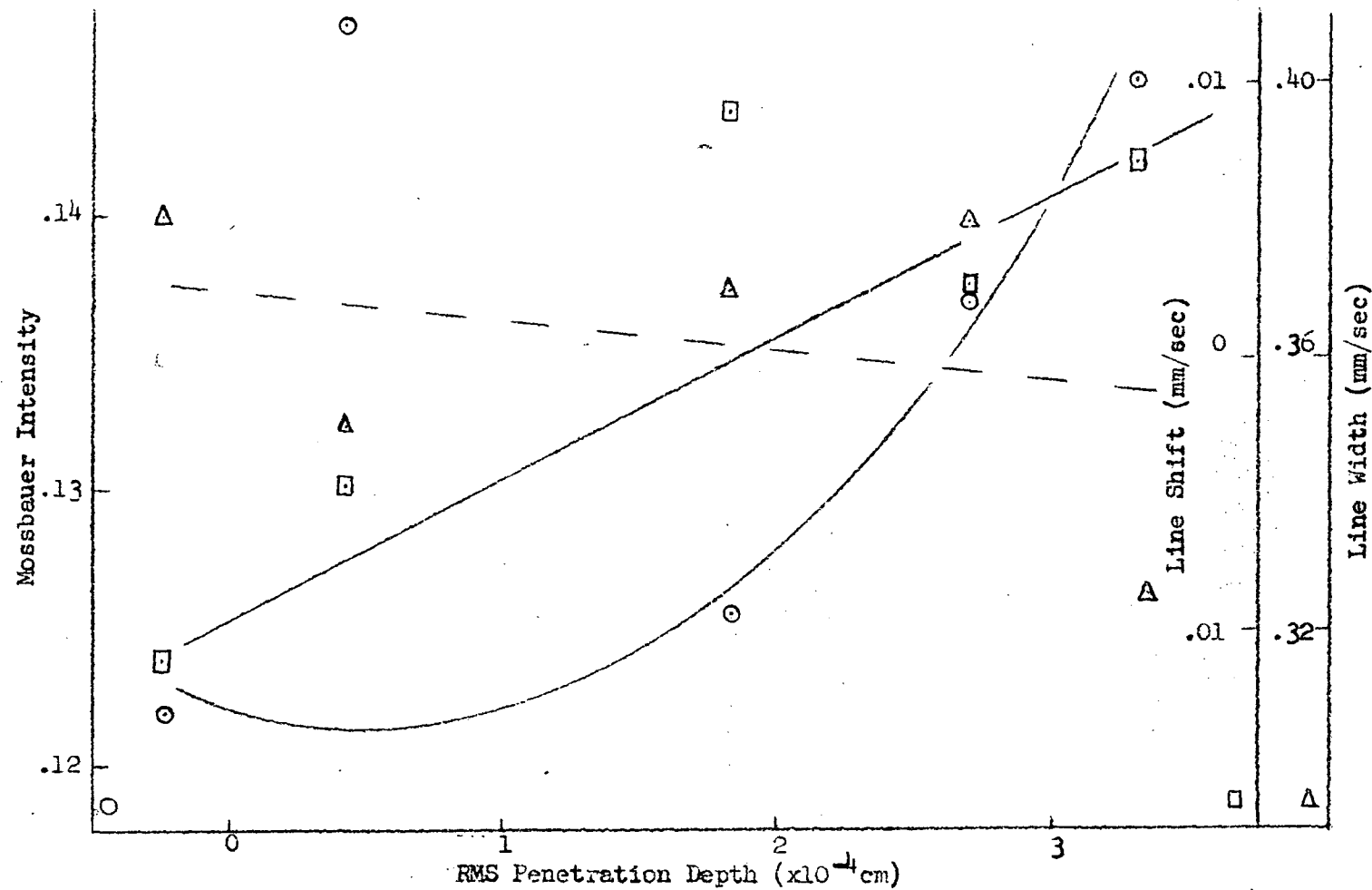
FIGURE IV-6   The Mossbauer line width, intensity and shift as a function of the rms penetration depth of the Co^{57}.

The diffusion coefficient was calculated by the method given in section 4.1. From the data of the diffusion runs, r = .690, from which D was calculated to be 2×10^{-11} cm^2/sec. This value of D is consistent with the value of D obtained for the diffusion of Fe[55] into FeO$_x$ and CoO at 900°C.[22] The rms diffusion depth for the total treatment was 3.3×10^{-4} cm (see Appendix E).

Diffusion Time	Total Diffusion Time	θ°C	h (mm/sec)	Δ (mm/sec)	ℓ (mm/sec)
10 min.	10 min.	898°C	.122	.38	-.007
10 min.	20 min.	895°C	.147	.34	-.0024
10 min.	30 min.	890°C	.126	.37	.0045
10 min.	40 min.	900°C	.137	.38	.0013
10 min.	50 min.	910°C	.145	.31	.0035

Table IV-2

Summary of Diffusion of Co[57]
into .00055" Armco Iron

4.5 Discussion of Results

An inspection of Table IV-2 shows that an appreciable value of h appears after very little diffusion at 900°C (less than ten minutes). Further, the increase of h after the initial ten minutes of diffusion is only from .122 to .145. From these results it can be concluded that if one desired to measure the initiation and build-up of h or of the Mossbauer intensity as a function of diffusion time, then diffusion runs shorter than ten minutes must be used. Hence, it would be necessary to construct a diffusion apparatus which would reach a stable temperature faster than the 'boat' used for this experiment.

Although the change in the width of the experimental lines was rather irregular, there is a trend for the width to decrease with each diffusion run. As noted earlier, a difference of the internal fields at the Fe^{57} nuclei in the source and absorber produces a broadened line. Therefore, the decrease in line width indicates that the diffusion of the Co^{57} into the Fe lattice changed the effective internal field at the radiating Fe^{57} nuclei from that characteristic of the Co lattice to one more similar to an Fe lattice. The final line width, .031 cm/sec (1.5 x 10^{-8}ev.) was larger than the theoretical line width thus indicating that possibly a difference in internal fields still existed.

From an examination of Fig.IV-4, it can be seen that the Mossbauer line is accompanied by two small peaks, one on either side of the main line. These satellite absorption curves are evident on the spectra obtained for the unannealed source and for the first three diffusion runs but appear to be almost absent from the spectra obtained from the last two diffusion runs. However, the better resolution and increased number of points used to plot the spectra discussed in Chapter V, show that these satellites were still present with considerably reduced amplitude. The position of these satellite peaks is between .80 mm/sec to 1.0 mm/sec, which is comparable to the position of the peaks obtained from an unsplit, unshifted emission line and Fe absorber, .86 mm/sec. The small absorption peaks are therefore attributed to the presence of a small region within the source in which the internal magnetic field at the Fe^{57} nuclei is effectively zero. The nuclei in such a region would emit an unsplit line, similar to that emitted from non-magnetic stainless steels.

In equation II-40 it was noted that the isomeric shift δ was

given by the equation:

$$\delta = \frac{2}{3} Ze^2 \left[<Re>^2 - <R_g>^2 \right] \left[|\Psi_a(0)|^2 - |\Psi_s(0)|^2 \right] \quad \text{II-40}$$

where the quantity $<Re>^2 - <R_g>^2$ is negative for Fe^{57}. Assuming that $<R>$ is independent of the annealing and that the line shift during the diffusion runs can be regarded as the isomeric shift, then

$$l = \delta = -\alpha \left[|\Psi_a(0)|^2 - |\Psi_s(0)|^2 \right] \quad \text{IV-7}$$

where α is a constant. Hence a variation in l would imply a variation in the electron density $|\Psi_s(0)|^2$ at the nucleus. As indicated in Table IV-2, a variation in l does indeed occur. This variation from -.007 mm/sec to a maximum of .0045 mm/sec implies that $|\Psi_s(0)|^2$ increased with the diffusion. However, this change in l was not a permanent change. The break in the variation of l noted between runs 3 and 4 is attributed to the fact that the two runs were separated by two days wereas all other runs were separated by $1\frac{1}{2}$ hours. This time dependent change in l indicates that some sort of relaxation process with a long time constant must have taken place.

Chapter V

TEMPERATURE INDEPENDENT EFFECTS

5.0 Introduction

In this chapter a summary is given of all the temperature inde-
pendent effects that could produce either a line shift or a line broadening
of the Mossbauer line. This chapter then describes the experimental measure-
ment of the parameters of the Mossbauer line as a function of the absorber
thickness, t'. Four values of t' were used, .0002", .00035", .00055" and
.001". For each thickness the parameters measured were the line intensity
h, the line width Δ, and the line shift δ. The results are summarized in
Table V-1.

Equation II-18 was programmed and evaluated numerically on the U.
B.C.'s IBM 1620 computer. This equation, yielding a theoretical value for
$R(v)$, was based upon the theory published by Margulies and Ehrman but in-
cluded the multiple emission and absorption lines of Fe^{57} in metallic iron
and the effect of the source thickness. The results of the numerical evalu-
ation show that the theory of Margulies and Ehrman is valid only when the
source thickness,t, is negligible in which case the Mossbauer effect in the
source does not effect the numerical results. If t is not negligible as was
the case in this thesis, then the Mossbauer effect in the source affects the
calculated results to such an extent that $R(v = \infty) \neq 1$. The Mossbauer effect
in the source can be taken into account by the renormalization of equation
II-18 as indicated at the end of this chapter. A detailed discussion of the
computer program with some of the test results has been included in Appendix
A.

5.1 A Brief Discussion of the Relevant Theory

a) Theoretical Mossbauer Intensity

The conditions which govern the characteristics of the Mossbauer effect for a given nucleus were summarized in table I-1. Among these conditions, the three most important are the lifetime of the excited state, the free recoil energy, and the Debye temperature. The latter two are the primary factors in determining the Debye-Waller factor, f, which in turn determines the intensity, ξ, of the Mossbauer effect. ξ also depends, but to a lesser extent, upon the source and absorber thickness. These factors are all taken into consideration in the theoretical derivation of $R(v)$ given by the equation III-7. In terms of $R(v)$, the intensity, ξ, is

$$\xi = 1 - R(v) \hspace{3cm} \text{V-1}$$

b) Line Shift Mechanisms

i) Isomer Shift

An isomer shift, (see Chapter II, section 2.3) can be caused by a small difference in the chemical environment (i.e. bonds) between the source and the absorber nuclei. This shift, however, is detected only if $\langle R_g \rangle \neq \langle R_e \rangle$. The magnitude of the isomer shift may be calculated from the equation

$$(\delta/c)_i = \frac{4\pi Ze^2}{3c} \left[\langle R_e \rangle^2 - \langle R_g \rangle^2 \right] \left[|\psi'(0)|^2 - |\psi(0)|^2 \right] \hspace{1cm} \text{II-40}$$

ii) Debye Temperature Difference

It is possible for a difference between the Debye temper-

atures of the source and absorber to produce a line shift. (See

Chapter II, section 2.2). The size of this shift can be calculated

from the equation

$$(\delta/c)_{ii} = \frac{9Nk\theta^4}{2Mc^2}\left[\frac{1}{\Theta_0^3}\int_0^{\Theta_D/\theta}\frac{x^3dx}{e^x-1} - \frac{1}{\Theta_0'^3}\int_0^{\Theta_D'/\theta}\frac{x^3dx}{e^x-1}\right] + \frac{9Nk}{16Mc^2}\left[\Theta_D-\Theta_D'\right] \quad \text{II-31}$$

iii) Impurity Effects

For Fe^{57} in Fe, the localized mode shift is expected to be

small. (See Chapter II, section 2.6). The shift is

$$(\delta/c)_{iii} = \frac{\frac{1}{2}\langle n\rangle h\nu_0}{m_0c^2} \times \frac{\tau(\text{localized mode})}{\tau(\text{gamma decay})} \quad \text{V-2}$$

where τ(localized mode) is the relaxation time for the localized mode

to come to thermal equilibrium with the lattice, and τ(gamma decay) is

the lifetime of the 14.4 kev state in Fe^{57}. τ(localized mode) $< 10^{-12}$

appears to be a reasonable value for τ(localized mode).

iv) Mass Defect

The diffusing of the radioactive impurity into the source

lattice changes the average mass of the source and thus its internal

energy relative to that of the absorber. (See Chapter II, section 2.2).

This mass defect, through its influence on the internal energy,

produces a shift of the Mossbauer spectrum of

$$(\delta/c)_{iv} = \frac{\Delta M}{2M'c^2}\int_0^\theta C_L d\theta - \frac{\Delta M}{(M')^2c^2} \times \frac{9k\Theta_D}{16} \quad \text{II-37}$$

v) Hydrostatic Compression

The isomeric shift has been shown to be dependent upon the

pressure to which the lattice is subjected.[13] (See Chapter II, section 2.2)

That is, the electron configuration is dependent upon the pressure.
The pressure coefficient is given by

$$\frac{1}{E_0}\left(\frac{\partial f}{\partial P}\right)_\theta = \frac{1}{E_0}\left(\frac{\partial \nu_{isom}}{\partial \ln V}\right)\left(\frac{\partial \ln V}{\partial P}\right)_\theta + \frac{1}{E_0}\left(\frac{\partial \nu_{rel}}{\partial \ln V}\right)\left(\frac{\partial \ln V}{\partial P}\right)_\theta \qquad V-3$$

$$= -(2.61 \pm 0.10) \times 10^{-18}/\text{kg/cm}^2$$

The first term represents the effect of the changing electron density
at the nucleus, and the second, the relativistic effect of changing the
mean vibrational energy. The second effect is less than 5% of the
total, measured coefficient and hence, the volume dependence of the
isomeric shift accounts for the major part of the pressure coefficient.
Thus a pressure difference between the source and absorber results in
a shift of the Mossbauer spectrum of

$$(\delta/c)_v = \frac{1}{c}\left(\frac{\partial \nu_{isom}}{\partial \ln V}\right)\left(\frac{\partial \ln V}{\partial P}\right)_\theta + \frac{1}{c}\left(\frac{\partial \nu_{rel}}{\partial \ln V}\right)\left(\frac{\partial \ln V}{\partial P}\right)_\theta \qquad V-4$$

c) Line Broadening Mechanisms

i) Magnetic Field Effects

In Chapter II, section 2.4 it was seen that the magnetic
Zeeman splitting of the excited and ground state energy levels of Fe^{57}
is determined by the magnetic field at the nucleus. A difference of the
magnitude of the internal field at the source and absorber nuclei
produces a broadened Mossbauer line. A difference in the internal magnetic
fields could arise from the partial magnetization of either or both of
the source and absorber by the annealing process, or, by the presence
of the Co^{57} in the source lattice.

ii) Localized Modes

The localized modes, (see above and Chapter II, section 2.6), also give rise to a line broadening as a result of the uncertainty of the occupation number of the localized mode. The magnitude of the broadening is given by

$$\Delta = \frac{\frac{1}{2}E}{m_0 c^2} \kappa_2 \; (\langle n^2 \rangle - \langle n \rangle^2)^{\frac{1}{2}} \hbar w_0 \frac{\Upsilon(\text{localized modes})}{\Upsilon(\text{gamma decay})} \qquad V\text{-}5$$

iii) Source and Absorber Thickness

The line width of the Mossbauer spectrum should equal 2Γ where Γ is the line width of the nuclear transition. (See Chapter II, section 2.1). However, only when the source and absorber thicknesses can be approximated to zero is this the case.[15] The use of nonzero source and absorber thicknesses produces a broadened line. The quantity $R(v)$ depends upon both thicknesses, and hence, the expected line width in the nonzero thickness case should be determinable from the theoretical spectrum.

iv) Random Shifts

Random isomeric shifts,(see Chapter II, section 2.3) caused by a variable chemical environment of the Co^{57} nuclei could produce a broadening of the Mossbauer spectrum rather than a shift. In addition, a difference in the quadrupole splitting of the excited state of the source and absorber would also produce a broadening of the line.

5.2 Experimental Procedure

a) Source and Absorber

The source used for the comparison between theory and

experiment was NSEC #2. The preparation and treatment of this source was discussed in Chapters III and IV. Four absorbers were used; 1. armco iron .00020" thick, 2. armco iron .00035" thick, 3. armco iron .00055" thick, and 4. shim steel .001" thick.

b) Procedure

1. The source was mounted in the high temperature source holder (see Chapter III) but the outer pot was not evacuated. The source holder was attatched to the lathe 27" from the proportional counter window.

2. The E. H. T. of the counter was turned on 12 hours before measurements were begun. The gas flow of the counter was checked at intervals for an hour before measurements were begun and also throughout the collection of data.

3. The .00020" Fe absorber was mounted in the absorber mount and the mount was attatched to the lathe.

4. The copper-constantan thermocouples were connected and a continuous record of the source and absorber temperature begun.

5. With 3.5 volts across the helipot, the output spectra of the pulser for setting of 1.00 to 4.00 in steps of 0.50 were super-imposed upon the 14.4 kev spectrum by the C. D. C. 100 channel kicksorter. The window settings of the single channel kicksorter were placed at pulser amplitudes of 2.00 and 3.50 corresponding to a "Baseline" of 330, and a "Channel Width" of 731. The amplifier settings used were; differentiation time constant - $1.6\mu s$, integration time constant - $0.8\mu s$, attenuation - 12 db, The discriminator bias on the NP II scaler was 1.0 volts and the dead time $15\mu s$.

6. The count rate of the gamma rays transmitted through the Fe absorber and through a 1/16" Al absorber were measured for equal counting times, i.e. correction was made for the instrumental dead time.

7. The areas within the single channel kicksorter settings of the background radiation transmitted through the Fe absorber and through the Al absorber were measured.

8. The gamma ray transmission through the Fe absorber within the above window settings was measured for 22 different positive and negative velocities of the absorber relative to the source. The measurements were made in groups of 4, separated by a measurement of the transmission at $v = 0$, and $v = \infty$ (i.e. .144 cm/sec). A record of the time at which the individual measuring periods ended was kept.

9. Steps 6, 7, and 8 were repeated for the other three absorbers.

c) Discussion of the Procedure

The data used in this section of the thesis was collected in one continuous run to eliminate any possible drifts in the apparatus. Furthermore, the source was kept at room temperature to eliminate a Josephson shift, and at room pressure to eliminate a hydrostatic compression shift in the Mossbauer spectrum. Steps 6 and 7 were included so that the background correction, explained in Chapter III, could be made on the data. The numerous measurements of the transmission at $v = 0$, and $v = \infty$, were made so that $R_m(v)$ could be plotted as a function of time to check for shifts in the proportional counter. Also, the continuous determination of $R_m(v)$ automatically corrected for the decay of the source strength.

5.3 Calculations and Corrections

The transmitted count rate, $N(v)$, was calculated from the measured data and corrected for the background count rate as outlined in Chapter III. The background correction is

$$N_b \quad N_{Al}(v) \times \frac{A(Fe)}{A(Al)} \qquad \qquad \text{III-15}$$

For each absorber thickness, $N(v = 0)$ was plotted as a function of time in order to calculate the pressure drift of the proportional counter.(see Chapter III). For these particular measurements however, it was found that the drift was negligible and hence, no correction for counter drift was necessary.

Using the background corrected values of $N(v)$, the ratio $R_m(v)$ was calculated and plotted as a function of v in figures V-1, V-2, V-3 and V-4. The line shift was calculated from equation IV-6.

5.4 Results

The mossbauer lines obtained for each of the four absorber thicknesses are shown in figures V-1, V-2, V-3 and V-4. From these figures the maximum intensity, h, of the Mossbauer lines were obtained. Also, the width of the measured line at $\frac{1}{2}h$ was determined and called the width, $\triangle$.

The measured values of h, $\triangle$ and δ are summarized in Table V-1. These results show the expected increase of h and $\triangle$ as the absorber thickness increased.
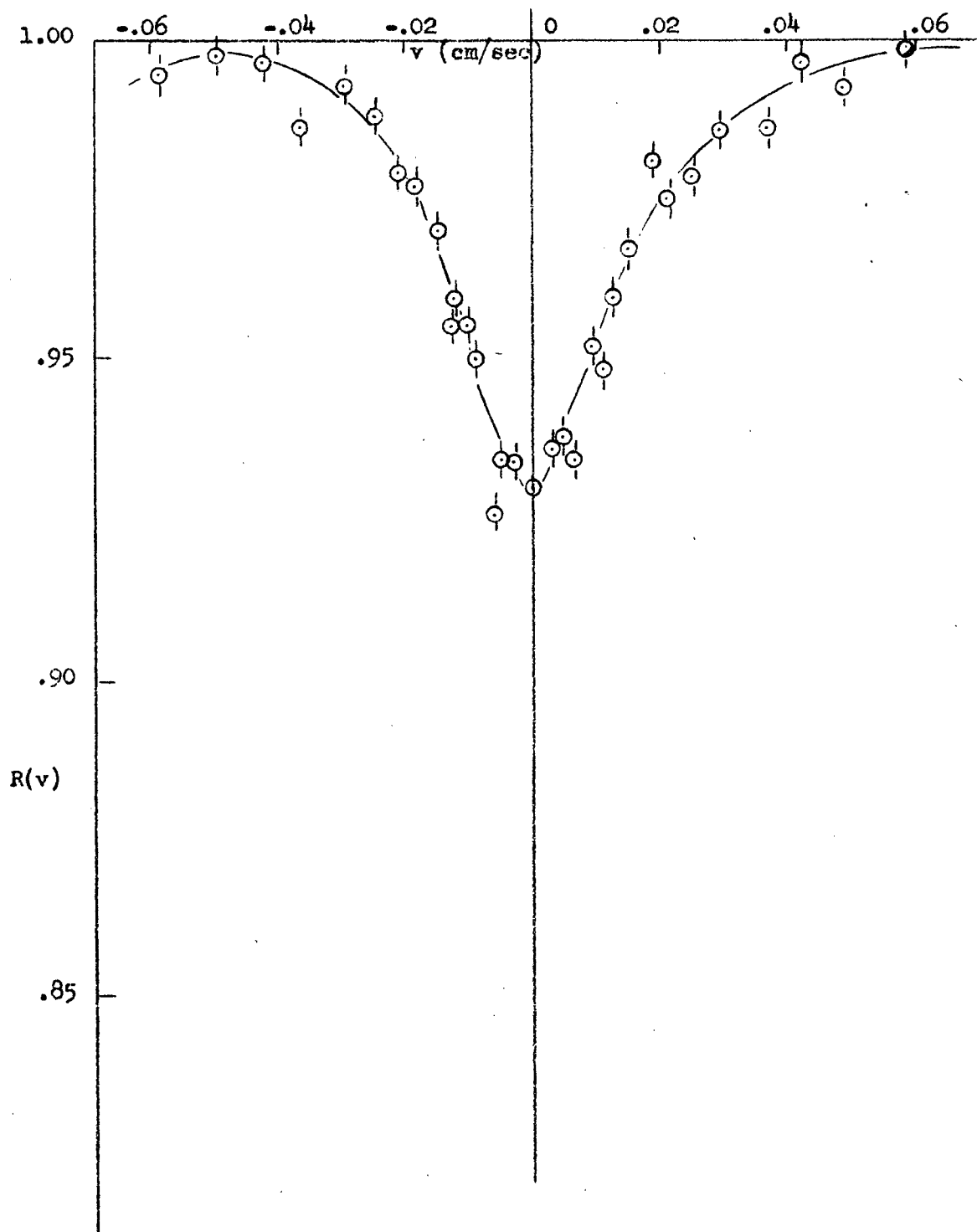
Figure V-1 The Mossbauer absorption spectrum for an absorber thickness of .0002".

Absorber Thickness	h	$\triangle$ (cm/sec)	δ (mm/sec)
.0002"	.070	.285	-.002
.00035"	.113	.300	-.003
.00055"	.169	.310	-.002
.001"	.228	.320	-.007

Table V

Measured Mossbauer Spectrum parameters as a function of absorber thickness.

5.5 Discussion of Results and Conclusions

The line shifts measured for the first three absorbers used agree within the experimental error (± .001 mm/sec) but disagree with that obtained for the fourth absorber. This difference is attributable to the fact that the absorber used in the fourth case was shim steel while the absorbers used in the first three cases were Armco iron. The difference between these two materials was so small that it was concluded that the line shift was an isomer shift since all other shift mechanisms would yield the same shift for the two types of absorbers.

The theory by which a theoretical value of R(v) was calculated was based upon that published by S. Margulies and J. R. Ehrman[5]. In their work, the transmission calculated for a gaussian source distribution was, in the notation used in this thesis:

$$T(v) = \left[1 - f\right] \exp(\tfrac{1}{2}\mu t)^2 \left[1 - \Phi\left(\tfrac{1}{2}\mu t\right)\right] + \frac{f\Gamma}{2\pi} \int_{-\infty}^{\infty} \frac{dE}{(E+S)^2 + \Gamma^2/4} \exp\left(\frac{-\tau'\Gamma^2/4}{E^2+\Gamma^2/4}\right)$$

$$\times \left[1 - \Phi\left(\frac{\tau\Gamma^2/4}{2[(E+S)^2+\Gamma^2/4]}\right)\right] \exp\left(\frac{\tau\Gamma^2/4}{2[(E+S)^2+\Gamma^2/4]}\right)^2 \qquad \text{V-6}$$
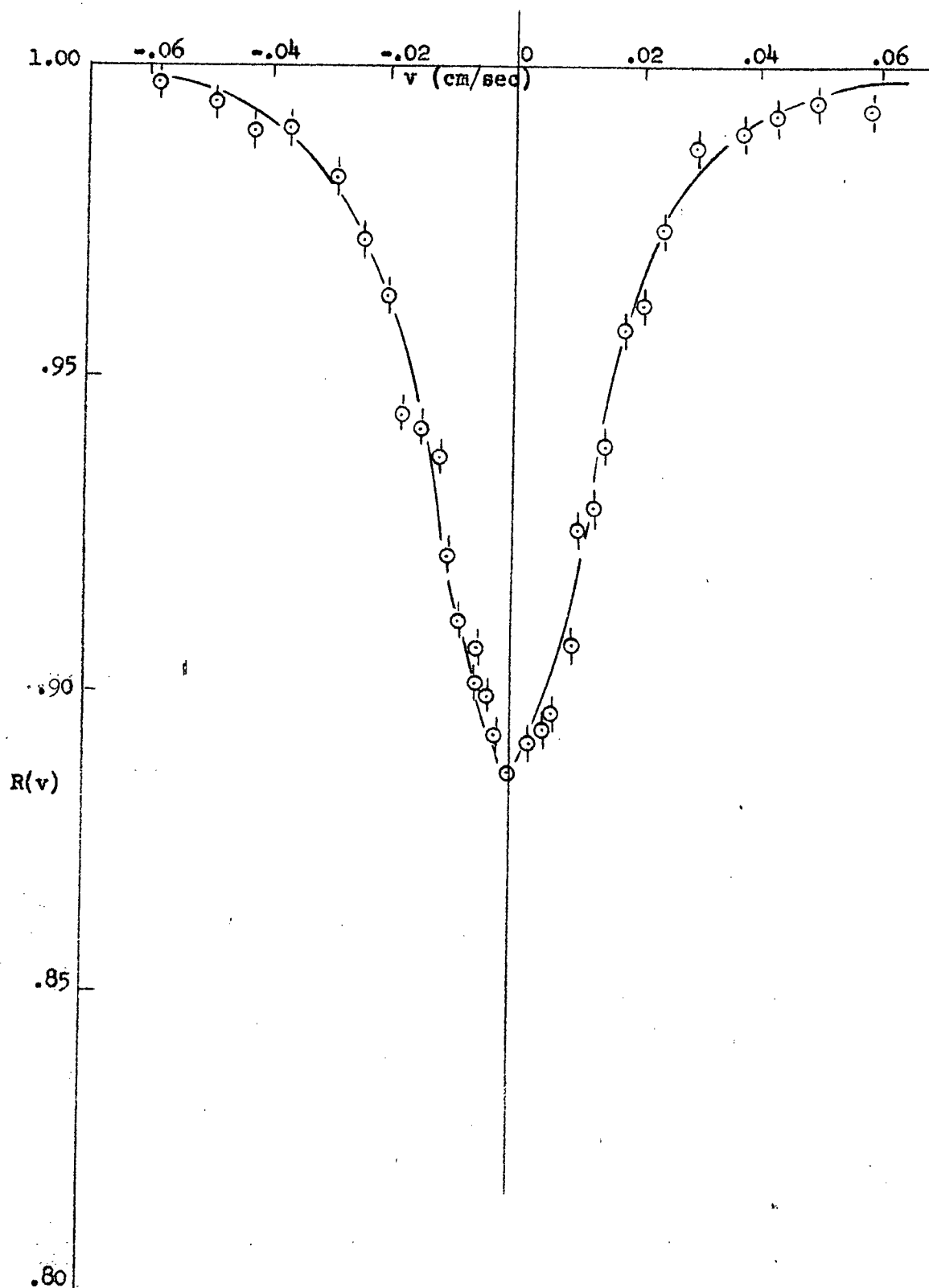
Figure V-2   The Mossbauer absorption spectrum for an absorber thickness of .00035".

It is seen that the Doppler shift, $S = vE_0/c$, has been included in the source part of the integration rather than the absorber part and also, that the Mossbauer absorption in the source has been neglected, implying a negligible source thickness.

The above equation was modified to include the source thickness and also the six line emission and absorption spectra of Fe^{57} in metallic iron. The transmission was normalized to yield R(v) by dividing through by what Margulies and Ehrman indicated to be the nonresonant absorption portion of equation V-6, $\exp(\frac{1}{2}\mu t)^2 \left[1 - \phi(\frac{1}{2}\mu t)\right]$. This process yielded the equation

$$R(v) = 1 - f + \sum_{j=1}^{3} \frac{W_{jk} f \Gamma}{\pi} \int_{-\infty}^{\infty} \frac{dE}{(E+S)^2 + \Gamma^2/4} \exp\left(\frac{-W_{k1}T\Gamma^2/4}{E^2 \quad {}^2/4}\right) \quad \text{II-18}$$

$$x \left[1 - \phi\left(\frac{W_{jk}T\Gamma^2/4}{2[(E+S)^2 + \Gamma^2/4]} + \frac{1}{2}\mu t\right)\right] \exp\left(\frac{W_{jk}T\Gamma^2/4}{2[(E+S)^2 + \Gamma^2/4]} + \frac{1}{2}\mu t\right)^2$$

$$\div \exp(\frac{1}{2}\mu t)^2 \left[1 - \phi(\frac{1}{2}\mu t)\right]$$

At $v = \infty$, the integral of equation II-18 should be reduced to f times the nonresonant term so that $R(v = \infty) = 1$. In practice, however, evaluation by the program outlined in appendix A yielded $R(v = \infty) = .97$. Testing proved that $R(v = \infty)$ increased to .9957 when t was reduced by a factor of 10 to 3.3×10^{-5} cm. From these results it was concluded that equation II-18 would yield valid results only when the source thickness is negligible and that the Mossbauer absorption in the source affects the calculated value of R(v) when t is not negligible. Furthermore, it was concluded that to fully allow for the Mossbauer absorption in the source when t is not negligible equation II-18 must be modified to

$$R(v) = T_c(v)/T_c(v = \infty) \qquad \text{V-7}$$
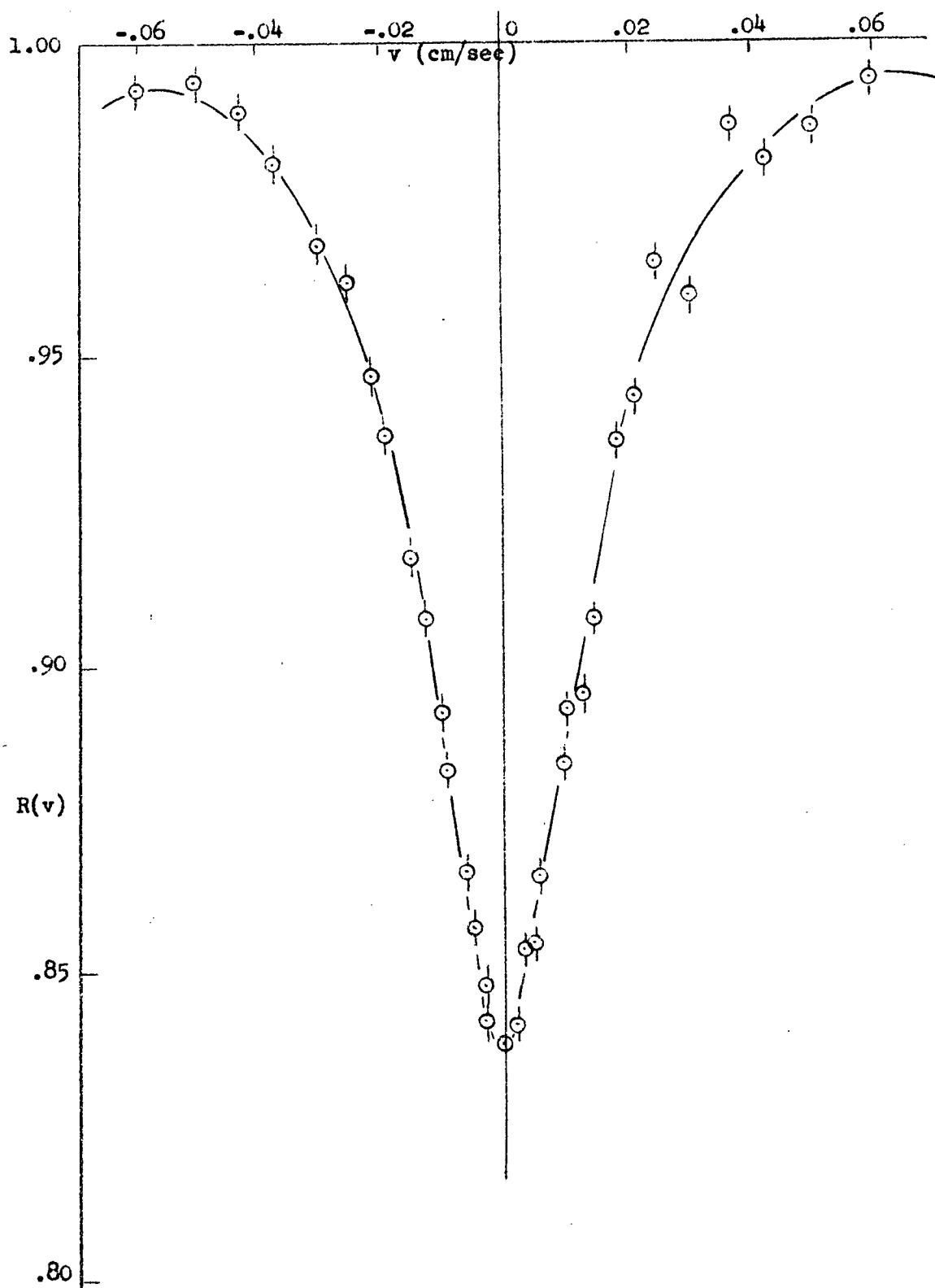
Figure V-3   The Mossbauer absorption spectrum for an absorber thickness of .00055".

where

$$T_c(v) = (1 - f) \exp(\tfrac{1}{2}\mu t)^2 \left[1 - \bar{\phi}(\tfrac{1}{2}\mu t)\right] + \sum_{j=1}^{2} W_{jk} \frac{f\Gamma}{\pi} \int_{-\infty}^{\infty} \frac{dE}{(E+S)^2 + \Gamma^2/4}$$

$$\times \exp\left(\frac{-W_{ij}\Gamma'\Gamma^2/4}{(E+S)^2 + \Gamma^2/4}\right)\left[1 - \bar{\phi}\left(\frac{W_{jk}\Gamma\Gamma^2/4}{2(E^2 + \Gamma^2/4)} + \tfrac{1}{2}\mu t\right)\right] \quad \text{V-8}$$

$$\times \exp\left(\frac{W_{jk}\Gamma\Gamma^2/4}{2(E^2 + \Gamma^2/4)} + \tfrac{1}{2}\mu t\right)^2$$

By means of this equation, R(v) could be evaluated numerically and the
values of the line intensity and line width determined and compared with
the experimentally determined values.
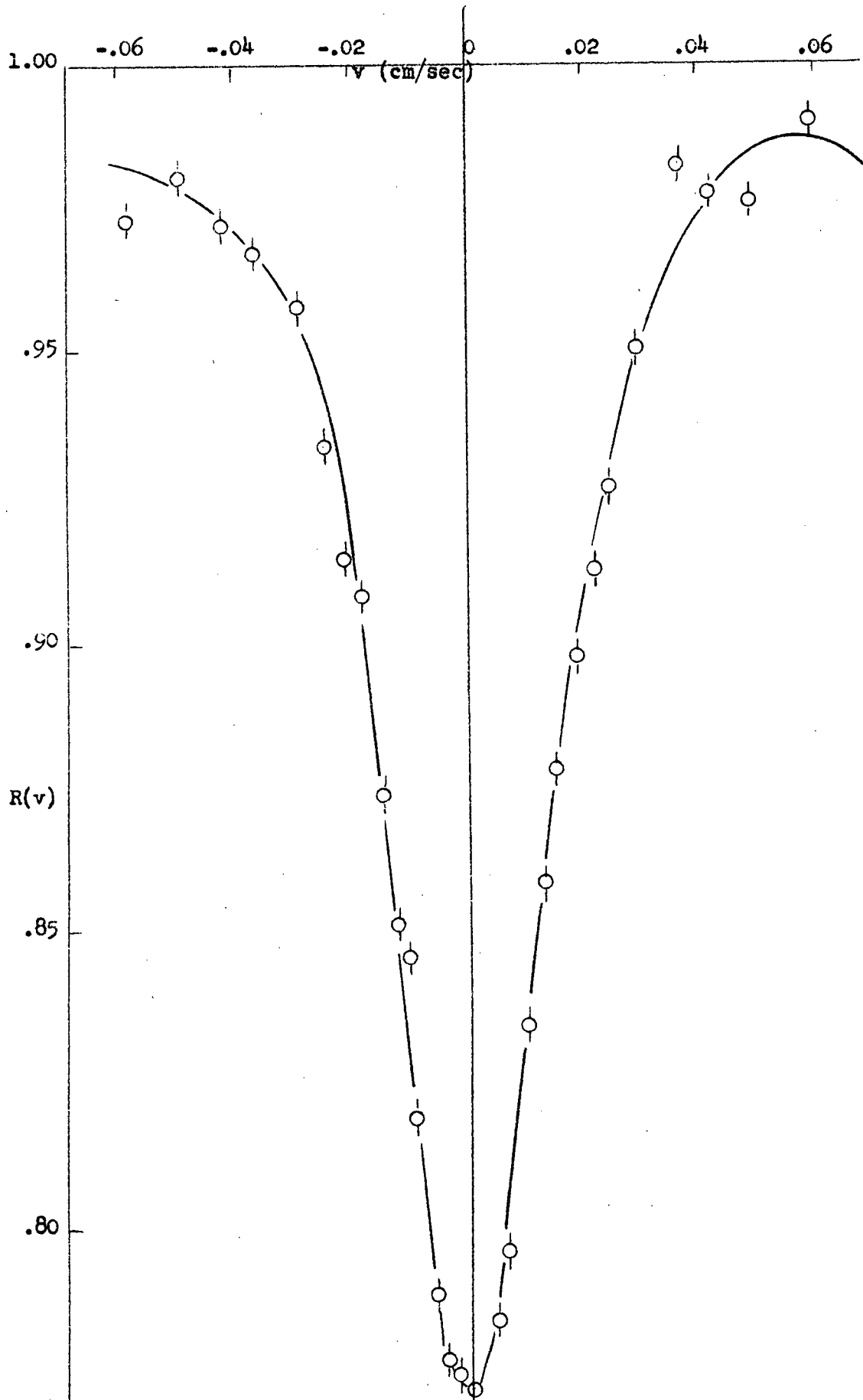
Figure V-4   The Mossbauer absorption spectrum for an absorber thickness
of .001"

Chapter VI

TEMPERATURE DEPENDENT EFFECTS

6.0 Introduction

A summary of the temperature dependence of the quantities discussed in Chapter II is given at the beginning of this chapter. The experimental work discussed in this chapter was divided into two sections; one section considered large temperature differences, i.e. greater than $50^{O}K$, and the other, small temperature differences, i.e. less than $50^{O}K$. This division was made so that very small changes caused by small temperature differences could be measured as well as the general temperature dependence. The analysis of the data at small temperature differences required the use of special formulae and techniques, both of which are discussed herein. The experimental procedure by which the data was accumulated for both sections is given in detail and the results summarized in table and graphic form. As in Chapter V, the relationship between the theoretical and experimental temperature dependence is investigated. It is seen that the agreement between the experimental and theoretical Josephson effect is good. The measurements indicate a Debye temperature of $420^{O}K$ for both the source and absorber. It is also found that the minimum line width does not occur when the source and absorber are at the same temperature, a possibility that was discussed in Chapter V. The shape of the Mossbauer spectrum proved to be temperature dependent. This dependence is shown and discussed near the end of the chapter. In the last section of the chapter, a discussion of the possible causes of the slight variation between theory and experiment is given.

6.1 Brief Discussion of Relevant Theory

a) Josephson Effect

The Josephson effect was discussed in Chapter II section 2.2. The magnitude of the effect is calculated from equation II-27.

b) Hydrostatic Compression Effect

The details of this effect were given in Chapter II section 2.2. The magnitude of this effect is calculated from equation II-30.

c) Temperature Dependence of f

The Mossbauer intensity is determined, in part, by the Debye-Waller factor, f, which is given, in the Debye approximation to the lattice vibrations, by the expression

$$f = \exp(-3E_0^2/kmc^2\Theta_D)\left[\frac{1}{4} + (\theta/\Theta_D)^2\int_0^{\Theta_D/\theta} \frac{x\,dx}{e^x - 1}\right] \qquad \text{I-5}$$

As the temperature increases, f decreases so that the intensity, h, also should decrease. Table VI-1 shows the variation of f as a function of temperature. For this table, f was calculated using $\Theta_D = 420^\circ K$

(°K)	f	(°K)	f
80	.910	300	.784
100	.900	350	.755
150	.875	400	.730
200	.843	450	.701
250	.813	500	.675

Table VI-1

The temperature dependence of f also affects the effective source and absorber thicknesses, T and T'. Using the values of f given in table VI-1, T and T' have been plotted as a function of temperature in figure VI-1.

d) Temperature Dependence of the Magnetic Field

As noted in Chapter II, section 2.4, the internal magnetic field, $\underset{\sim}{H}$, at the emitting or absorbing nucleus is temperature dependent - its dependence is given by the Weiss Law. This temperature dependence of $\underset{\sim}{H}$ affects the Mossbauer spectrum in two ways. First, as the difference between the internal magnetic fields of the source and absorber increases, the width of the Mossbauer line also increases. Secondly, as the Mossbauer line is broadened, its intensity will decrease so that either an increase or a decrease in the source temperature will reduce the intensity.

6.2 Experimental Analysis of the Effects of Small Temperature
Differences Between Source and Absorber

a) Line Shifts

An equation that can be used to detect line shifts is

$$\delta = \frac{1}{2}\Delta v \frac{(A + B) - (C + D)}{(A + C) - (B + D)} \qquad \text{VI-1}$$

where $\Delta v = v_2 - v_1$, A is the count rate at $+v_1$, B is the count rate at $+v_2$, C is the count rate at $-v_1$, and D is the count rate at $-v_2$. The assumption contained implicitly in this equation is that $\delta \ll \Delta$. In fact, as will be seen below, this approximate formula yields a value for δ
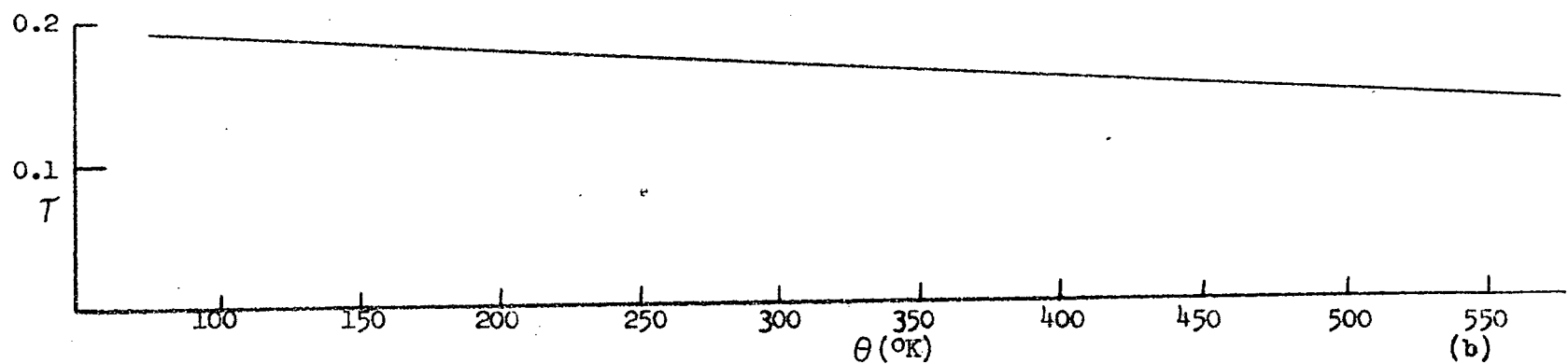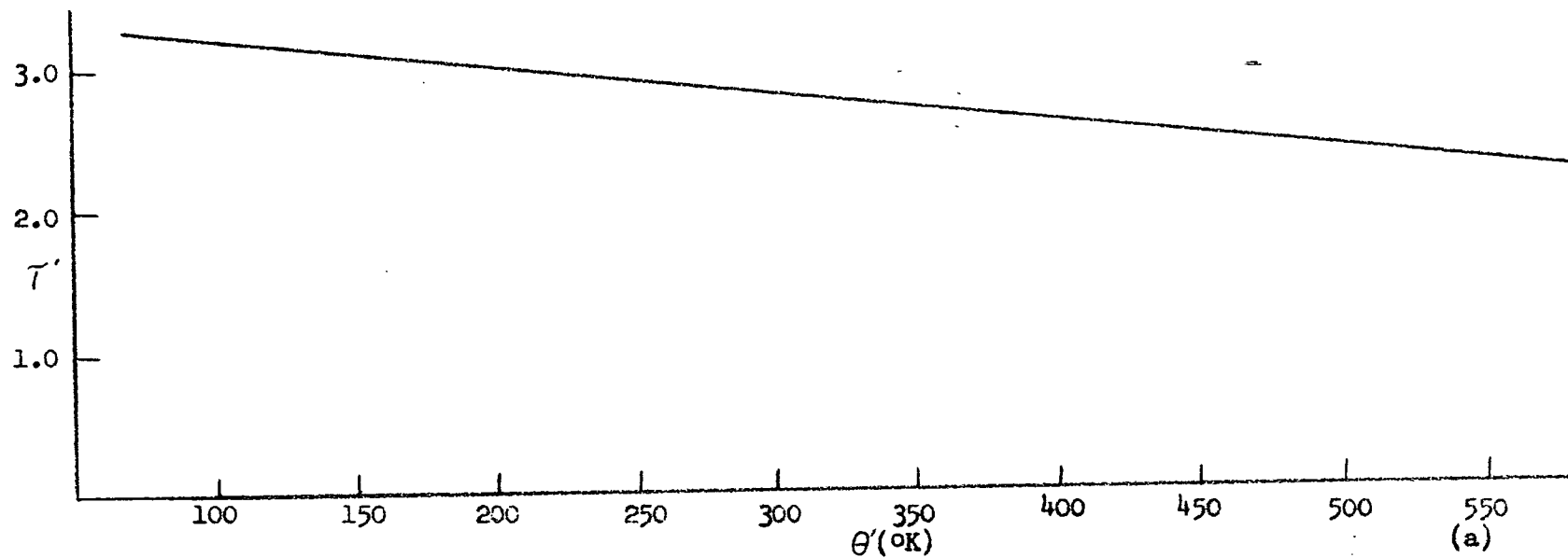
FIGURE VI-1   The variation of the apparent source and absorber thicknesses, T, and $\widetilde{\tau}{}'$, as a function of temperature.

that is in error by a factor of 1.5. A more accurate formula (Moss II,p 58) is

$$\delta = \frac{4\Delta}{3\sqrt{3}}(1/h - .75)\frac{(R^+ - R)}{(R^+ + R)} \qquad \text{IV-6}$$

where R^+ and R^- are the count rates at $+v$ and $-v$. The disadvantage of equation IV-6 is that it necessitates a knowledge of h and Δ, whereas equation VI-1 does not.

It is possible, by careful measurement of δ as a function of θ to evaluate Θ_D, the Debye temperature of the source. δ/c, where c is the velocity of light, was plotted as a function of θ and Θ_D in figure II-3. If δ is measured as a function of θ, then the slope, $d(\delta/c)/d(\theta)$, determines the Debye temperature.

b) Line Widths

In Chapter V it was noted that the line width depended upon the temperature dependent internal magnetice field $\underline{H}$. As seen there, the measured line width was greater than the theoretically determined line width. It is expected that if $\Delta H = 0$ at $\Delta\theta = 0$, then the minimum line width would be found at $\Delta\theta = 0$. The true position of the minimum line width can be determined by measuring Δ as a function of $\Delta\theta$. The location of the minimum requires that small temperature differences be used, and the accuracy of the location requires that the counting statistics be good. Thus, the determination of the minimum line width is better done with a few points with good statistics rather than from the total spectrum. Assuming that A, B, C, and D have the same definitions as in section 6.2.a, Δ can be calculated from the equation

$$\Delta = 2|v_1| + \frac{dv}{dR_1} (h/2 - A) + \frac{dv}{dR_2} (h/2 - C) \qquad\qquad \text{VI-2}$$

where $dv = v_1 - v_2$, $dR_1 = A - B$, and $dR_2 = C - D$. This equation requires that A, B, C, and D be located on the linear portion of the Mossbauer spectrum. For large $\Delta\theta$, the spectrum will be shifted to such an extent that the two sets of count rates, A and B, and C and D, will not both be in the linear portion, so that equation VI-2 is not valid for large $\Delta\theta$.

c) Line Intensities

In equations VI-1 and VI-2 it is noted that h appears as a variable that must be known before either Δ or δ can be calculated. Therefore, a similar expression to determine h from a limited number of points on the Mossbauer spectrum, independent of Δ and δ is impossible. However, for small $\Delta\theta$, h varies very little and hence can be determined by interpolation from a plot of h against $\Delta\theta$ for large $\Delta\theta$.

6.3 Experimental Procedure

a) Source and Absorber

The source used for all temperature dependent measurements was the NSEC #2. For large temperature differences between the source and the absorber, the source was mounted in the high temperature source holder shown in figure III-14. The source holder shown in figure III-15 was used only when the source temperature was lowered below $0^\circ C$. A similar system was followed for small temperature differences between the source and the absorber.

For these measurements, only the .00055" Fe absorber was used. It was determined that the maximum significance of results could be obtained with this absorber. (see appendix D). The absorber was mounted on the lathe carriage by means of the holder described in Chapter III.

b) Source Temperature Greater Than Absorber Temperature

1. The source was mounted firmly in the high temperature holder and the outer pot was evacuated to 15 microns

2. The absorber was firmly clamped in its holder and the holder was clamped onto the lathe carriage.

3. The thermocouples were connected to the Varian recorder. The cold junctions were put into an ice-water mixture.

4. The setting on the apparatus were the same as used in Chapter V.

5. The background correction, as outlined in Chapter V, was determined.

6. The transmission of the gamma rays through the absorber was measured as a function of velocity for 14 positive and negative velocities.

7. The heating unit was inserted into the inner pot and the source temperature increased.

8. Steps 5, 6, and 7 were repeated for source thermocouple readings of 3.15 mv, 5.25 mv, and 8.3 mv. In each case sufficient time was allowed for the source temperature to become stable before the measurements were begun.

c) Source Temperature Less Than Absorber Temperature

1. Steps 1 to 4 of section 6.3.b were repeated with the source in the low temperature holder.

2. A 600 watt heater was placed in the liquid nitrogen reservoir and the variac was set to produce a thermocouple reading of -1.95 mv.

3. The background correction was determined as in Chapter V.

4. The transmission of the gamma rays through the absorber was measured as a function of the velocity for 14 positive and negative velocities.

5. Steps 2, 3, and 4 were repeated for source thermocouple readings of -3.00 mv and -3.89 mv.

d) Small Temperature Differences Between Source and Absorber

1. Steps 1 to 5 of section 6.3.b were repeated. The variac was set to give thermocouple readings of 1.00 mv, 1.52 mv, 1.72 mv, 2.05 mv, and 2.55 mv. The gamma ray transmission was determined at each temperature. The measurements were made at velocities of $\pm$.1444cm/sec, $\pm$.0185 cm/sec, $\pm$.0123 cm/sec, $\pm$.0062 cm/sec, $\pm$.0046 cm/sec, and 0 cm/sec.

2. Steps 1 to 3 of section 6.3.c were repeated. The variac was set to give thermocouple readings of .25 mv, .012 mv, and -.85 mv. The gamma ray transmission was determined at each temperature. The measurements were made at the same velocities as used for step 1.

In all the measurements, it was found that the counter drift, in any set of measurements was negligible in the short period of data collecting time. The number of counts registered per point for small temperature differences was of the order of 10 greater than that for

large temperature differences.

6.4 Calculations and Results

a) Large Temperature Differences Between Source and Absorber

For each source temperature, $R_m(v)$ was calculated using the corrected transmission values and plotted as a function of velocity as illustrated in figure VI-2. The intensity, h, was determined directly from these plots. The line width, $\triangle$, was recorded as the width of the spectrum at $\frac{1}{2}$h. Since equation VI-1 was not valid for large temperature shifts, the line shift, , was measured directly from the graphs of the Mossbauer spectrum, and was taken as that velocity about which the spectrum was symmetrical at $\frac{1}{2}$h. The measured values of these parameters are given in table VI-2.

$\triangle \theta ^{O}K$	h	$\triangle$ (cm/sec)	$\mathcal{L}$ (cm/sec)
179	.093	.060	.0130
100	.124	.036	.0075
50	.166	.031	.0035
0	.174	.031	-.0003
-76	.168	.037	-.0055
-108	.160	.041	-.0065
-138	.153	.040	-.0085

Table VI-2

The gross temperature dependence of the parameters
of the Mossbauer spectrum

In order to compare the measured temperature shift with the Josephson effect, several corrections had to be made with the measured
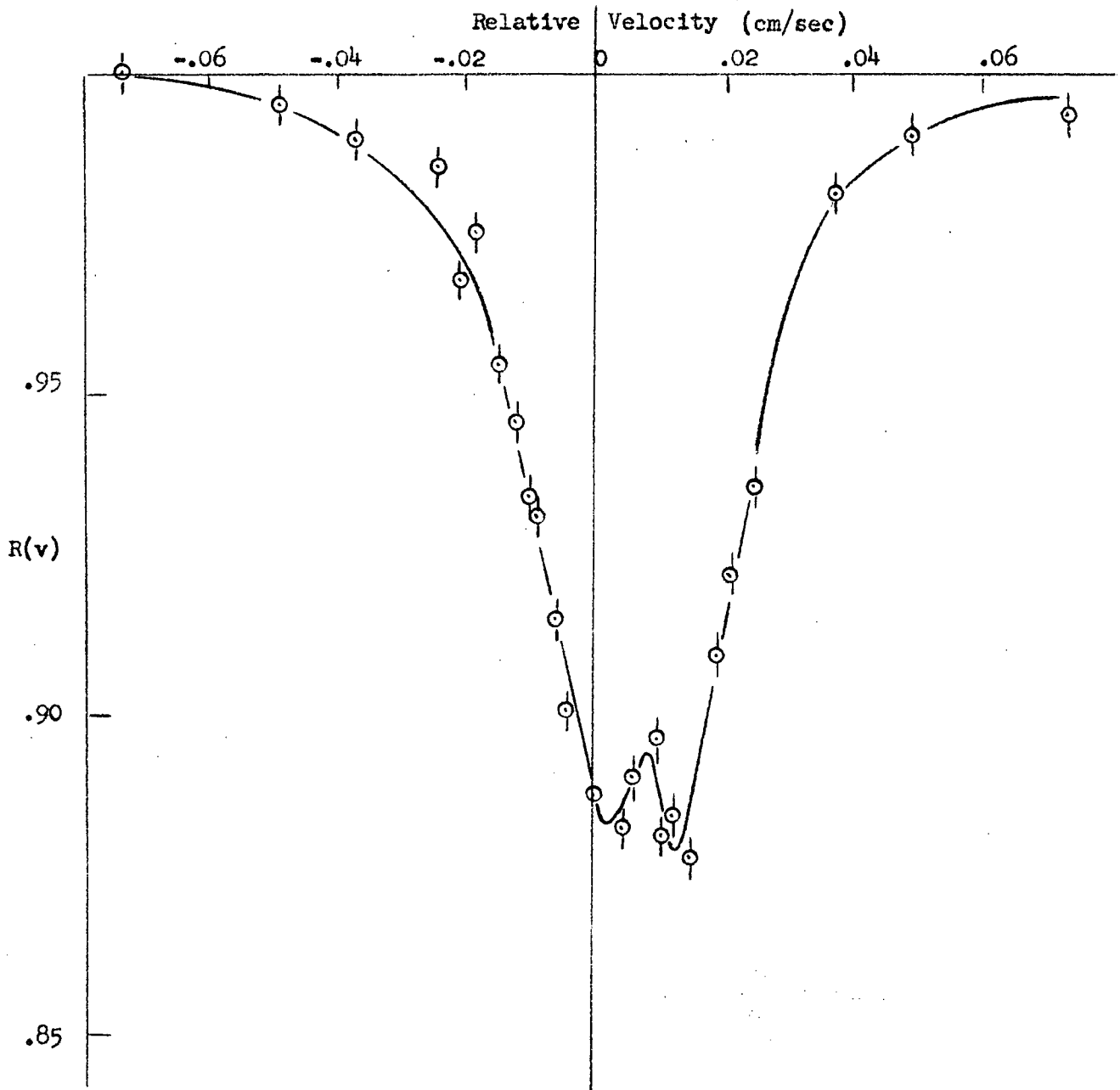
FIGURE VI-2 The Mossbauer spectrum obtained with a source temperature of 126°C and an absorber temperature of 26°C. This spectrum illustrates both the temperature shift and the appearance of the hyperfine structure.

shift. First, it was noted that at $\triangle\theta = 0$ a small residual shift was measured. This residual shift was subtracted from the measured shift. Second, it was noticed that the absorber temperature, θ', was not constant for all measurements. This variation was compensated by adding a shift δ' given by

$$\delta' = -2.24 \times 10^{-15} \triangle\theta'c \qquad \text{VI-3}$$

where $\triangle\theta' = \theta' - 297°K$, to the measured shift. Third, the temperature dependent hydrostatic compression shift was added to the measured shift. This hydrostatic compression shift was calculated from the data contained in figure II-3. The values of the measured shift, the three corrections, and the measured Josephson shift are summarized in table VI-3. The Josephson shift has been plotted as a function of the source temperature in figure VI-3 . The solid line in this figure is the theoretical Josephson shift calculated from equation II-27 using $\Theta_D = 420°K$ and $\theta' = 297°K$.

°K	1×10^{-4} cm/sec	$\delta_r \times 10^{-4}$ cm/sec	$\delta' \times 10^{-4}$ cm/sec	$\delta_{hc} \times 10^{-4}$ cm/sec	$1_c \times 10^{-4}$ cm/sec
478	130	-3.0	-1.3	6.4	139.2
379	65	-3.0	-1.3	4.5	73.8
349	35	-3.0	-1.3	2.3	41.6
299	-3	-3.0	-1.3	0.0	-1.3
219	-55	-3.0	1.3	-3.4	-56.7
186	-65	-3.0	2.0	-4.9	-68.9
156	-85	-3.0	2.0	-6.2	-86.0

Table VI-3

The three corrections applied to the measured temperature shift of the Mossbauer spectrum to obtain the measured Josephson shift.
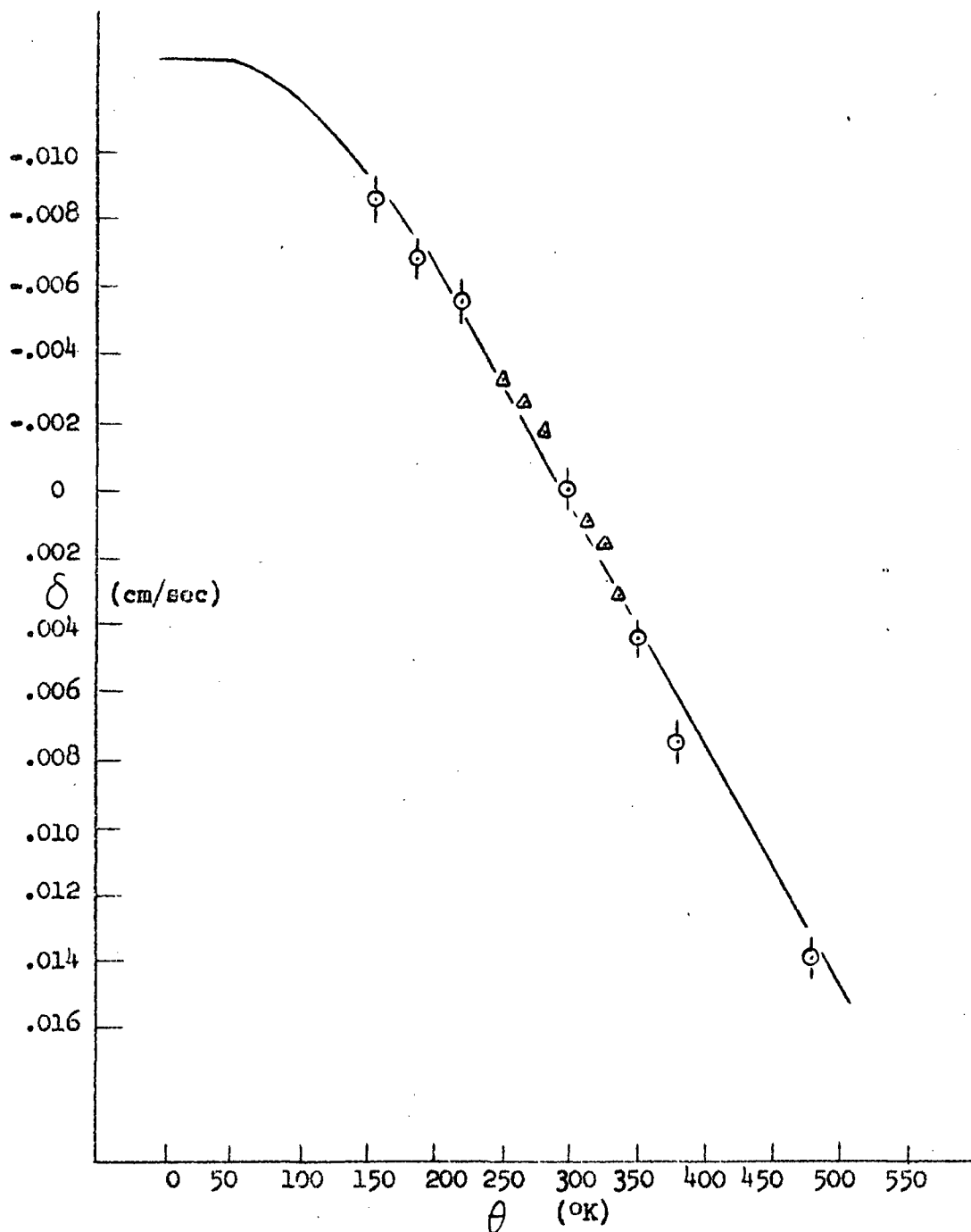
FIGURE VI-3   The measured temperature dependent Josephson shift
plotted as a function of the source temperature.
The solid line is the theoretical shift calculated
for a Debye temperature of 420°K.

The line intensity has been plotted as a function of $\Delta\theta$ in figure VI-4. Included in this figure is the variation of the theoretical value of the Mossbauer intensity, ξ, with $\Delta\theta$. This variation takes into account only the temperature variation of f and not of $\underline{H}$. The theoretical points were calculated from equation II-18 on the IBM 1620 computer.

b) Small Temperature Differences Between Source and Absorber

The line shifts were calculated from the two equations referred to above, first, δ_1 by equation VI-1 and secondly, δ_2 from equation IV-6. These calculated shifts were corrected for the residual shift, the variation in θ', and the hydrostatic compression shift as outlined in section 6.4.a. The uncorrected and corrected values of δ_1 and δ_2 are tabulated in table VI-4.

$\theta\,^\circ K$	$\theta'\,^\circ K$	$\delta_1(m)$ cm/sec	$\delta_1(c)$ cm/sec	$\delta_2(m)$ cm/sec	$\delta_2(c)$ cm/sec
335	298.5	.00214	.00270	.00241	.00297
323	297.5	.00113	.00157	.00113	.00157
315	297	.00093	.00131	.00112	.00150
310.5	297.5	.00087	.00123	.00043	.00082
298.5	299.5	-.00009	.00030	-.00042	.00000
279	299.5	-.00278	-.00232	-.00226	-.00190
268.5	297.5	-.00330	-.00310	-.00290	-.00270
250	297	-.00490	-.00479	-.00386	-.00340

Table VI-4

The uncorrected and corrected small temperature shifts of the Mossbauer spectrum.
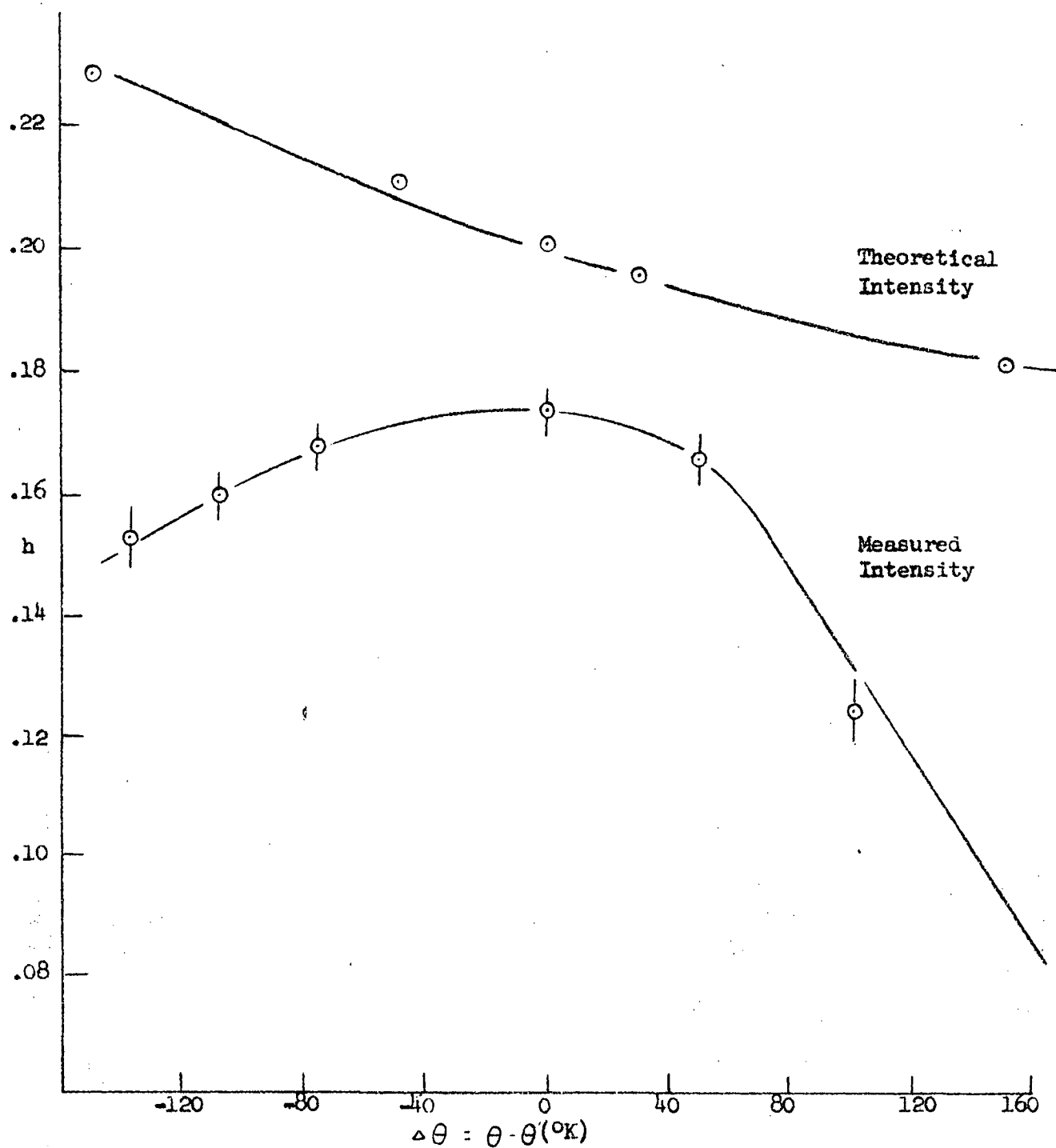
FIGURE VI-4 The measured and theoretical temperature variation of the
Mossbauer intensity plotted as a function of the temperature
difference between the source and absorber.

Inspection of the values of δ_1 and δ_2 given in table VI-4 shows, as expected, that the two are different, with the magnitude of δ_1 usually greater than the magnitude of δ_2. This difference between the magnitudes of the two shifts is also obvious in the plot of δ_1 and δ_2 as a function of $\Delta\theta$ in figure VI-5. From this figure the slopes $d(\delta/c)/d\theta$ of δ_1 and δ_2 were found to be

$$d(\delta_1/c)d\theta = 3.28 \times 10^{-15}/^{\circ}K \qquad\qquad VI-4$$

and

$$d(\delta_2/c)d\theta = 2.36 \times 10^{-15}/^{\circ}K \qquad\qquad VI-5$$

The latter slope is equal, within experimental error, to the slope obtained from the measurements made in the previous section of the gross temperature shifts versus temperature. This agreement shows that equation VI-3 is sufficiently accurate to use for calculating temperature shifts. The shifts, δ_2, were added to figure VI-3 and are seen to lie on the solid theoretical line. For $\Theta_D = 420^{\circ}K$ the theoretical slope between $\theta = 250^{\circ}K$ and $\theta = 350^{\circ}K$ is

$$d(\delta/c)/d\theta = 2.34 \times 10^{-15}/^{\circ}K \qquad\qquad VI-6$$

The line widths calculated for small temperature differences between the source and absorber by means of equation VI-2 are tabulated in table VI-5. The values of h used in these calculations were obtained from figure VI-2. Figure VI-6 shows the variation of the Mossbauer line widths as a function of temperature for both large and small temperature shifts. The experimental points are shown with their error bars. The results indicate that the minimum line width lies not at $\Delta\theta = 0^{\circ}K$ but at $\Delta\theta = 24^{\circ}K$. Hence if it is assumed that the residual line broadening

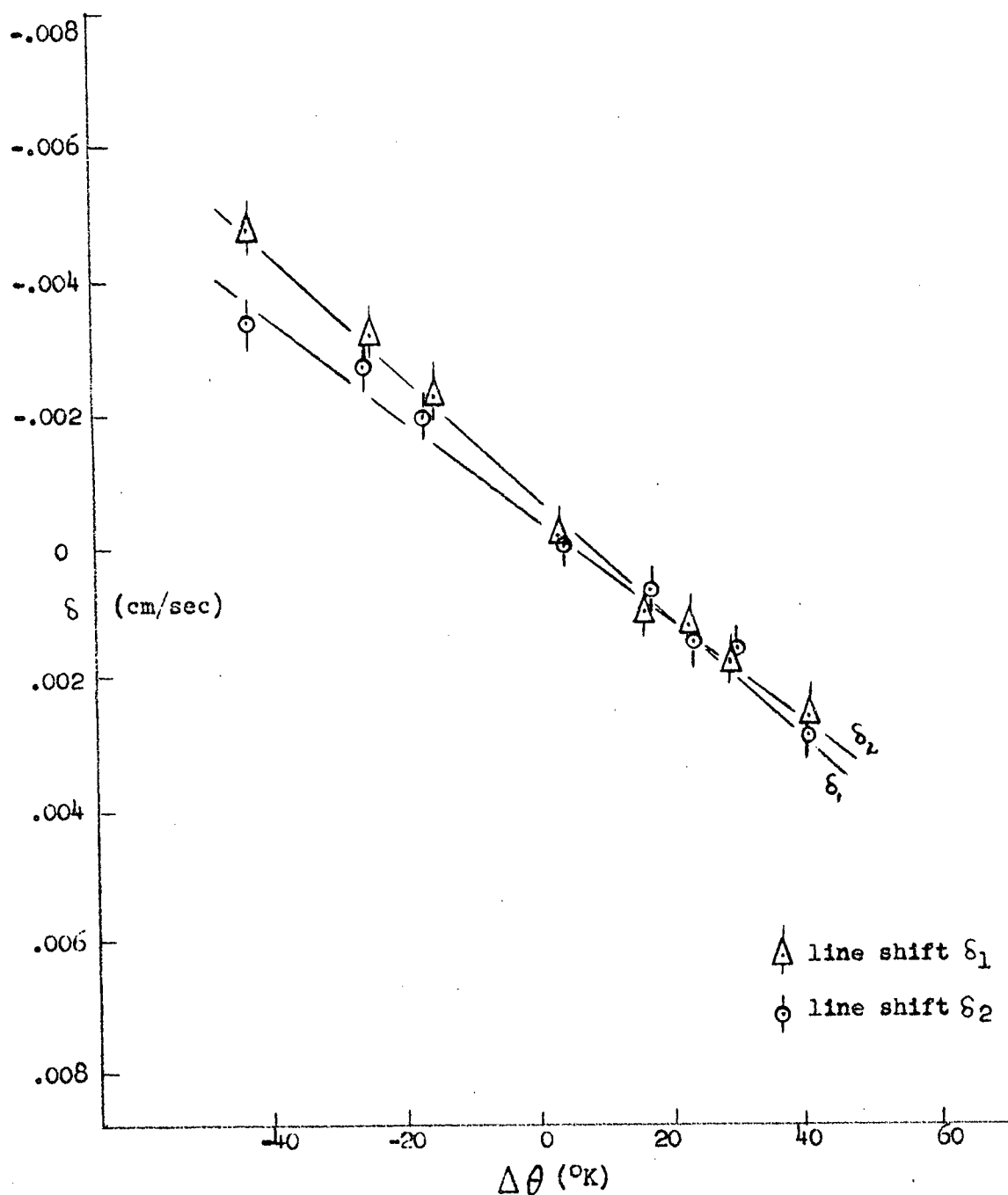FIGURE VI-5 A comparison of the temperature dependent line shifts, δ_1, and δ_2, calculated from equations VI-1 and IV-6.

at $\Delta\theta = 0^\circ K$ is due to some residual internal magnetic field difference, ΔH, at $\Delta\theta = 0^\circ K$, the resulting value calculated for ΔH is .01 x 10^5 oe which is the field difference required to produce a line broadening at $\Delta\theta = 0^\circ K$ of .0025 cm/sec. (See table II-3). The solid line in figure VI-6 is the broadening of the Mossbauer spectrum calculated from the temperature dependence of H. For this calculation the minimum line width was taken as .0305 cm/sec at $\Delta\theta = 24^\circ K$. The theoretical points are indicated on the figure without error bars.

6.5 Discussion of Results and Conclusions

a) The Shape of the Spectra

At $\Delta\theta = 100^\circ K$, $189^\circ K$ and $-138^\circ K$ a hyperfine structure appeared on the Mossbauer spectrum. This structure, shown at $\Delta\theta = 100^\circ K$ in figure VI-2, indicates that the Zeeman splitting of the nuclear levels

$\theta^\circ K$	$\theta'^\circ K$	$\Delta\theta^\circ K$	h	Δ(cm/sec)
335.0	297.5	36.5	.17	.0335
323.0	297.5	25.5	.18	.0325
315.0	297.0	18.0	.18	.0320
310.5	297.5	13.0	.18	.0334
298.5	299.5	-1.0	.18	.0318
279.0	299.5	-20.5	.17	.0330
250.0	297.0	-47.0	.17	.0340

Table VI-5

The line width of the Mossbauer spectrum as a function of small temperature differences between source and absorber
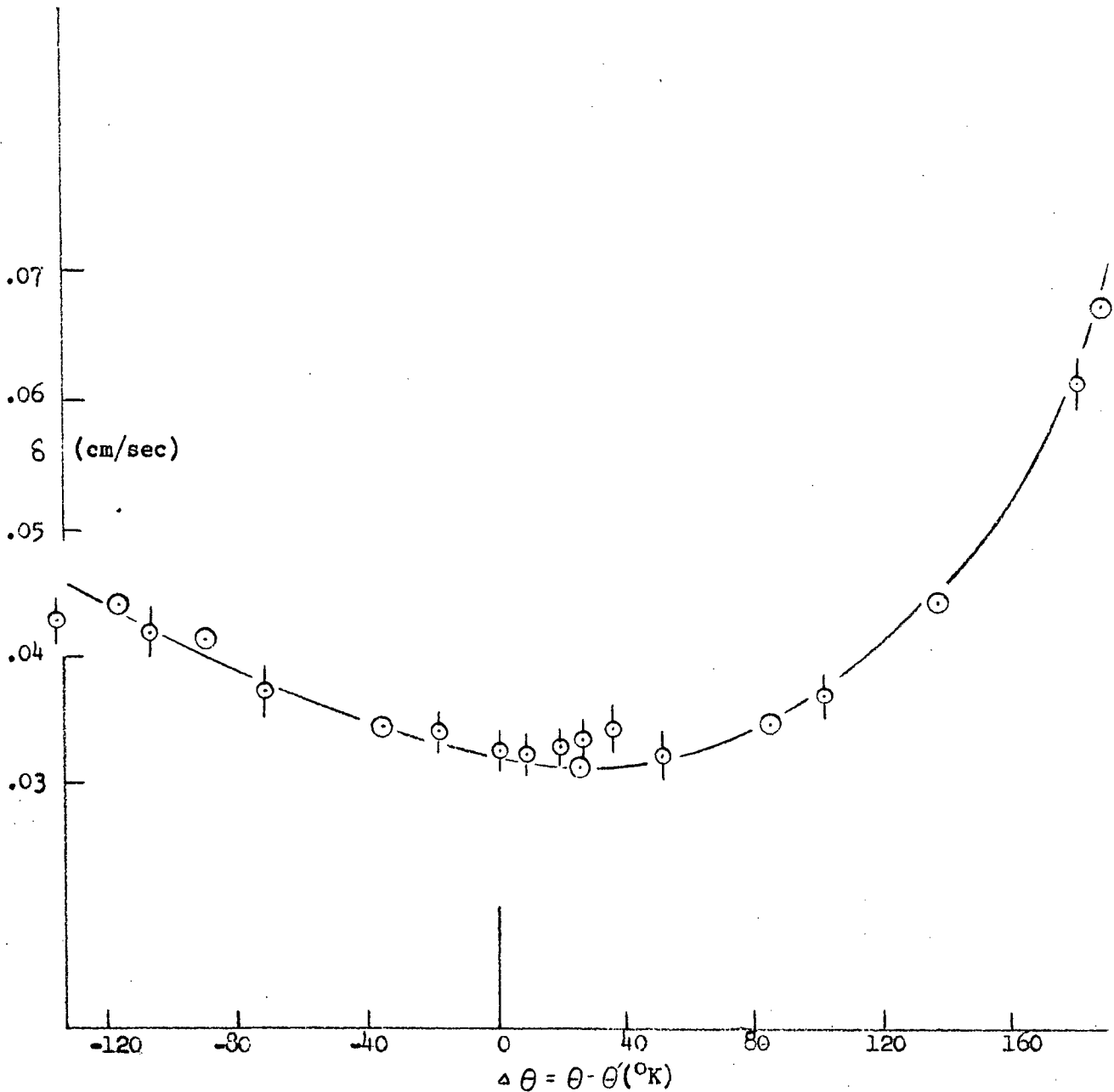
FIGURE VI-6 The variation of the Mossbauer line width as a function of the
temperature difference between the source and absorber. The
solid line and the points without error bars represent the
theoretical temperature dependence calculated from the known
temperature dependence of $\underset{\sim}{H}$.

of the source and absorber nuclei is sufficiently different to be detected at these temperature differences. That is, the difference between the Zeeman splitting of the nuclear levels no longer produces only a broadening, but also a multiple line. This splitting is consistent with the fact that at these large temperature differences, large differences in the internal magnetic fields at the nuclei of the source and absorber are present. Assuming that $H = H'$ at $\Delta\theta = 24^\circ K$, then $\Delta H = .06 \times 10^5$ oe, $.12 \times 10^5$ oe, and $-.12 \times 10^5$ oe, for each of the above temperature differences. To illustrate the effect that a large temperature difference can have on the energy levels of the nuclei consider the transition $-3/2 \rightarrow -1/2$ at $\Delta\theta = 189^\circ K$. The difference in the transition energies of this line of the source and absorber is calculated, from equation II-44, to produce a line shift of $.0195$ cm/sec. This shift is comparable to the measured line width at $\Delta\theta = 0^\circ K$ of $.031$ cm/sec. The shift in transition energy is greatest for the two transitions $-3/2 \rightarrow -1/2$ and $3/2 \rightarrow 1/2$. (See table II-2). Moreover, the transmission probabilities, W_{jk} for these two transitions are greater than those of the four remaining transitions. Therefore, at the velocities at which the emission and absorption lines corresponding to these two transitions overlap, the resonant absorption should reach a maximum thereby producing the observed doublet structure.

b) The Line Shift

In the temperature range considered ($\theta = 156^\circ K$ to $\theta = 478^\circ K$), The measured line shifts agree, within experimental error, with the shift predicted by the Josephson effect for $\Theta_0 = 420^\circ K$. The agreement, implies that, in this temperature range and for this source and absorber combination, the quadrupole moment and the isomer shift are

magnetic fields between the source and absorber at $\Delta\theta = 0^\circ K$ could be caused by the fact that the source lattice is an alloy of Co^{57} and Fe whereas the absorber lattice is natural Fe. However, it has been found experimentally that the internal field at an Fe nucleus arises primarily from the contributions of its own electrons and depends only slightly upon the magnetization of the surrounding atoms.[16] For example, the internal field at $300^\circ K$ at the Fe nuclei in an Fe lattice is 3.33×10^5oe, whereas it changes to 3.045×10^5oe in a Co lattice. Since the concentration of Co^{57} in the source used was less than 2.00×10^{-4}, any broadening caused by this mechanism is negligible. Also, if the alloying of Co^{57} and Fe affected the internal magnetic field, then the magnetic field at the source nuclei should be less than that at the absorber nuclei. However, the fact that $\Delta H = 0$ for $\Delta\theta > 0^\circ K$ indicates that at $\Delta\theta = 0^\circ K$ the magnetic field at the source is greater than that at the absorber nuclei, since the magnetic field decreases as the temperature increases. A possible cause of the difference in H between the source and absorber is the presence of a residual magnetic field left in the source as a result of the annealing treatment. Moreover, the nuclei at the boarders of the magnetic domains are subjected to nonuniform magnetic fields so that a small amount of broadening of the Mossbauer line can be expected to appear. Unfortunately, it is impossible to estimate the amount of this broadening.

An additional temperature dependent broadening mechanism that could be operating to increase the width of the observed line is the change in the apparent source thickness, τ, through the temperature dependence of f. This mechanism would operate so as to increase Δ for $\Delta\theta > 0^\circ K$ and decrease Δ for $\Delta\theta < 0^\circ K$. However, the variation in τ is very small. (See figure VI-1)
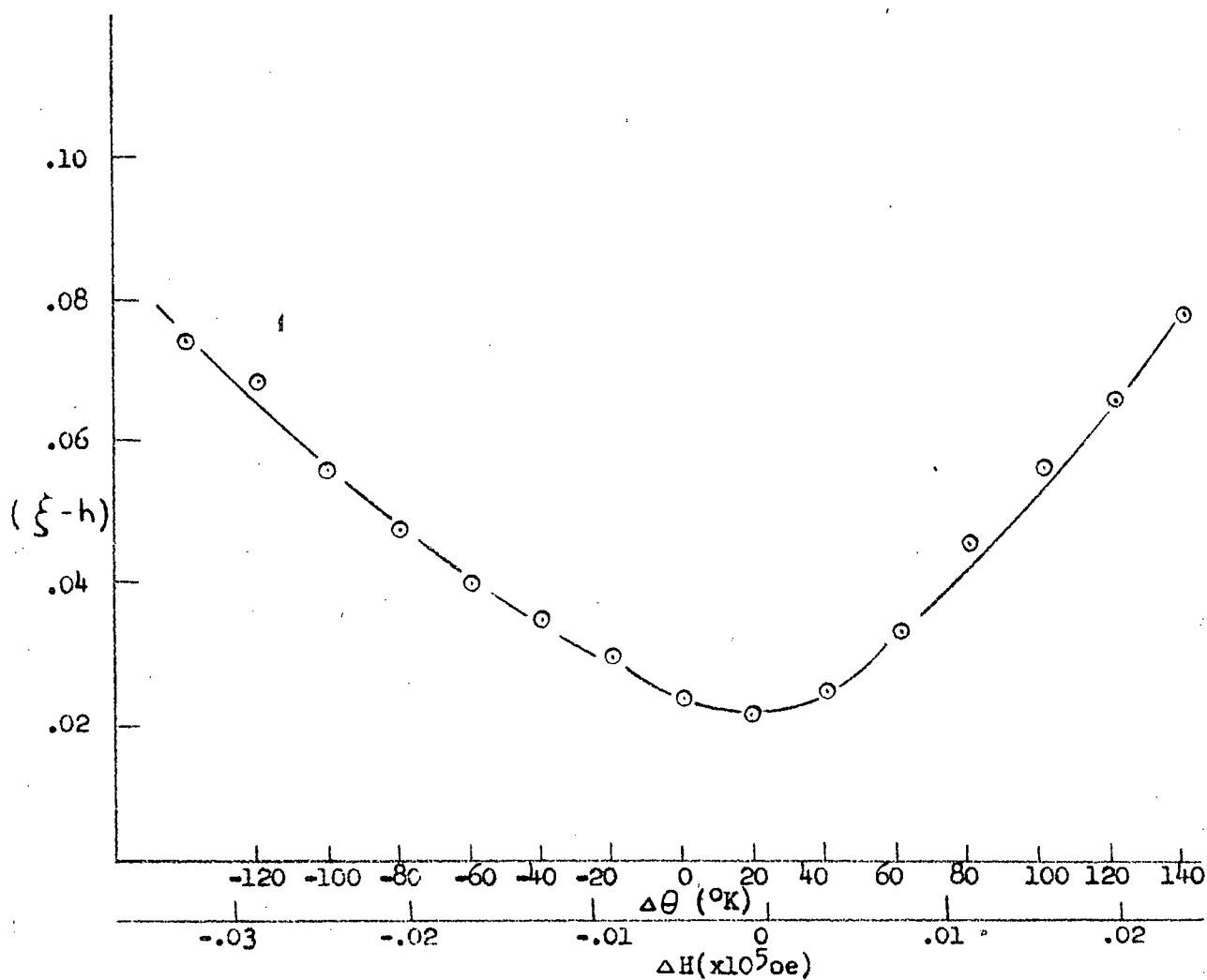
FIGURE VI-7 The difference between the theoretical and measured Moss-
bauer intensity plotted as a function of the temperature
difference between the source and absorber and the diff-
erence between the internal magnetic fields.

temperature independent or, at the most, their temperature variation is within the experimental error. Hence any variation of these two quantities, such as that found by S. DeBenedetti et al, was not observed with this source and absorber combination.[28] Figure II-4 showing δ/c as a function of θ for $\Theta_0 = 420^{\circ}K$ and $\Theta_0 = 355^{\circ}K$ illustrates the weak dependence of δ/c on Θ_0 above $200^{\circ}K$, so that the agreement between experimental and theoretical line shifts merely means that any variation caused by a temperature dependence of Θ_0 is small compared with the experimental error. This weak dependence of Θ_D on θ also means that an error of $\pm 20^{\circ}K$ must be associated with the assignment of $\Theta_D = 420^{\circ}K$ to the source and absorber. In order to reduce this error, and to detect a difference in Debye temperature between the source and absorber, measurements would have to be conducted in the region below $\theta = 150^{\circ}K$.

The residual shift found for $\Delta\theta = 0^{\circ}K$ does not arise from a difference in Debye temperature between the source and absorber. Since the source was an alloy of Co^{57} and Fe, it is expected that $\Theta_D < \Theta_D'$ which would produce a positive shift whereas the observed residual shift is negative. It is concluded, therefore, that the residual shift is essentially an isomer shift.

c) The Line Width

The observed temperature dependence of the line width is predicted, within experimental error, by the temperature dependence of the internal magnetic field and its effect upon the Zeeman splittings of the nuclear levels of the source and absorber nuclei. This result, however, is based upon the observation that the minimum line width occurs at $\Delta\theta = 24^{\circ}K$ and not at $\Delta\theta = 0^{\circ}K$. The difference in the internal
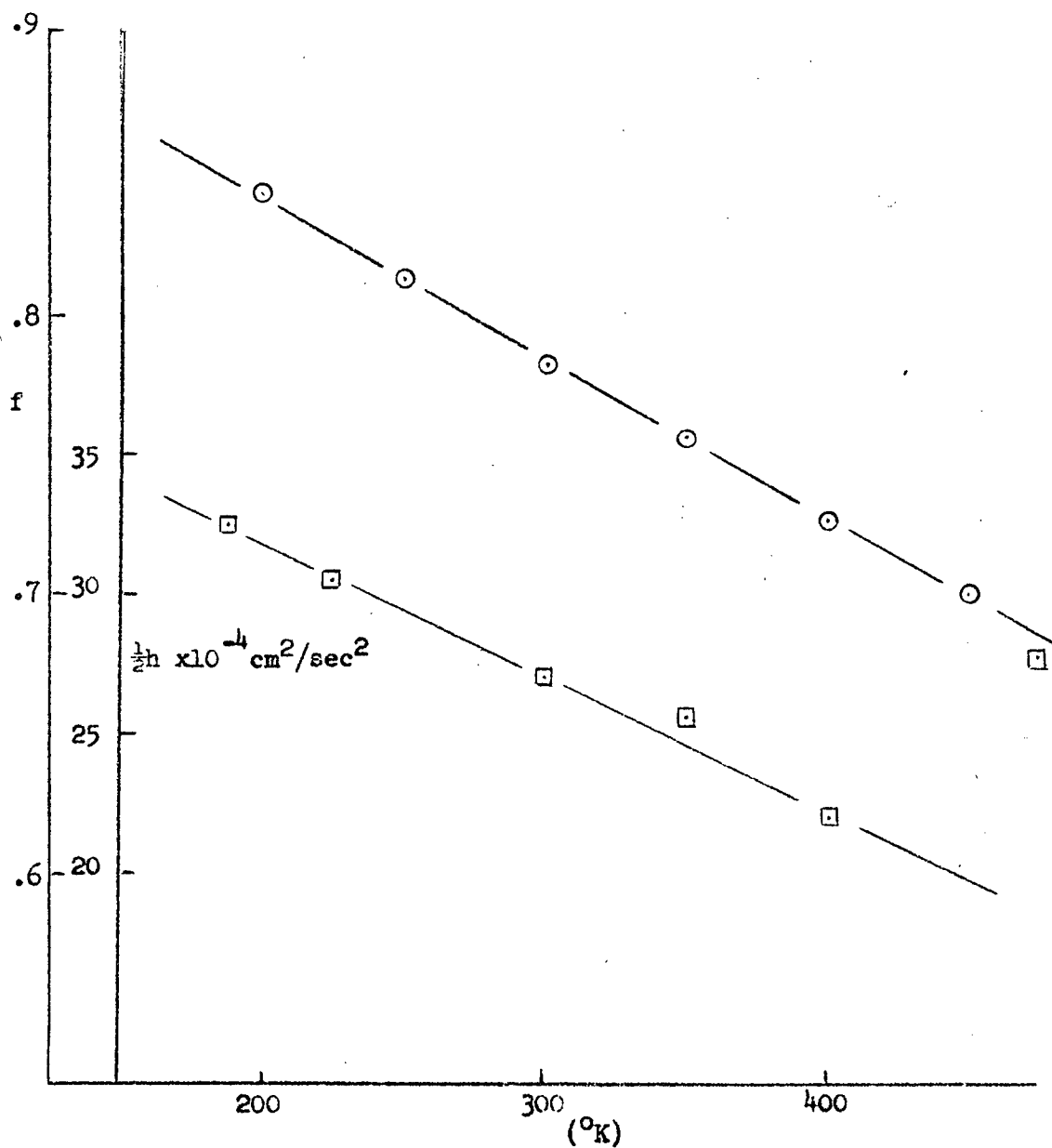
Figure VI-8 The temperature dependence of the Debye-Waller factor, f, and the approximate area beneath the Mossbauer spectrum, $\frac{1}{2}h\Delta$.

d) The Line Intensity

The temperature dependence of f predicts that h should decrease as θ increases. However, since $\underset{\sim}{H}$ and therefore $\triangle$ are temperature dependent, the temperature dependence of f alone is insufficient to explain the temperature dependence of h. This fact is clearly demonstrated in figure VI-4. The difference between h and $\underset{\varsigma}{\zeta}$ has been plotted as a function of $\triangle\theta$ in figure VI-7. The $\triangle\theta$ axis in this figure has also been labeled with the corresponding values of $\triangle H$. This curve illustrates a definite relationship between $\triangle H$ and h. The probable mechanism producing this relationship was discussed in section 6.1.d. It is interesting to note that the curve of figure VI-7 has a minimum at approximately $\triangle\theta = 24^{\circ}K$ similar to the curve of figure VI-6, thereby supporting the conclusion that $\triangle H = 0$ at $\triangle\theta = 24^{\circ}K$. The temperature dependence of h, therefore appears to be the resultant of the temperature dependence of f and H.

It is expected that the product, $\frac{1}{2}h\triangle$, which is the approximate area under the Mossbauer spectrum, should follow the same temperature dependence as f. In figure VI-8 $\frac{1}{2}h\triangle$ and f are plotted as functions of θ. From this figure it is seen that, between $200^{\circ}K$ and $400^{\circ}K$, these two quantities do have the same temperature dependence but beyond these limits the agreement breaks down.

Appendix A

THE COMPUTER PROGRAM

In order to compare the theoretical parameters of the Mossbauer line with those obtained experimentally, equation II-18 had to be evaluated. This evaluation was to be done numerically using the IBM 1620 at the UBC Computing Centre and the IBM 7090 at the University of Toronto's Computing Centre.

Originally, the program was formulated using Simpson's rule for the evaluation of the integral. The difficulty in producing a correct program lay in determining suitable values for the step size and the limits of integration. The final values used were step size, 1×10^{-9}ev, number of steps, 601, and the limits of integration, -3×10^{-7}ev to 3×10^{-7}ev. The time required to evaluate the program using these values was 53 minutes per point using the IBM 1620. The number of points that were required for each of the four absorber thicknesses was 30, hence arrangements were made to send the program to the University of Toronto's Computing Centre where the complete evaluation of the 120 points would require only 20 minutes on the IBM 7090.

If the program used was correct, $R(v = \infty)$ should be 1. The difficulty that remained, however, was that $R(v = \infty)$, calculated by the above program was .970125 rather than 1. Since this error was thought to be inherent in the step size, the limits of integration, or the value of v used for $v = \infty$, a series of check runs were made on the IBM 1620 in which these values were varied. In each case, however, the value of $R(v = \infty)$ was less than .97 indicating that the error lay elsewhere. Before further tests were made on the program, it was changed by replacing all divisions by constants, by multiplications, and by

replacing Simpson's rule by a Gaussian formula for the integration. Eight, four-point Gaussian integrations were used over the range of integration indicated above. This program yielded the same results as did the former program but in an average time of $2\frac{1}{2}$ minutes per point. Some final results obtained with this program are summarized in Table A-1. Both the original and final programs are on file in the care of Dr. B. L. White, Department of Physics, UBC.

v cm/sec	$R(v,t_1')$	$R(v,t_2')$	$R(v,t_3')$	$R(v,t_4')$
0	.9060	.8614	.8099	.7393
.01	.9400	.9171	.8892	.8481
.04	.9690	.9662	.9627	.8572
.11	.9723	.9720	.9717	.9710
.26	.9726	.9729	.9723	.9726

Table A-1

Test results of the numerical evaluation of $R(v)$. t_1', t_2', t_3' and t_4 refer to the absorber thicknesses of .0002", .00035", .00055" and .001".

Appendix B

THE PREPARATION OF AN ENRICHED Fe^{57} ABSORBER

An investigation was made into the possibility of making an enriched Fe^{57} absorber. Enriched Fe^{57} is supplied in the compound Fe_2O_3 so that the following procedure was devised to prepare the metallic absorber from the oxide.

1. Reduce the ferric oxide to Fe by placing the oxide in a hydrogen atmosphere at $900^{\circ}C$ for one hour.

2. Add H_2SO_4 (dilute) to the Fe to prepare $Fe_2(SO_4)_3$ containing 10 mg of Fe/ml.

3. Prepare the following electroplating solution[27]

   2.5 ml $Fe_2(SO_4)_3$

   85.0 ml $(NH_4)_2C_2O_4$ (saturated)

   1.0 ml 3M H_2SO_4

4. Use the following plating characteristics

current	0.85 amps
voltage	8 - 10 volts
time	2.25 hours
initial pH	4
final pH	less than 7
initial solution colour	yellowish green
time for colourless solution	0.75 hours

5. Use Pt for the anode and Cu for the cathode.

6. Maintain the plating solution temperature at $70^{\circ}C$

7. Offset the tendancy of the plating solution to become basic by dropwise additions of 3M H_2SO_4.

The above procedure was used to produce several discs of natural Fe electroplated on Cu. The layer of Fe was shiny but was unevenly distributed in every case. This uneven distribution made

the preparation of the enriched absorber impractical since a uniform

absorber thickness is necessary for the interpretation of the experi-

mental results. Also, the thickness of the absorber had to be known

but no method could be devised whereby the electroplated layer could

be measured except by destroying the absorber.

Appendix C

GEOMETRIC CORRECTIONS TO R(v)

To determine the effect the experimental geometry had on R(v), the two assumptions

1. the source thickness is zero and

2. the emission and absorption spectra each consist of a

single line

were made. Under these conditions equation II-18 becomes

$$R(v,\phi_m) = 1 - f + \frac{f\Gamma}{2\pi} \int_0^\infty dE \frac{\int_0^{\phi_m} d\phi \curlywedge(\phi)\eta(\phi)e^{-[\sigma_e + \sigma_m(E,v_0,\phi)] n/\cos\phi}}{\int_0^{\phi_m} d\phi \curlywedge(\phi)\eta(\phi)e^{-\sigma_e n/\cos\phi}} \quad \text{C-1}$$

In the above equation

$$\curlywedge(\phi) = 2\pi\sin\phi \qquad\qquad\qquad\qquad\qquad \text{C-2}$$

$$\eta(\phi) = (1 - e^{-\mu_p x/\cos\phi}) \qquad \text{where } \mu_p \text{ is the linear absorption coefficient for Ar} \qquad \text{C-3}$$

$$\beta = v_0/c \qquad\qquad\qquad\qquad\qquad\qquad\qquad \text{C-4}$$

$$\sigma_m(E,v_0,\phi_m) = f'\sigma_0\Gamma^2/4 \bigg/ \left[E - E_0(1 + \beta\cos)\right]^2 + \Gamma^2/4 \qquad \text{C-5}$$

and n is the number of Fe^{57} atoms/cm^2.

When $\phi = 0$, $\curlywedge(\phi) = \curlywedge(0)$, $\eta(\phi) = \eta(0)$, $\cos\phi = 1$ and

$$R(v_0,0) = 1 - f\left[1 - \frac{\Gamma}{2\pi} \int_0^\infty \frac{dE e^{-\sigma_m(E,v_0)n}}{[E - E_0(1 + \beta)]^2 + \Gamma^2/4}\right] \qquad \text{C-6}$$

When ϕ_m is small, the substitution $\cos\phi = 1 - \phi^2/2$ can be used. For a proportional counter window of 6" width, and a source to counter distance of 15", $\phi_m = .2$rad. and the use of the expansion of $\cos\phi$ introduces an error of .7% in the value of $\cos\phi$. Hence, when ϕ_m is small

$$\wedge(\phi) = 2\pi(\phi - \phi^3/6) \tag{C-2'}$$

$$\eta(\phi) = \eta(0)\left[1 + .42\phi^2\right] \tag{C-3'}$$

where the fact that $\mu_p x = 0.85$ for the Ar-CH$_4$ proportional counter has been used, and

$$\exp(-\sigma_e n/\cos\phi) = \exp(-\sigma_e n)(1 - .7\phi^2) \tag{C-7}$$

Hence

$$\int_0^{\phi} d\phi \wedge(\phi)\eta(\phi)\exp(-\sigma_e n/\cos\phi) = 2\pi\eta(0)\exp(-\sigma_e n)\int_0^{\phi_m} d\phi(\phi - \phi^3/6)$$
$$x \ (1 + .42\phi^2)(1 - .7\phi^2) \tag{C-8}$$

Also

$$\exp(-\sigma_m n/\cos\phi) = \exp(-\sigma_m(\phi=0)n)\left[1 - \sigma_m(\phi=0)n3\phi^2/2\right] \tag{C-4'}$$

in the derivation of which the approximation $(E - E_0(1 + \beta/3)) = 2\Gamma$ has been made. $\sigma_m(\phi=0)n$ has a maximum value at $E = E_0$ of 4 (for Fe^{57}, a .001" thick natural Fe absorber, and $f = .7$), and an average value of 1 over the range of integration, hence

$$\frac{f\Gamma}{2\pi}\int_0^\infty dE \int_0^{\phi_m} \frac{d\phi \wedge(\phi)\eta(\phi)\exp\left[-(\sigma_e + \sigma_m(E,v_0\phi))n/\cos\phi\right]}{\left[E - E_0(1 + \beta\cos\phi)\right]^2 + \Gamma^2/4}$$

$$= f\Gamma\eta(0) e^{-\sigma_e n}\int_0^\infty dE \int_0^{\phi_m} \frac{d\phi \ e^{-\sigma_m n}(\phi - .16\phi^3)(1 + .42\phi^2)(1 - .7\phi^2)(1 - \frac{\sigma_m n3\phi^2}{2})}{\left[E - E_0(1 + \beta)\right]^2 + \Gamma^2/4}$$

$$= f\Gamma\eta(0) e^{-\sigma_e n}\int_0^\infty \frac{dE \ e^{-\sigma_m n}}{\left[E - E_0(1+\beta)\right] + \Gamma^2/4}\int_0^{\phi_m} d\phi \ (\phi - 2\phi^3)$$

Thus

$$R(v,\phi_m) = 1 - f\left[1 - \frac{\Gamma}{2\pi}\int_0^\infty \frac{dE\exp(-\sigma_m n)}{[E-E_0(1+\beta)]^2 + \Gamma^2/4} \frac{\int_0^{\phi_m} d\phi(\phi - 2\phi^3)}{\int_0^{\phi_m}d\phi(\phi - \phi^3/6)(1 - .28\phi^2)}\right]$$

$$= 1 - f\left[1 - \frac{A\Gamma}{2\pi}\int_0^\infty \frac{dE\exp(-\sigma_m n)}{[E-E_0(1+\beta)]^2 + \Gamma^2/4}\right.$$

C-10

where A is the geometrical correction factor. Values of A corresponding to the four absorber thicknesses used in the experimental work are given below.

Absorber Thickness	Correction Factor - A
.0010"	.97
.00055"	.98
.00035"	.99
.0002"	.996

Appendix D

STATISTICAL DESIGN OF THE EXPERIMENT

Since a variety of absorber thicknesses were available for the experimental work, (.0002", .00035", and .001"), the following analysis was made to determine which thickness would give the most significant results in a given counting time T. The assumption made in this analysis is that the emission and absorption spectra consist of single lines.

Assuming that $\cos\emptyset = 1$, the change in count rate from that at $v = \infty$, to that at $v = 0$, is given by

$$
\begin{aligned}
\chi &= N(v=\infty) - N(v = 0) \\
&= N_s e^{-\mu_e x} - N_s (f e^{-\mu_e x} \overline{^{-\mu_m x}} + (1-f)e^{-\mu_e x}) \\
&= N_s f(1 - e^{-\mu_m x})e^{-\mu_e x}
\end{aligned}
\tag{D-1}
$$

where N_s is the count rate with no absorber, and μ_m and μ_e are the linear absorption coefficients of the Mossbauer and electronic absorption respectively. Also

$$
\begin{aligned}
e^{-\mu_m x} &= \frac{\displaystyle\int_0^\infty \frac{e^{-\sigma_m n}}{(E_o-E)^2 + \Gamma^2/4} dE}{\displaystyle\int_0^\infty \frac{dE}{(E_o-E)^2 + \Gamma^2/4}} \\
&= e^{-\mu_m x/2} I_o(\mu_m x/2)
\end{aligned}
\tag{D-2}
$$

where $I_o(\mu_m x/2) = J_o(i\mu_m x/2)$ is the Bessel function of the first order[10]. The statistical error in the count rate is

$$
e = (N_s e^{-\mu_e x})^{\frac{1}{2}}
\tag{D-3}
$$

Then, for the given counting time T, the absorber thickness x, for

which the most signigicant results are obtained is that value at which the ratio χ/e has its maximum value. Now

$$\chi/e = f(N_S T)^{\frac{1}{2}} e^{-\mu_e x/2} (1 - e^{-\mu_m x/2} I_0(\mu_m x/2))$$ D-4

so that for a fixed N_S and T, when χ/e is a maximum

$$d(\chi/e)/dx = 0$$
$$= \mu_e/2 \left[1 - e^{-\mu_m x/2} I_0(\mu_m x/2) \right] + \mu_m x/2 e^{-\mu_m x/2} I_0(\mu_m x/2)$$
$$- \mu_m x/2 e^{-\mu_m x/2} I_1(\mu_m x/2)$$ D-5

where the relationship $I_0'(z) = I_1(z)$ has been used. Using $z = \mu_m x/2$, the condition determining the value of x at which χ/e is a maximum is that

$$e^{-z} I_0(z) = \mu_e/(\mu_m + \mu_e) + \mu_m/(\mu_m + \mu_e) e^{-z} I_1(z)$$ D-6

Since the experimental measurements were done with Zeeman split spectra rather than with the single line spectra that the above theory assumes, a difference between the experimentally determined value of x at which χ/e is a maximum and the theoretical value is not unexpected.

Appendix E

THE ROOT MEAN SQUARE DIFFUSION DEPTH

Using the assumptions given in Chapter IV, the number of diffused atoms between x and $x + dx$ is

$$c(x) = \frac{Q \exp(-x^2/4Dt)}{\sqrt{\pi Dt}} \qquad \text{E-1}$$

Therefore, the mean square penetration depth $\overline{x^2}$ is

$$\overline{x^2} = \frac{\int_o^\infty \frac{x^2 Q \exp(-x^2/4Dt)dx}{\sqrt{\pi Dt}}}{\int_o^\infty \frac{Q \exp(-x^2/4Dt)dx}{\sqrt{\pi Dt}}} \qquad \text{E-2}$$

$$= 2Dt$$

Hence, the root mean square diffusion depth is

$$\overline{x^2}^{\frac{1}{2}} = (2Dt)^{\frac{1}{2}} \qquad \text{E-3}$$

Bibliography

1. R. L. Mossbauer, Kernresonanzfluoreszenz von Gammastrahlung in Ir^{191}, Z. Physik, 151, 124 (1958)

2. H. Frauenfelder, (ed.), "The Mossbauer Effect", W. A. Benjamin, Inc., New York, 1962.

3. D. M. J. Compton, and A. H. Schoen, (eds.), "Proceedings of the Second International Conference on the Mossbauer Effect, Saclay, France, Sept. 13-16, 1961", Wiley, New York, 1962.

4. A. J. Boyle, and H. e. Hall, The Mossbauer effect, Strickland, A. C., (ed.), "Reports on Progress in Physics", The Institute of Physics and the Physical Society, London, 1962, Vol. 25, pp 441-525.

5. S. Margulies, and J. R. Ehrman, Transmission and line broadening of resonance radiation incident on a resonance absorber, Nuclear Instr., 12, 131 (1961a)

6. J. G. Dash, R. D. Taylor, D. E. Nagle, P. P. Craig, and W. M. Visscher, Polarization of Co^{57} in Fe metal, Phys. Rev., 122, 1116 (1961)

7. S. S. Hanna, J. Herberle, C. Littlejohn, G. J. Perlow, R. S. Preston, and D. H. Vincent, Polarized spectra and hyperfine structure in Fe^{57}, Phys. Rev. Letters, 4, 177 (1960a)

8. L. R. Walker, G. K. Wertheim, and V. Jaccarino, Interpretation of the Fe^{57} isomer shift, Phys. Rev. Letters, 6, 98 (1961)

9. J. C. von der Bosch, The Zeeman effect, P. H. XXVIII, 317.

10. E. Jahnke, and F. Ende, "Tables of Functions with Formulas and Curves", Dover, New York, 1945, pg. 226.

11. B. D. Josephson, Temperature dependent shift of gamma rays emitted by a solid, Phys. Rev. Letters, 4, 341 (1960)

12. A. J. Dekker, "Solid State Physics", Prentice Hall Inc., Englewood cliffs, New Jersey, 1960, pg. 42.

13. R. V. Pound, G. B. Benedek, and R. Drever, Effect of hydrostatic compression on the energy of the 14.4 kev gamma ray from Fe^{57} in iron, Phys. Rev. Letters, 7, 405 (1961)

14. A. H. Wilson, "Thermodynamics and Statistical Mechanics", Cambridge University Press, Cambridge, 1957, pg. 158.

15. S. L. Ruby, and J. M. Hicks, Line shape in Mossbauer spectroscopy, Rev. Sc. Instr., 33, 27, (1962)

16. G. K. Wertheim, Mossbauer effect; applications to magnetism, J. Appl. Phys., (suppl.), 32, 110S (1961b)

17. P. G. Klemens, Localized modes and spin-lattice interactions, Phys. Rev., 125, 1795 (1962)

18. R. Brout, and W.Vischer, Suggested experiment on approximate localized modes in crystals, Phys. Rev. Letters, 9, 54 (1962)

19. T. E. Bortner, and G. S. Hurst, Ionization of pure gases and mixtures of gases by 5 Mev alpha particles, Phys. Rev., 93, 1236 (1954)

20. R. V. Pound, and G. A. Rebka, Jr., Resonant absorption of the 14.4 kev gamma ray from 0.10μ sec Fe^{57}, Phys. Rev. Letters, 3, 554 (1959a)

21. W. Boas, "Physics of Metals and Alloys", John Wiley and Sons, Inc., 1947

22. P. P. Craig, D. E. Nagle, and D. R. F. Cochran, Zeeman effect in the recoilless gamma ray resonance of Zn^{67}, Phys. Rev. Letters, 4, 561 (1960)

23. R. E. Carter, and F. D. Richardson, An examination of the decrease of surface activity method of measuring self-diffusion coefficients in wushite (FeO_n) and cobaltous oxide, Jour. of Metals, 6, 1244 (1954)

24. O. C. Kistner and A. W. Sunyar, Evidence for quadrupole interaction of Fe^{57m} and influence of chemical binding on nuclear gamma ray energy, Phys. Rev. Letters, 4, 412 (1960)

25. R. V. Pound and G. A. Rebka, Apparent weight of photons, Phys. Rev. Letters, 4, 337 (1960)

26. D. E. Nagle, H Frauenfelder, R. D. Taylor, D. R. F. Cochran, and B. T. Mathais, Temperature dependence of the internal field in ferromagnets, Phys. Rev. Letters, 5, 364 (1960)

27. C. L. Maletskos, and J. W. Irvine, Jr., Quantitative electro-deposition of radioactive cobalt, zinc and iron, Nucleonics, 14, 84 (1956)

28. S. DeBenedetti, G. Lang, and R. Ingalls, Electric quadrupole splitting and the nuclear volume effect in the ions of Fe^{57}, Phys. Rev. Letters, 6, 60 (1961)